CHALMERS
UNIVERSITY OF TECHNOLOGY

Future Mould Growth Index

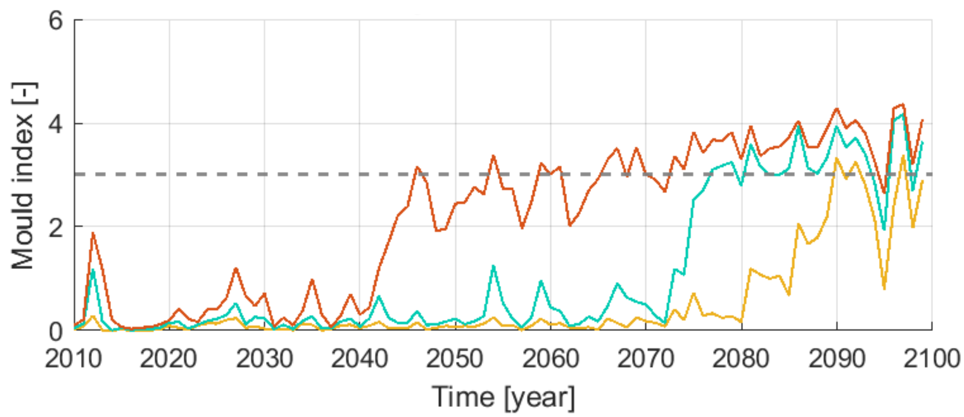

Future Risks on Moisture Safety in Ventilated Parallel Roofs

A Numerical Study of a Common Roof Type in Sweden Subjected to Future Weather Data Sets

Master's thesis in Master Programme of Structural Engineering and Building Technology

ALICE ALLINGER

DEPARTMENT OF ARCHITECTURE AND CIVIL ENGINEERING,
DIVISON OF BUILDING TECHNOLOGY,
BUILDING PHYSICAL MODELLING

CHALMERS UNIVERSITY OF TECHNOLOGY
Gothenburg, Sweden 2022
www.chalmers.se

MASTER'S THESIS 2022

Future Risks on Moisture Safety in Ventilated Parallel Roofs

A Numerical Study of a Common Roof Type in Sweden Subjected to Future Weather Data Sets

ALICE ALLINGER

CHALMERS
UNIVERSITY OF TECHNOLOGY

Department of Architecture and Civil Engineering
Division of Building Technology
Building Physical Modelling
CHALMERS UNIVERSITY OF TECHNOLOGY
Gothenburg, Sweden 2022

Future Risks on Moisture Safety in Ventilated Parallel Roofs
A Numerical Study of a Common Roof Type in Sweden Subjected to Future Weather Data Sets

ALICE ALLINGER

Supervisor: Angela Sasic Kalagasidis, Department of Architecture and Civil Engineering
Supervisor: Fredrik Säfblad, PE Teknik & Arkitektur
Supervisor: Martina Stockhaus, PE Teknik & Arkitektur
Supervisor: Gabriel Odén, PE Teknik & Arkitektur
Examiner: Angela Sasic Kalagasidis, Department of Architecture and Civil Engineering

Master's Thesis 2022
Department of Architecture and Civil Engineering
Division of Building Technology
Building Physical Modelling
Chalmers University of Technology
SE-412 96 Gothenburg
Telephone +46 31 772 1000

Cover: Mould Growth Index of a Bright-coloured Roof Oriented in South, East, and North for a Future Climate

Gothenburg, Sweden 2022

Future Risks on Moisture Safety in Ventilated Parallel Roofs
A Numerical Study of a Common Roof Type in Sweden Subjected to Future Weather Data Sets

ALICE ALLINGER

Department of Architecture and Civil Engineering
Chalmers University of Technology

Abstract

The climate is changing. The prognoses are a higher outdoor temperature and an increased absolute vapour content in outdoor air for all of Sweden. In Sweden today many roofs are already subjected to moisture-related damages and the guidelines for moisture safe design roofs are sparse.

Two different roof constructions are normally used in Sweden today: the attic and the ventilated parallel roof. The ventilated parallel roof has not been evaluated for a future climate. The purpose of this study is to investigate the moisture safety of ventilated parallel roofs subjected to a data set of future climates. The effect of orientation, inclination, colour and additional exterior insulation is evaluated for different locations in Sweden.

Parallel roofs in Sweden are often ventilated by natural driving forces: wind and thermal buoyance. The model of the study considers a full data set of meteorological data for calculating directional dependent thermal buoyance, moisture infiltration from indoor to outdoor due to pressure differences, and moisture and heat transport through the roof.

The result shows a future increased risk of mould growth in ventilated parallel roofs in all of Sweden. North is the dimensioning orientation. The most efficient way of reducing the risk is to use a reflective and bright-coloured roof.

Keywords: moisture safety, mould growth, numerical study, ventilation, parallel roof, air cavity, climate change, gable roof

Framtida risker i fuktsäkerhet för ventilerade parallelltak
En numerisk studie av en vanlig takkonstruktion i Sverige utsatta för dataset av framtida väder

ALICE ALLINGER

Institutionen för arkitektur och samhällsbyggnadsteknik
Chalmers Tekniska Universitet

Sammanfattning

Klimatet förändras. Prognosen är högre temperatur och en ökad absolut fukthalt i utomhusluften i hela Sverige. Redan idag är många tak i Sverige ansträngda av fuktproblem, och riktlinjerna för fuktsäkerdesign för tak är sparsamma.

Två typer av takkonstruktioner är vanliga i Sverige idag: kallvindar och ventilerade parallelltak. Det ventilerade parallelltaket har inte blivit undersökt ur fuktsynpunkt för framtida klimatpåverkan. Syftet med denna studie är att undersöka fuktsäkerheten i ventilerade parallelltak utsatta för dataset av framtida väder. Påverkan av orientering, luftning, färg och extra isolering utanpå kommer utvärderas för olika platser i Sverige.

Parallelltak i Sverige ventileras oftas av naturliga drivkrafter som vind och skorstenseffekten. Modellen som används i studien tar hänsyn till stora dataset av meteorologiska data för att beräkna skorstenseffekten beroende på vindriktning och fukttransporten genom luftläckage beroende av tryckskillnader, samt värme- och fukttransport genom konstruktionen.

Resultatet visar på en framtida ökad risk av mögelpåväxt i ventilerade parallelltak i hela Sverige. Det nordliga taket är dimensionerande. Effektivaste sättet att minska risken är att ha ett reflekterande och ljust tak.

Sökord: fuktsäkerhet, mögeltillväxt, numerisk studie, ventilation, parallelltak, luftspalt, klimatförändringar, sadeltak

Acknowledgements and Preface

This study and report are the product of a master thesis project in the Master Programme of Structural Engineering and Building Technology at the Chalmers University of Technology. The study has been done under close supervision by supervisors at Chalmers and with supervisors at the consultant firm PE Teknik & Arkitektur.

As the author of this study, I firstly want to thank my supervisor at Chalmers, Angela Sasic Kalagasidis for all her enthusiasm, for her deep and wide knowledge and for believing that I always can do more. I also want to thank docent Pär Johansson for giving me useful advice on numerical studies.

Secondly, I want to give a great thank to my supervisors at PE Teknik & Arkitektur: Martina Stockhaus, Fredrik Säfblad and Gabriel Odén. Thank you for giving me a close connection between the subject and real applications, for helping me understand the subject in-depth, and for helping me delimitate my work by choosing interesting study objects. A special thanks to Gabriel Odén who has put a lot of time into guiding me in troubleshooting my numerical model and helped me proofreading the report.

At last, I want to thank my father Lennart Allinger for proofreading the reports and giving useful feedback.

Alice Allinger, Gothenburg, April 2022

List of Acronyms

Below is a list of acronyms that have been used throughout this thesis listed in alphabetical order:

.txt	File format for a textfile
.mat	File format for a binary Matlab file for storing data
.wac	File format for a climate data file
A1B	Emission scenario
A2	Emission scenario
B1	Emission scenario
ECHAM5	A global climate model developed at the Max-Planck Institute for Meteorology
ECMWF	European Centre for Medium-range Weather Forecasts
ENLOSS Model	A building energy calculation program developed by SMHI
ERA40	A reanalysis project with 40 years of meteorological data
FEBY 18	Forum för Energieffektivt Byggande 2018[1]
GCM	Global Climate Model
GOT	Gothenburg
GtC	Emissions of CO_2 measured in Gigatonne of Carbon
IPCC	Intergovernmental Panel on Climate Change
MGI	Mould Growth Index
OST	Östersund
RCA2	Rossby Centre Regional Atmospheric Climate Model 2
RCA3	Rossby Centre Regional Atmospheric Climate Model 3
RCM	Regional Climate Model
SMHI	Swedish Meteorological and Hydrological Institute
SOLTIMSYN Model	A model for calculating the intensity of shortwave direct radiation based on spectral distribution, developed by SMHI
SRES	Special Report on Emissions Scenarios
STO	Stockholm

[1] In english: Forum for Building Energy Efficient Construction 2018

STO STD	A standard case for simulations considering a dark-coloured roof with an inclination of 30° located in Stockholm for the period 2010-2100
WUFI	WUFI Wärme- Und Feuchtetransport Instationär – A numerical software for hygrothermal calculations. When WUFI is used in this report, it is a reference to WUFI 2D.

Contents

Nomenclature

Below is a list of letters used throughout this thesis listed in alphabetical order in three groups: Roman Upper-case Letter, Roman Lower-case Letter and Greek Upper-case Letter

Roman Upper-case Letter

A_{cavity}	is the cross-section area of the cavity [m2]
D_w	is the liquid transport coefficient [m^2/s]
G_{inf}	is the moisture source, which is the amount of moisture accumulated in the structure per time [kg/s]
H_{in-out}	is the vertical height between the inlet and the outlet [m]
H_{np}	is the vertical distance between the neutral pressure plane and the inlet of the cavity [m]
$I_{e,body}$	is the longwave radiation emitted by a body [W/m^2]
$I_{lw,terr}$	is the terrestrial longwave radiation that can strike the body [W/m^2]
$I_{lw,refl}$	is the longwave radiation from the sky reflected by the ground [w/m^2]
$I_{lw,refl,sky}$	is the longwave radiation from the sky [W/m^2]
I_{sol}	is the solar heat load striking horizontally on a horizontal roof surface [W/m^2]
I_{sw}	is the global shortwave radiation [w/m^2]
$I_{sw,dir,\vartheta}$	is the direct shortwave radiation parallel to the solar beams [W/m^2]
$I_{sw,dir,h}$	is the horizontal direct shortwave radiation [W/m^2]
$I_{sw,dif,h}$	Is the horizontal diffuse shortwave radiation [W/m^2]
$I_{sw,refl}$	Is the shortwave radiation reflected on the ground [W/m^2]
L_{cav}	is the length of the cavity [m]
M	is the mould growth index [-]
M_{max}	is the maximum mould growth at the present conditions [-]

$\Delta P_{driving\ forces}$	is the pressure difference between inlet and outlet [Pa]
$\Delta P_{frictional\ loss}$	is the pressure drop due to friction [Pa]
ΔP_{roof}	is the total pressure difference over the roof [Pa]
ΔP_{wind}	is the pressure difference due to wind [Pa]
R_a	is the specific gas constant of dry air, which is 287.0058 [J/(kgK)]
Re	is the Reynolds number [-]
R_{ext}	is the thermal resistance of the external roof structure [m^2K/W]
RH	is the relative humidity [%]
RH_{crit}	is the critical relative humidity [%]
R_{int}	is the thermal resistance of the internal roof structure [m^2K/W]
R_v	is the specific gas constant of water vapour [J/(kgK)]
$\sum S_{cav}$	is the airflow resistance in the cavity [$Pa/(m^3/s)$]
ΔT	is the difference in temperature between the body's surface and the surroundings [K]
T	is the temperature [°C]
T_0	is the effective temperature of the condensate thermal network [°C]
T_a	is the temperature of the air in the cavity [°C]
T_C	is the air temperature in Celsius [C]
$T_{a,cav}$	is the temperature of the air in the cavity [K]
$T_{a,cav}\,(l)$	is the temperature of one air cavity as a function of the length variable [K]
T_{ext}	is the temperature of outdoor air [°C]
T_{int}	is the temperature of surroundings facing the roof surface [°C]
T_K	is the air temperature in Kelvin [K]
T^r	is the equivalent temperature of the sky [°C]
V_{cav}	is the volume of air that is exchanged [m^3]
$\dot{V}_{cav}$	is the airflow rate in the cavity [m^3/s]

Roman Lower-case Letter

b_{cav}	is the width of the cavity [m]
Δc_p	is the difference in wind pressure coefficient between windward and leeward sides [-]
c	is the specific heat capacity of the material (including the moisture content) [W/m^2K]
c_a	is the specific heat capacity of air [J/(KgK)]
d_H	is the hydraulic diameter [m]
g	is the gravity constant [m/s^2]
h_{cav}	is the height of the cavity [m]
h_e	is the evaporation enthalpy of water [J/kg]

k_1	is a correction factor for calculating mould growth index [-]
k_2	is a correction factor for calculating mould growth index [-]
n	is the air exchange rate [1/hr]
p_a	is the partial pressure of dry air, which is 100352 at ground level [Pa]
p_v	is the pressure of water vapour [Pa]
p_{vapour}	is the water vapour pressure [Pa]
q	is the heat flow to and from a body [W/m^2]
q_{50}	is the leakage through the roof at 50 Pa pressure difference [l/(sm^2)]
$q_{sw,dir}$	is the heat flow due to global shortwave radiation [W/m^2]
q_{inf}	is the leakage through the roof [l/(sm^2)]
t	is the time [s]
t_m	is the response time, in favourable conditions before the growth begins [week]
t_v	is the response time, in favourable conditions before the mould growth becomes visible [week]
u	is the wind scalar of the wind horizontal direction West-East [m/s]
u_{cav}	is the airspeed in the cavity [m/s]
$u_{90,m}$	is the mean velocity of the airflow at the 90° bend [m/s]
$u_{cav,m}$	is the mean velocity of the airflow in the cavity [m/s]
$u_{inlet,m}$	is the mean velocity of the airflow right after the inlet [m/s]
$u_{outlet,m}$	is the mean velocity of the airflow right before the outlet [m/s]
$u_{w,10}$	is the wind speed at the measurement station height of 10 m [m/s]
v	is the wind scalar of the wind vertical direction West-East [m/s]
v_a	is the moisture content of air [kg/m^3)]
$v_{a,int}$	is the moisture content in the indoor air [kg/m^3)]
v_m	is the vapour content of the air in the material [kg/m^3]
$v_{kin,a}$	is the kinematic viscosity of air [m^2/s]
v_s	is the saturated vapour content of the air in the material [kg/m^3]
$v_{a,ext,sat}$	is the moisture content at 100 % relative humidity in the outdoor air [kg/m^3]
w	is the moisture content of the material [kg/m^3]
w_{80}	is the practical water content, at 80 % relative humidity [kg/m^3]
w_{free}	is the free water content [kg/m^3]
w_{max}	is the maximum water content [kg/m^3]
$\frac{\partial w}{\partial \varphi}$	is the moisture capacity [kg/m^3 %]
x	is the position in the material [m]

Greek Letter

α	is the absorbed part of the incoming radiation [-]
α_0	is the effective heat transfer coefficient of the condensate thermal network [W/m^{2}K]
α_0	is the effective heat transfer coefficient of the condensate thermal network [W/m^{2}K]
α_c	is the convective surface heat transfer coefficient in the cavity [W/m^{2}K]
α_c	is the convective heat transfer coefficient [W/m^{2}K]
$\alpha_{c.e}$	is the convective surface heat transfer coefficient of the external roof surface [W/m^{2}K]
α_{direct}	is the part of the global shortwave radiation that is absorbed by the surface [-]
α_r	is the radiant surface heat transfer coefficient in the cavity [W/m^{2}K]
α_r	is the radiant heat transfer coefficient [W/m^{2}K]
$\alpha_{r.e}$	is the radiant surface heat transfer coefficient of the external roof surface [W/m^{2}K]
α_t	is the total heat transfer coefficient [W/m^{2}K]
β_{exp}	is the coefficient of thermal expansion [1/K]
$\beta = 0.7$	is an exponent dependent on the flow resistance. The normal value used in engineering calculations is 0.7 [-]
δ_v	is the vapour permeability [m^2/s]
ε	Is the convergence criterium [-]
η	is the coefficient for fitting a curve, determined by Lunelove through measurements of shortwave radiation for the period 1927-1933 [-]
θ	is the error of relative humidity φ in WUFI [-]
θ_r	is the inclination of the roof [°]
$\theta_{sol,h}$	is the solar height [°]
$\theta_{sw,dir}$	is the angle between the normal of the building surface and the solar beams [°]
θ_{wind}	is the wind direction clockwise, with north = 0 and 360 [°]
κ	is the relative roughness of the cavity's surfaces [m]
λ_{90}	is the frictional factor before the 90° bend, treated in section 4.1.3 [-]
λ_{cav}	is the frictional factor of the cavity [-]
λ_m	is the heat conductivity of the material, dependent on the moisture content [W/mK]

ξ	is a loss coefficient, depending on the inlet, outlet or 90° bend [-]
$\xi_{sur90} = 0.8$	is a geometrical factor of the design of the cross-section before and after the 90° bend. Månhardt and Odén (2020) used this value for the reference case based on figure 2.3.2.4.1 in *Air Flows in Building Components* (Kronvall, 1980) [-]
ρ	is the reflected part of the incoming radiation [-]
ρ_m	is the density of the material (including moisture content) [kg/m^3]
$\rho_{a,cav}$	is the density of the air in the cavity [kg/m^3]
$\rho_{a,hum}$	is the density of humid air [kg/m^3]
$\rho_{a,int}$	is the density of indoor air, equation [kg/m^3]
$\rho_{a,ext}$	is the density of outdoor air [kg/m^3]
τ	is the transmitted part of the incoming radiation [-]
φ	is the relative humidity [%]
φ	is the relative humidity of the air in the material [%]
ψ	is the error of temperature T in WUFI [-]

List of Figures

Below is a list of figures that have been used throughout this thesis listed in chronological order:

Chapter 6 Result

List of Tables

Below is a list of tables that have been used throughout this thesis listed in chronological order:

1
Introduction

For a long time, humans have constructed buildings for shelter. One of the most crucial parts of a building is the roof. Roofs are important for protection against the climate:

- Precipitation: Rain and snow
- Wind
- Radiation, both shortwave (solar) and longwave
- Temperature loads

In Nordic countries, a harsh outdoor climate, high demands on indoor climate as well as a will of minimizing the energy losses require a well-constructed roof that performs well throughout all its lifespan.

Traditionally, roofs with a cold attic have been the most common roof construction in Sweden. Due to a will to maximize the heated volume of the building, and since mould growth is common in attic constructions, foremost in southern Sweden, ventilated parallel roofs have become another common construction. Moisture damage due to mould growth may result in poor indoor air quality, odours, discolouration, and in severe cases, even rot, which will affect the structural strength of the materials.

Climate change will result in new climate loads on buildings. In a Nordic climate, common wall constructions, as well as attic constructions, have been studied. In the attics, the new climate will increase the risk of mould growth. In this study, the risk of mould growth in ventilated parallel roof constructions in a future climate is studied.

1.1 Background

Ventilated parallel roofs have become popular as they make it possible to have a larger heated indoor area and volume. The simple difference between attics and ventilated parallel roofs is that on the latter, the insulation is put directly underneath the exterior roof, instead of creating an open space above the insulation. An advantage of attics when it comes to moisture safety is that they are easy to inspect. This has provided the knowledge that moisture problems are common in attics, which have been known for years (Hägerhed Engman & Samuelsson, 2006).

Before the contemporary strive to increase energy efficiency, the insulation was relatively thin. This meant that higher heat flux from the interior would heat the exterior roof resulting in a lower relative humidity in the air cavity, and therefore a higher moisture safety. With today's well-insulated parallel roofs a lower heat flux reduces the heating of the exterior roof. This is good in a sense of energy efficiency but will theoretically result in lowered moisture safety since the exterior part of the roof becomes colder. This is especially dangerous in ventilated parallel roofs which are not possible to inspect.

Another aspect of parallel ventilated roofs that differs from attics is that the air exchange rate is much higher because an inlet of a similar size is supposed to change a much smaller volume. In the standard procedure in Sweden today, a constant number, which is relatively low is assumed for the calculations. Svantesson and Säwén (2019) have recently done a study on how the buoyancy effect affects the wind speed in a ventilated parallel roof, and Månhardt and Odén (2020) further developed the model and implemented it on an existing building. These driving forces of exchanging the air highly affect the moisture safety of the roof construction.

Moisture safety is an umbrella term for all moisture-related consequences (Bjurström, 2007). Different materials react differently: metals corrode; concrete, natural stone and brick can be broken by frostbite; organic materials mould, and wood can even rot. Many materials also submit unhealthy emissions and odours. Housepaint and paper flake off. In roof constructions in Sweden today, wood is a commonly used material. With its exposed location in the construction, it is the most vulnerable part when it comes to moisture safety. In this study, the mould growth index model (Hukka & Vittanen, 1999) is used to describe the degree of mould that evolves at the exposed wood in the construction.

Today, many buildings with ventilated parallel roofs are built in Sweden. No one knows for sure how they will react to future climate change.

The Rossby Centre of The Swedish Meteorology and Hydrological Institute (SMHI) has simulated climate data for the period from 1961 to 2100. In the data sets, there is a forecast of the future climate.

In this study, a model is developed for evaluating the moisture safety with the mould growth index in a parallel ventilated roof construction subjected to data sets of the future climate.

1.2 Aim and Research Question

The aim of the study is firstly to evaluate how climate change will affect the risk of moisture-related damage in a common parallel ventilated roof construction with natural convection as a driving force. Secondly, the aim is to find the parameters that most affect moisture safety in a parallel ventilated roof design in a future climate. The goal is to find the corresponding mould growth index for each setup of data in the set of future climate data.

The aim of the study will be found by answering the main research question:

> *How will parallel ventilated roofs withstand the future climate in consideration of mould growth?*

This question is answered by the following sub-research questions:

> *How can a model of parallel roof be formulated to evaluate the mould growth index from climate data?*
>
> *How can climate data be used in building modelling for getting reliable results?*
>
> *How do design parameters, such as orientation, inclination, colour, and additional insulation affect the results?*

1.3 Scope

The main factor for delimiting the study is the number of hours of the master thesis project. The study is delimited to well-insulated parallel due-pitched roofs (saddle roofs) with an inlet and outlet at the eaves (closed ridge) and ventilated by natural driving forces (wind and thermal buoyance). Materials prone to moisture damage (in this case wooden board) are exposed directly to the air in the cavity. The design of the air cavity is delimited to one single case: a building of 10 meters in width, a cavity height of 45 mm, and a width of 555 mm. The length of the air cavity is depending on the building width and the inclination. The height of the roof is assumed to be at 10 meters height and therefor standard weather station data can be used without any further calculations. Otherwise, windspeed is non-linearly increasing with increasing height. Built-in moisture is not considered in the study, and precipitation and driving rain are not investigated as main loads.

The study is delimited to moisture assessment in WUFI 2D using an model for predicting the airflow in the cavity and thereby the air exchange rate per hour, the moisture gain from infiltration from a simplified air leakage model based on the interior climate of the European Standard 13877, and a small spread leakage of rain through the construction.

The setup of the model is delimited to be validated with one other study Månhardt and Odén (2020) where the same model setup was used and validated.

The moisture safety evaluation is delimited to the mould growth index developed by Vittanen (Hukka & Vittanen, 1999).

The study is delimited to climate data from the Rossby Centre Regional Atmospheric Climate Model 3 (RCA3) with climate data from the year 1961 to 2100. The initial condition of the model is delimited to condition 1. The spatial resolution is delimited to 50 km. The global climate model is delimited to ECHAM5. The climate model parameters are explained in section 2.1.

To find the magnitude and importance of different parameters a parametric study is done. The parametric study is delimited to:

- Changing climates (four different locations in Sweden)
- The future climate data emission scenarios A1B, A2 and B2.
- Orientation of the roof: south, east, north and west
- The inclination of 30° and 45°
- The uttermost material of the roof is dark-coloured or light-coloured metal sheets.
- The amount of insulation between the cavity and the exterior climate is varied between none and a 100 mm layer.

1.4 Methodology

In the first part of this project, a literature study was conducted to achieve an overview of previous research concerning parallel ventilated roof constructions and climate modelling. The literature study on climate modelling was delimited to understand the concept of climate modelling and the specific geographical region of interest. Since this project intended to use models developed by Svantesson and Säwén (2019) and Månhardt and Odén (2020), and data processed by Nik (2010), their work was studied carefully.

The second part of the project was to process three sets of data for the numerical simulations: climate data, airflow data and moisture infiltration data. This included large data handling programming of the future climate data, implementing and adjusting the airflow model created by Svantesson and Säwén (2019) and developed by Månhardt and Odén (2020), and creating a moisture infiltration model.

The third part of the project was to create a hygrothermal model in WUFI 2D, based on a model in WUFI Pro, and validate it in comparison with the results of Månhardt and Odén (2020).

The fourth, and last part of the project was to implement future climate data in the model and evaluate the achieved results.

The procedure is detailed and described in chapter 5, Methods.

1.5 Previous Research

A climate data set for weather data of the period 1961 to 2100 has been simulated by Kjellström et al. (2005). The regional climate model RCA3 of northern Europe are using boundary conditions from ECMWF Reanalysis experiment ERA40 which at the time was the most comprehensive set of climate data for simulations in Europe.

Nik (2010) has processed the data set for use in building physic modelling, using the data for heat, air, and moisture simulation of an attic model of a 2-storey building. He was comparing different global climate models (GCMs), regional climate models (RCMs), their parameters and emission scenarios. The difference between GCMs is up to 3°C for a period of 30 years (Kjellström et al., 2005). On relative humidity, all models show a more consistent increase with an increment during spring and autumn. Different emission scenarios have variabilities in multiple variables which may affect a building differently. The future climate is likely to be more favourable for moisture growth in attic construction (Nik et al., 2012).

Nik et al. (2012) have used the data processed by Nik to investigate cold attic construction in four different locations in Sweden: Lund, Gothenburg, Stockholm and Östersund. The greatest risk of mould growth was in the northern roof in Gothenburg, but in Lund, results were almost as high. In colder locations, the risk of mould growth was significantly lower. Different emission scenarios did not affect the risk of mould growth in the attics.

In his doctoral thesis (Gullbrekken, 2018) concludes that leakage from rain and moisture infiltration from indoors to outdoor are the main contributing factors to moisture damage in ventilated parallel roofs. Gullbrekken also studied how wind pressure coefficients depend on the wind direction in relation to the roof, on roofs with natural ventilation from eave to eave. He also shows a correlation between wind speed and air exchange rate in the cavity.

Mundt-Petersen and Harderup (2010) conclude that the air exchange rate is of great importance for wooden stud walls with a cavity to get reliable results. They also concluded that a wind dependent calculation with a low air exchange rate gives less reliability than a higher constant air exchange rate (Mundt-Petersen & Harderup, 2011). By evaluating different measurement positions in a ventilated parallel roof Mundt-Petersen (2015) concludes that simulation tools for moisture safety are reliable if the initial and boundary conditions are accurate. He also concludes that the north-facing roof is the dimensioning orientation in ventilated parallel roofs. Mundt-Petersen (2016) concludes that in well-insulated ventilated parallel roofs the greatest risk of moisture damage exists close to the exterior, on the wooden board on the exterior side of the cavity. The air exchange rate should be as low as possible, but still enough to be able to ventilate excessive moisture away.

A model for thermal buoyancy as a driving force for the ventilation in the cavity of a parallel roof has been developed by (Svantesson & Säwén, 2019) based on experimental data and simulated analysis with good correlations.

Månhardt and Odén (2020) developed a model based on the model of thermal buoyancy (Svantesson & Säwén, 2019) combined with wind pressure coefficients (Gullbrekken, 2018) and moisture infiltration from indoors. They made blind calculations which they validate with measurements from an existing building. It was concluded that the model was able to describe the climate in the cavity more accurate than the recommended methods in Swedish literature, with a constant low air exchange rate and that the most important design parameters were to include the cavity as well as the tightness to infiltration of vapour through the roof. Different geometries only make a small difference to the result.

1.6 Thesis Outline

The report is structured into three chapters describing theories and knowledge about the subject, followed by four chapters describing the method, result, discussion and conclusion.

In chapter 2, Weather Data, the principles of climate modelling are described. The character and the processing of the climate data are presented. The result of this chapter is used for weather input in the airflow model, the infiltration model and the hygrothermal numerical model.

In chapter 3, Ventilated Parallel Roof, the roof construction of the study is presented along with theory, design, and historical usage. In the chapter, the study subject, as well as the validation subject, is presented.

In chapter 4, Physical Models, the physics behind the models used in the study is presented. The models are the airflow model, the moisture infiltration model, and the mould growth model. A short physical description of the coupled heat and moisture transport used by the hygrothermal numerical software is also presented.

In chapter 5, Methods, a detailed procedure of the study is presented supported by the theory and knowledge from chapters 2-4.

In the remaining chapters, 6-8, Result, Discussion and Conclusion, the result is presented, discussed, and a conclusion is submitted.

2
Weather Data

The weather data used in this study is based on data from the Rossby Climate Research Centre of the Swedish Meteorology and Hydrological Institute (SMHI). The data has been processed by Nik in his licentiate thesis (2010). In this chapter knowledge needed for understanding the weather data is presented.

2.1 Climate Modelling

Models of varying complexity are used for describing the climate. In this study, two different types of climate models are distinguished: GCMs (global climate models) and RCM (regional climate models). A GCM is a mathematical model describing the general circulation of either the atmosphere, ocean or land, based on the thermodynamics of a rotating sphere with various energy sources as forcing. In a GCM individual components represent large parts of the climate. The model describes interactions between the atmosphere and ocean, but also with the land surface, snow, ice and the biosphere. The spatial resolution of GCMs are rather coarse (100-300 km). By downsizing a model, using the general circulation data from the GCM as a boundary conditions, adding more specific parameters like local topography and land properties, a RCM, with a higher spatial resolution (25-50 km) than a GCM, can be created. In the models, different parts of the environment are coupled in a network (Nik, 2010).

The GCMs and RCMs are describing how the climate is reacting to different external forcing, for example, changing levels of greenhouse gases, solar intensity, and other aspects. The solution to the GCM is used as a boundary condition in the RCM. The initial conditions for weather models are normally set to the weather data (greenhouse gas, concentrations, aerosol content, etc) of the year 1860, which is before any large climate changes due to human society began, but also when a more systematic collection of weather data started. The problem is both that not enough weather data is known from that time, and that the time period from 1860 until today is to short too make an accurate calculation on weather cycles. A solution to this is to set up arbitrary pre-industrial initial values 1000 years before the initial conditions of the year 1860. The control run is satisfactory if it in short time varies, but in long time is fairly constant, meaning no drifting of the climate is allowed. In this study, the weather data used is from an RCM called RCA3 (Rossby Centre Regional Atmospheric Climate Model 3), which is developed by the Rossby Centre of SMHI, because that is a model created for the region in interest. RCA3 boundary and initial conditions are based on a GCM called ECHAM5 which has been developed at the Max-Planck Institute (Nik, 2010).

In climate modelling, there are uncertainties about the resulting climate change. The first aspect is that the external forcing emission scenario (greenhouse gas, aerosol, etc.) is unknown. Another influencing factor is the general circulation pattern of the GCM. A way of decreasing the uncertainties is to compare different GCMs, RCMs and forcing emission scenarios. The model is assumed somewhat robust if the variations between the models and simulations are small (Persson et al., 2007). The emissions scenarios relevant for this study are presented in section 2.2.

In his licentiate thesis Nik (2010) researched which parameters affect RCA3 when applying it for moisture safety design in an attic. Different spatial resolution, boundary conditions and initial conditions did only marginally influence. The forcing emission scenarios, on the other hand, had a significant impact on the result.

2.2 Future Emissions Scenarios

Emission scenarios are assumptions about the level of emissions and greenhouse gases that will enter the climate system. Different emission scenarios are based on assumptions of different socioeconomic scenarios (future development of population, GDP, energy use, etc). These scenarios are called SRES scenarios because they were presented in IPCC's Special Report on Emissions Scenarios (Nakicenovic et al., 2000). The process of climate modelling was at the time of the creation of RCA3 a linear process (figure 2.1) where a specific socioeconomic scenario resulted in a specific emission scenario which resulted in a specific radiative forcing scenario that is affecting the climate.

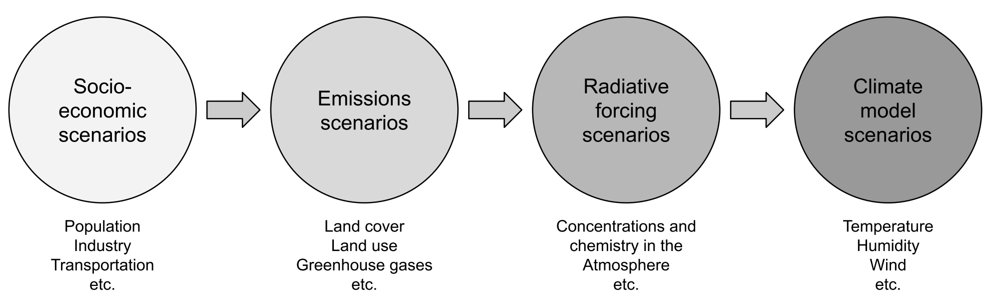

Figure 2. 1. *The Development of Climate Model Scenarios*

Note: Different socio-economic scenarios (population growth, development of the transport system, etc.) of the world’s societies are leading to different emission scenarios (the use of land, amount of greenhouse gases, etc.), which are described by a more physical radiative forcing scenario (atmospheric concentrations and chemistry, etc.) which is formulating different climate model scenarios (temperatures, humidity, wind, etc.). Figure based on Moss et al, The next generation of scenarios for climate change research and assessment (figure 3, p.752), Nature 747-756.

The radiative forcing scenario is how the atmospheric concentrations, carbon cycle and atmospheric chemistry are together creating a greenhouse effect. The radiative forcing leads to different values in the future climate: air temperature, precipitation, humidity, etc (Moss et al., 2010).

In IPCC Special Report on Emissions Scenarios, four families of SRES scenarios are presented: A1 (A1B is a variant of A1), A2, B1 and B2 (figure 2.2).

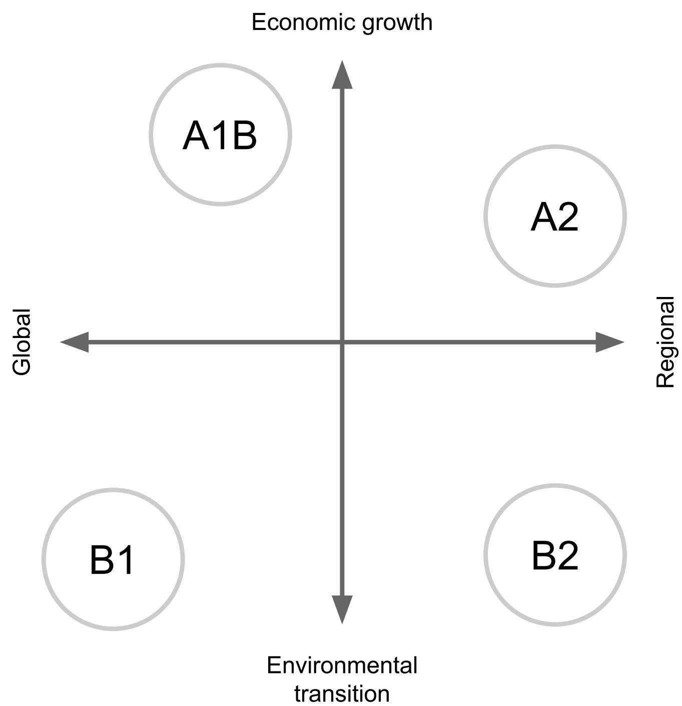

Figure 2. 2. *The Emission Scenarios*

Note: The emission scenarios A1B, A2, B1 and B2 are representing different development according to the amount of economic growth and environmental transition, and if the world is more global or more regional.

A1B is a scenario characterized by rapid economic growth with a lot of new and more efficient technologies, as well as a population growth that will peak in mid-century and thereafter declines. The interaction between regions will increase and the world will become more global. A2 is a scenario less global than A1 with a focus on regional economic growth. The population growth is slower than in A1 but is not declining. New technologies are introduced more slowly than in A1B. B1 is a scenario where the world unites for realizing the transition to a global world with less material intensity and more environmentally friendly and resource-efficient technologies, as well as a rapid change of the economic structure toward a service and information economy. The population is peaking in mid-century and is declining afterwards. B2 is a scenario that is more regionally and local than B1 with a higher focus on local transition in economics, society and sustainability. The population growth is happening at a lower rate than in A2 but is not peaking in mid-century like A1 and B1. The technology growth is slower than in B1. In the A1 family, there are three different versions presented here: A1FI, where FI stands for fossil fuel-intensive; A1B, where B stands for balanced (both fossil fuel and non-fossil fuel); and A1T, where there is mostly non-fossil fuel. The estimated total global annual CO_2 emissions from all sources from 1990 to 2100 are presented in figures 2.3-2.6 (Nakicenovic et al., 2000).

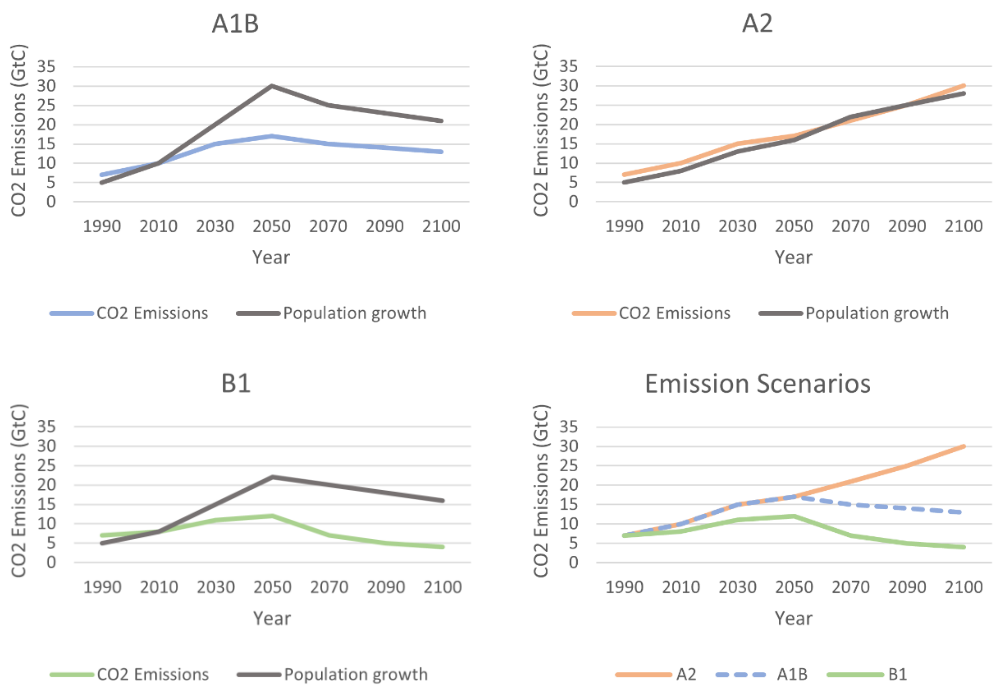

Figure 2. 3, *2. 4, 2. 5 &* 2. 6. *The CO_2 Emissions and Population Growth of Emission Scenario A1B, A2 and B1.*

Note: The parameters: CO_2 emissions in gigatonne of carbon (GtC) and population growth (dimensionless but relative between the plots) for the emission scenarios A1B, A2, B1 and B2. The global and rapid economic growth scenario A1B leads to the rapid growth of population and GtC peaking in mid-century and then declining. The regional and rapid economic growth scenario A2 leads to slightly slower growth of population and a similar rapid GtC, but with no decline at mid-century. The regional B2 scenario with a focus on the environmental transition before economic growth will have slower growth in both population and GtC leading to at the end of the century a similar GtC as scenario A1B, but with a smaller amount GtC released on the way.

2.3 Weather Data from Rossby Centre

Weather data for this study is produced by Rossby Centre (section 2.3.1) and processed by Nik (2010) for building physics modelling (section 2.3.2).

2.3.1 Data from Rossby Centre

In the available data from Rossby Centre, the following data is used in the study:

- Global data from ECHAM5
- Regional data from RCA3
- Three different emissions scenarios: A2, B2, A1B
- Initial condition 1 for all the scenarios. Which is a set-up for how the initial conditions were produced using simulation for 1000 years before pre-industrial time (Nik, 2010).
- For each scenario, there is data for four Swedish cities: Lund, Gothenburg, Stockholm and Östersund.
- For each city, there exists data for 140 years spanning from 1961 to 2100.
- Each data set consists of 14 climate parameters, presented in table 2.1.

Lund is in the most southern part of Sweden, Gothenburg and Stockholm are also in southern Sweden, and Östersund is in middle Sweden. Lund and Gothenburg are close to the western sea, and Stockholm is close to the eastern sea. Östersund has an inland climate.

Table 2. 1. *Data of the Rossby Centre Data Set.*

Name	**Description**	**Unit**	**Resolution**
Longwave Radiation	Downward longwave radiation at the surface	[W/m^2]	30 minutes
Global Shortwave Radiation	Corresponding shortwave radiation: diffuse radiation + direct radiation	[W/m^2]	30 minutes
Air Temperature	Air temperature at a 2 m level	[K]	3 hours
Specific Humidity	Specific humidity at 2 m level	[kg water/kg air]	3 hours
Wind Speed: West-East	West-East component of wind speed at a 10-meter level	[m/s]	3 hours
Wind Speed: South-North	South-North component of wind speed, at a 10-meter level	[m/s]	3 hours
Total Precipitation	Snow and rain precipitation together	[mm/s]	30 minutes
Snow Precipitation	The amount of snow precipitation	[mm/s]	30 minutes
Rain Precipitation	The amount of rain precipitation	[mm/s]	6 hours

Total Air Pressure	The air pressure	[N/m^2]	30 minutes
Total Cloud Coverage	Total Cloud Coverage	[0-1]	3 hours
Cloudiness of Low-Level Clouds	Cloudiness of Low-Level Clouds	[0-1]	3 hours
Cloudiness of Mid-Level Clouds	Cloudiness of Mid-Level Clouds	[0-1]	3 hours
Cloudiness of High-Level Clouds	Cloudiness of High-Level Clouds	[0-1]	3 hours

Note: The parameters of Rossby Centre Weather Data and their units and time resolution.

The precipitation data is available in a different data set and is only available for scenario A1B.

2.3.2 Data for Building Physic Modelling

The weather data produced by RCA3 is not ready for usage in building physic modelling. This chapter is briefly explained how Nik (2010) processed the data for fitting building physic modelling. The data needed for the building physic modelling in this study are the following:

- Air temperature [°C]
- Relative humidity [%]
- Global horizontal shortwave radiation [W/m^2]
- Diffusive horizontal shortwave radiation [W/m^2]
- Direct horizontal shortwave radiation [W/m^2]
- Longwave sky radiation [W/m^2]
- Wind direction [°]
- Wind speed [m/s]
- Precipitation [mm/hr]

The air temperature data is to be converted from Kelvin to Celsius, and the longwave radiation is already present in the data from the climate model. The precipitation data is to be converted from periods of 30 minutes and 6 hours to periods of 1 hour, and from the unit mm/s to mm/hr. In his licentiate, Nik (2010) processed (figure 2.7) relative humidity is calculated from the air temperature, specific humidity and the total air pressure; global shortwave radiation and cloud coverage are used for calculating the direct shortwave radiation; and, global shortwave radiation and direct radiation are used for calculating the diffuse shortwave radiation. Wind speed of East-West and South-North is used for calculating the wind direction and the wind speed.

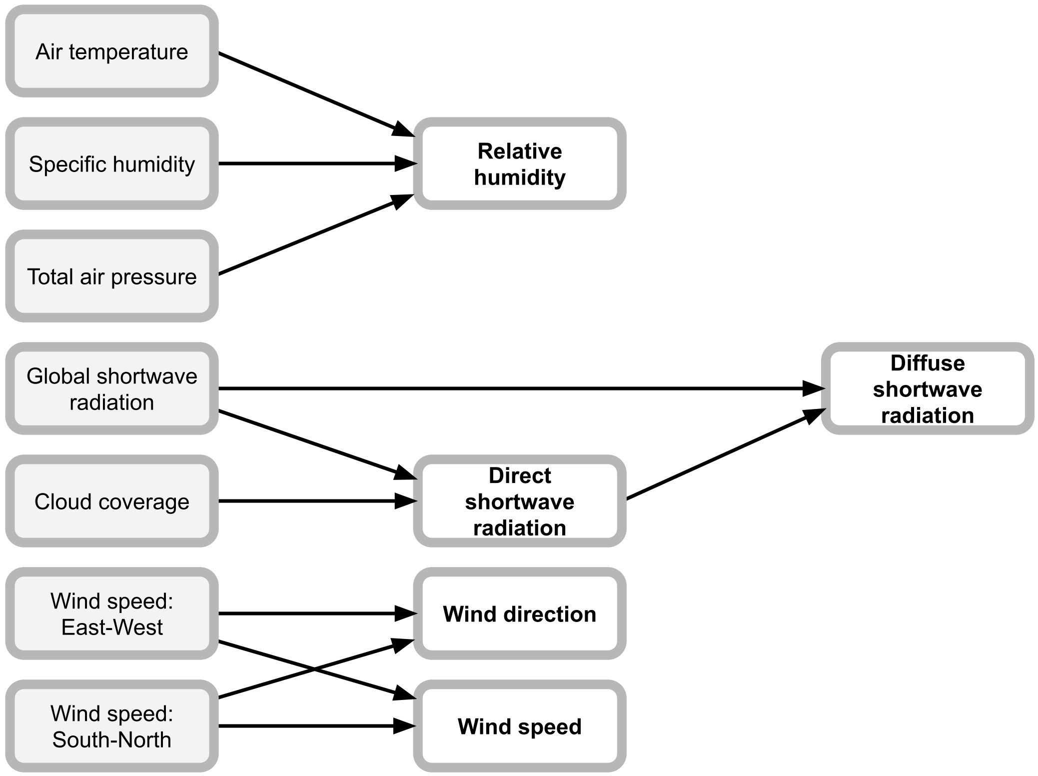

Figure 2. 7. *The Procedure of Processing the Climate Data for Building Applications.*

Note: The procedure Nik *(2010)* used processing the Rossby Centre weather data to fit building physical modelling.

All data is also to be converted into a consistent and relevant time resolution. In building physic modelling, a time resolution of 1 hour is convenient, and all data are therefore converted into a resolution of 1 hour per step. In a data set of 140 years, that equivalents 1227240 hours, including the lap years.

2.3.2.1 Radiation Data

All bodies emit electromagnetic radiation at temperatures above absolute zero K. Radiation has a different wavelength depending on the temperature of the body. In building physics thermal radiation is of interest. Thermal radiation is a way of transferring heat between surfaces without physical contact. It has a spectrum from 0.1 to 100 µm, which corresponds to emissions from a body at temperatures between -100 °C to 10000°C. This includes parts of ultraviolet radiation, visible light and infrared radiation. Radiation from the sun and light sources are emitted at shorter wavelengths, with the highest intensity of wavelength of visible light. Radiation with larger waves is in building physics called longwave radiation or infrared radiation (Hagentoft, 2001).

Radiation that strikes a body will be absorbed by, reflected from, and transmitted through the body according to equation 2.1 (Hagentoft, 2001):

$$\rho + \alpha + \tau = 1 \qquad (2.1)$$

Where:

ρ	is the reflected part of the incoming radiation [-]
α	is the absorbed part of the incoming radiation [-]
τ	is the transmitted part of the incoming radiation [-]

2.3.2.2 Global Shortwave Radiation

When shortwave radiation reaches the atmosphere, some parts of it are scattered, this radiation is called *diffuse shortwave radiation* $I_{sw,diff}$. The part, which is not scattered, is called *direct shortwave radiation* $I_{sw,dir}$. Together they make up the *global shortwave radiation* I_{sw} on a horizontal surface, equation 2.2. The unit of shortwave radiation is W/m^2 (Nik, 2010).

$$I_{sw} = I_{sw,diff} + I_{sw,dir} \qquad (2.2)$$

The global shortwave radiation is provided in the data set from Rossby Centre.

2.3.2.3 Direct Shortwave Radiation

The direct shortwave radiation is not available in the data set from Rossby Centre. Nik (2010) has calculated the direct shortwave radiation with the ENLOSS model (Taesler & Andersson, 1984), and in some parts with the SOLTIMSYN model (IEA, 1996).

The calculations are out of the scope of this study and will only be explained briefly (Nik, 2010). The complete procedure is the following:

1. Data is achieved from Rossby Centre:
2. Finding solar height by a numerical Heat, Air and Moisture Tool.
3. Finding the air mass
4. Finding partial vapour pressure at the surface
5. Finding the absorption of radiation by water vapour
6. Using data of turbidity – the cloudiness of a fluid
7. Using data of spectral distribution
8. Calculating the intensity of direct shortwave radiation parallel to solar beams
9. Calculating a correction factor, and correcting the direct shortwave radiation
10. Finding the horizontal direct shortwave radiation

The heat flow from direct shortwave radiation is defined as (Hagentoft, 2001):

$$q_{sw,dir} = \alpha_{dir} I_{sw,dir,\theta} \cos(\theta_{sw,dir}) = \alpha_{dir} I_{sw,dir,h} \tag{2.3}$$

Where:

$q_{sw,dir}$	is the heat flow due to global shortwave radiation [W/m^2]
$\alpha_{sw,dir}$	is the part of the shortwave radiation that is absorbed by the surface [-]
$I_{sw,dir,\theta}$	is the shortwave radiation energy flow striking a surface with normal components parallel to the solar beams [W/m^2]
$I_{sw,dir,h}$	is the shortwave radiation striking a surface horizontal at the normal component of a horizontal surface on the ground [W/m^2]
$\theta_{sw,dir}$	is the angle between the normal of the building and the solar beams [°]

The heat flow is used in the airflow model in chapter 4, and the hygrothermal simulations in chapter 5.

2.3.2.4 Diffuse Shortwave Radiation

The diffuse shortwave radiation is not available in the data set from Rossby Centre. Nik (2010) calculates it according to Taesler and Andersson (1984). The direct shortwave radiation and the cloud coverage are needed to calculate the diffuse shortwave radiation. It is calculated for horizontal radiation according to equations 2.11-2.15.

When the sky is clear:

$$I_{sw,diff,hrz} = \eta I_{sw} \tag{2.4}$$

$$\eta = \frac{1}{1 + 8(\sin\theta_{sol,h})^{0.7}} \tag{2.5}$$

$$I_{sw} = I_{sw,diff,h} + I_{sw,dir,h} \tag{2.6}$$

$$I_{sw,dir,h} = I_{sw,dir,\theta} \sin\theta_{sol,h} \tag{2.7}$$

When the sky is cloudy:

$$I_{sw,diff.h} = I_{sw} - I_{sw,dir,h} \tag{2.8}$$

Where:

I_{sw}	is the global shortwave radiation [W/m^2]

$I_{sw,diff,h}$	Is the horizontal diffuse shortwave radiation [W/m^2]
$I_{sw,dir,h}$	is the horizontal direct shortwave radiation [W/m^2]
$I_{sw,dir,\theta}$	is the direct shortwave radiation parallel to the solar beams [W/m^2]
η	is the coefficient for fitting a curve, determined by Lunelove through measurements of shortwave radiation for the period 1927-1933 [-]
$\theta_{sol,h}$	is the solar height [°]

2.3.2.5 Longwave Radiation

The longwave radiation from the sky is provided in the data set from Rossby Centre, where the longwave radiation is defined as a normal component to a horizontal surface of the earth (Nik, 2010), in building physics often a roof.

All bodies both absorb and emits longwave radiation. In the case of building physics, the transmittance of longwave radiation can be neglectable (Hagentoft, 2001). A building has longwave radiation exchange with all its surrounding: the sky, other buildings, nature, and the ground. The longwave part of the radiation from the sun is negligible in comparison with the rest of the sky because the solar disk has a much smaller angular extension (Fraunhofer IBP, 2008).

Bodies with temperatures at similar power exchange longwave radiation with each other. The net flow of the radiation energy that is passed back and forth is low compared to other sources of energy sources in building physics, e.g., shortwave radiation. In building physics, the longwave radiation can be approximated by a radiative heat transfer coefficient which is used together with the corresponding convective heat transfer coefficient. Knowing the heat transfer coefficients (equations 2.16), the heat flow to and from a body can be calculated by equation 2.17 (Hagentoft, 2001):

$$\alpha_t = \alpha_r + \alpha_c \tag{2.9}$$

$$q = \alpha_t \Delta T \tag{2.10}$$

Where:

α_t	is the total heat transfer coefficient [W/m^{2}K]
α_r	is the radiant heat transfer coefficient [W/m^{2}K]
α_c	is the convective heat transfer coefficient [W/m^{2}K]
q	is the heat flow to and from a body [W/m^2]
ΔT	is the difference in temperature between the body's surface and the surroundings [K]

Even due to the longwave radiative heat flows often are being small some cases are needed to be taken into consideration. A balance of radiation to and from a building body is shown in figure 2.8 (Fraunhofer IBP, 2008). From the sky direct shortwave radiation $I_{sw,dir}$, diffuse shortwave radiation $I_{sw,diff}$ and atmospheric counter-radiation $I_{lw,sky}$ are reaching the body. The atmospheric counter-radiation is the radiation emitted by the sky, including the atmosphere and clouds. The atmospheric counter-radiation also strikes the terrestrials, ground and surroundings, and some of it is reflected toward the building body, this is called reflected atmospheric counter-radiation $I_{lw,refl.sky}$. Some of the shortwave radiation that strikes the terrestrial is also reflected toward the building body, which is called reflected shortwave radiation $I_{sw,refl.}$. All terrestrials are emitting longwave radiation which can strike the building body, terrestrial counter-radiation $I_{lw,terr}$. Finally, the building body is also emitting longwave emissions $I_{e,body}$ in all direction, towards the terrestrials, the sky and the sun (Fraunhofer IBP, 2008).

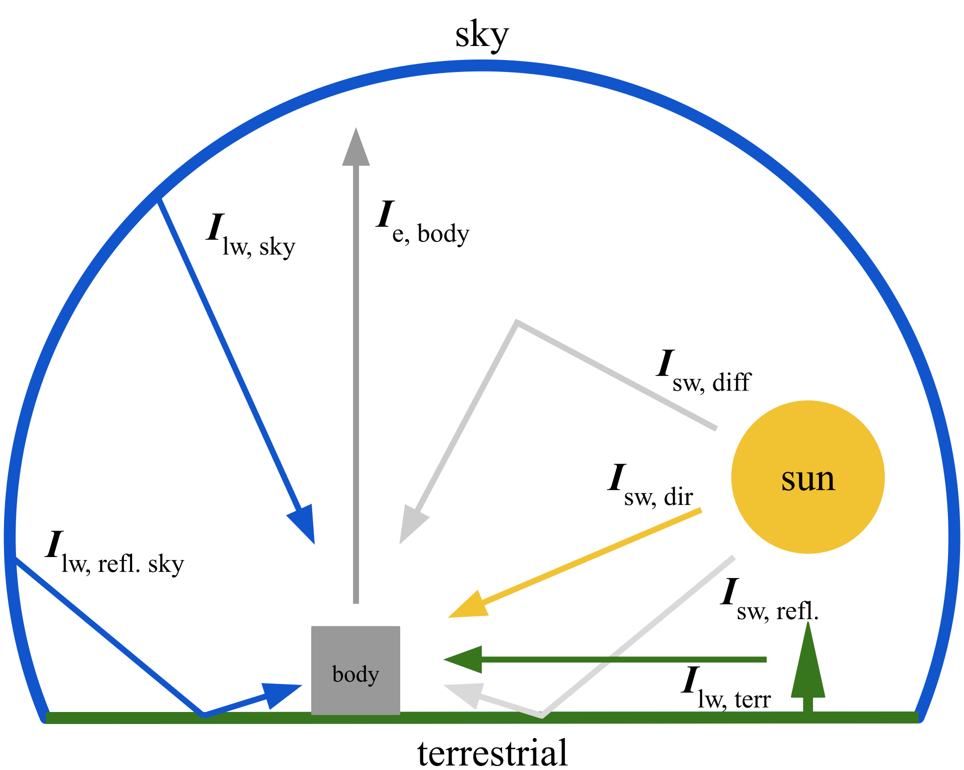

Figure 2. 8. *The Radiation Balance of a Body on Earth.*

Note: A visualisation of the different parts of shortwave radiation I_{sw} and longwave radiation I_{lw} reaching a building body as well as the part emitted from the building body.

The main loss due to longwave radiation is between the building body and the sky. This is because the molecule structure of the atmosphere makes it a poor thermal emitter. During the day, the loss is not noticeable because the incoming shortwave radiation is much larger. By night, when there is no shortwave radiation, surfaces viewing the sky can become severely cooled down. The inclination of the surface affects how much the surface views the sky, which also affects the amount of longwave radiative loss. A horizontal surface has the greatest loss, and a vertical surface has the least (Fraunhofer IBP, 2008).

A clear sky emits differently depending on the temperature and the content of humidity. Cold and dry air emits less than warm and humid air. The cloudier a sky is, the more it emits, resulting in less loss from the building body due to longwave radiation (Fraunhofer IBP, 2008).

2.3.2.6 Wind Speed and Wind Direction

The wind data from Rossby Centre were two vectors, which are seen in figure 2.9 (Nik, 2010):

- The horizontal component of the wind vector in the West-East direction
- The vertical component of the wind vector in the South-North direction

The wind vectors are converted into a wind speed and a wind direction.

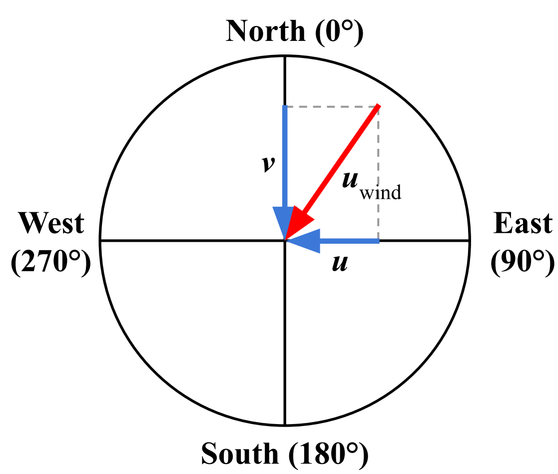

Figure 2. 9. *The Wind Vector in Relation to Wind Direction and Wind Speed.*

Note: In the Rossby Centre weather data wind is expressed in a south-north component v, and a west-east component u. A scalar u_{wind} is to be used to describe the wind speed depending on the angle θ, where north is defined as 0°, east 90°, south 180° and west 270°.

The wind direction is achieved by equation 2.18:

$$\theta_{wind} = arctan\left(\frac{u}{v}\right)\frac{180}{\pi} + 180 \tag{2.11}$$

Where:

θ_{wind}	is the wind direction clockwise, with north = 0 and 360 [°]
u	is the wind scalar of the wind horizontal direction West-East [m/s]

v is the wind scalar of the wind vertical direction West-East [m/s]

The wind speed u_{wind} is achieved by equation 2.19:

$$u_{wind} = \sqrt{u^2 + v^2} \tag{2.12}$$

2.3.3 Deviation on the RCA3

In chapter 2.1 it was presented that a way of dealing with the uncertainties of climate modelling is to compare simulation between GCMs, RCMs and forcing emissions scenarios. It was also noted that in this study, only the GCM ECHAM5 is used, and only one RCM RCA3 is used. The ECHAM5 is considered to be an accurate model for describing the circulations patterns in Europe (Nik, 2010). RCA3 is an improvement of previous models, like RCA2, and is considering giving accurate solutions for Europe (Kjellström et al., 2005).

ECMWF (European Centre for Medium-range Weather Forecasts) has done a Reanalysis experiment called ERA40. This experiment is according to Kjellström et al (2005) probably the most comprehensive model for describing the state and behaviour of the atmosphere of the region. By comparing the simulation of RCA3 for the period between 1961 and 2002 with the data set of ERA40 and with measured meteorological data, the credibility of RCA3 has been tested. In most areas the model produces accurate data, for example, the sea level pressure in Sweden correlates with 0.9 to ERA40. The largest deviation for Northern Europe is when it comes to air temperatures in winter and precipitation in summer. The mean deviation of air temperature for RCA3 for Europe is ±1°C, but in Northern Sweden, the deviation is positive between 3-4°C. A reason for this could be that all weather stations are placed in valleys, which tend to have lower air temperatures, due to micro-climate, than the surroundings, but also because too much longwave radiation reaches the surface. Comparing RCA3 with measured meteorologic data shows that the precipitation tends to be overestimated during summer (Kjellström et al., 2005).

2.4 Weather Data from Fuktcentrum

Another set of data that is used in the validation process of this study is four data sets from Fuktcentrum (2018). The data is based on measurements made by SMHI for 9 years, between 1990 and 1998, in the cities: of Lund, Stockholm, Borlänge and Luleå. The following parameters are available in the data sets:

- Air temperature [°C]
- Relative humidity [0-1]
- Global shortwave radiation on the horizontal surface [W/m^2]
- Diffuse shortwave radiation on the horizontal surface [W/m^2]
- Longwave radiation on the horizontal surface [W/m^2]
- Precipitation [mm/h]
- Wind direction [°]
- Wind speed [m/s]

To create the data sets Fuktcentrum (2018) had to process the raw data to make it coherent. The aim was to make the data realistic, but also with a high moisture load. The steps for doing this were:

1. Removing strange values in the data sets
2. Adding data for missing days, from the days close by
3. Adding data for missing hours by interpolating between hours before and after
4. Calculate the missing longwave radiation according to Wallentén (2010)
5. Distribute precipitation data from 12 or 24 hours to 1 hour according to Wallentén (2010)
6. Adjusting the data make at least one value on relative humidity reaching 100% every 3 months.

3
Ventilated Parallel Roof

The roof is the uppermost element of a building. Due to its high placement, and its large area facing the sky, it is more exposed to rain, snow, and ice than exterior walls (Arvidsson et al., 2017).

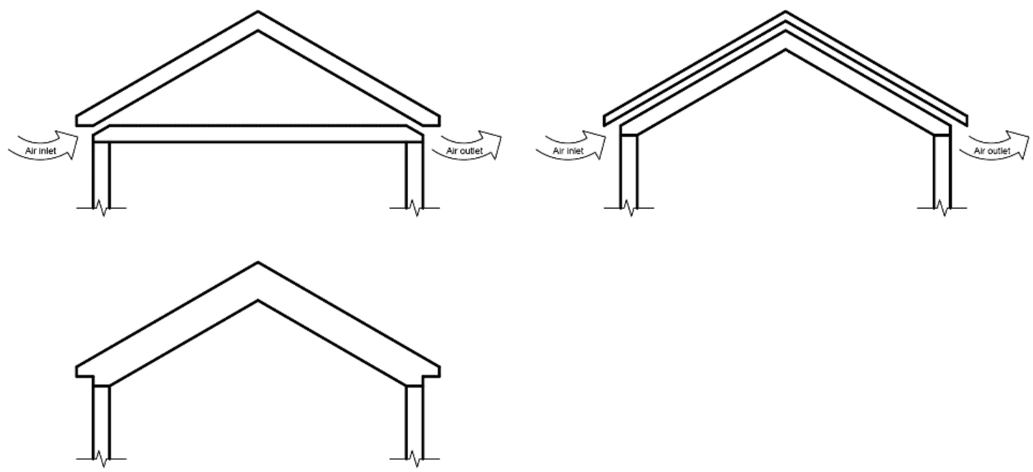

Figure 3. 1. *Common Roof Constructions.*

Note: From left to right, and from top to bottom: The attic is normally ventilated at the eaves; The parallel roof is ventilated at the eaves; The massive roof is not ventilated.

Traditionally in Nordic countries, there are two types of roof constructions, warm roofs, and cold roofs. In principle, through a warm roof heat losses and gains are only transported through the conductivity of the materials. The heat flow is perpendicular to the roof surface. Before the amount of insulation was as great as today, the heat flow through the roof made even the exterior roof surface heated in the winter which melted snow and ice, and from there the name *warm roof* originates (Arvidsson et al., 2017).

A *cold roof*, on the other hand, is a roof where the heat losses and gains are transported away by ventilation in the roof construction. A common construction is an attic, where the main part of the heat losses is due to the ventilation of the attic. In winter, the interior roof surface is warm and the exterior roof surface is cold (Arvidsson et al., 2017).

In the past decades, the increased amount of insulation has decreased the heat losses through warm roofs, resulting in that their exterior surface is not notable warmer than the outdoor air, leading to no melted snow on the modern warm roofs (Arvidsson et al., 2017).

Today, it is more relevant to distinguish between ventilated and non-ventilated roofs, figure 3.1. A ventilated roof consists of three parts, the exterior part, the cavity or attic, and the interior part. The function of the exterior part is to protect from wind rain and meltwater and, this is done through a windboard and a waterproof layer. The purpose of the cavity is to ventilate away moisture that is in the construction. The interior part is for protection against wind, and to insulate for keeping the temperature of the indoor climate. In Sweden, it is common to use wood as material on roofs. Wood is a material that is prone to moisture. Moisture that comes from indoors and from the construction phase is ventilated away in the cavity, which is illustrated in figure 3.2.

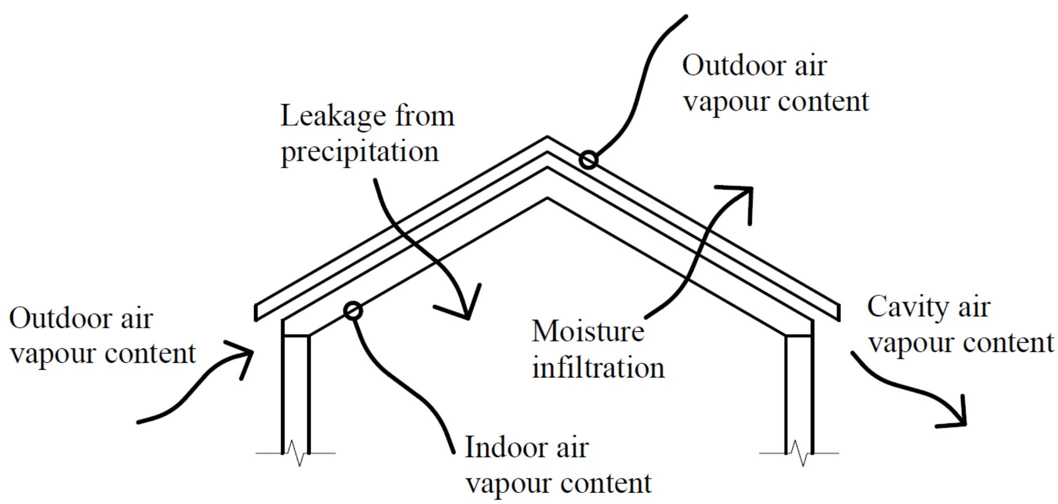

Figure 3. 2. *Moisture Gain and Losses to a Ventilated Parallel Roof*

Note: In a ventilated parallel roof, in this study, moisture is diffused through the roof depending on water content differences. Moisture is also infiltrating the construction due to air infiltration from indoors to outdoor. Moisture is entering the construction due to leakage from precipitation. Moisture is possibly built-in at the construction phase. Moisture is entering the cavity through ventilation of outdoor air and is ventilated away by the same cavity.

The driving force for the ventilation is wind, stack effect and fans. The normal procedure is to ventilate the cavity naturally using outdoor air. The ventilation is done through either a cavity, which is called a parallel ventilated roof, or an attic roof. Because of the relatively large volume of an attic, the air can be assumed to be perfectly mixed resulting in the same air temperature and vapour content everywhere in the space. In the cavity, on the other hand, the air will vary in temperature. The air in the cavity will be heated and cooled due to heat flux from the indoors, radiation from the sun, and longwave radiation towards the sky, which is illustrated in figure 3.3. At the inlet of the cavity, the air temperature is the same as outdoor air, further into the cavity the temperature will change, but quite soon after the inlet, a temperature equilibrium of the space will be reached. The air temperature in the cavity is also dependent on the amount of insulation both in the interior and the exterior part of the roof. A higher temperature in the cavity results in higher moisture uptake from the air and less moisture in the construction. Normally, the moisture capacity of air is enough to take care of diffusing moisture from the indoor climate. In case of leakages or condensation in the cavity due to a cold night, the moisture capacity of the air, at the temperature of the air in the cavity, might not be enough. In ventilated attics, the critical location according to moisture safety is the inner side of the exterior roof, because condensation can happen there due to longwave radiation on cold nights (Arvidsson et al., 2017).

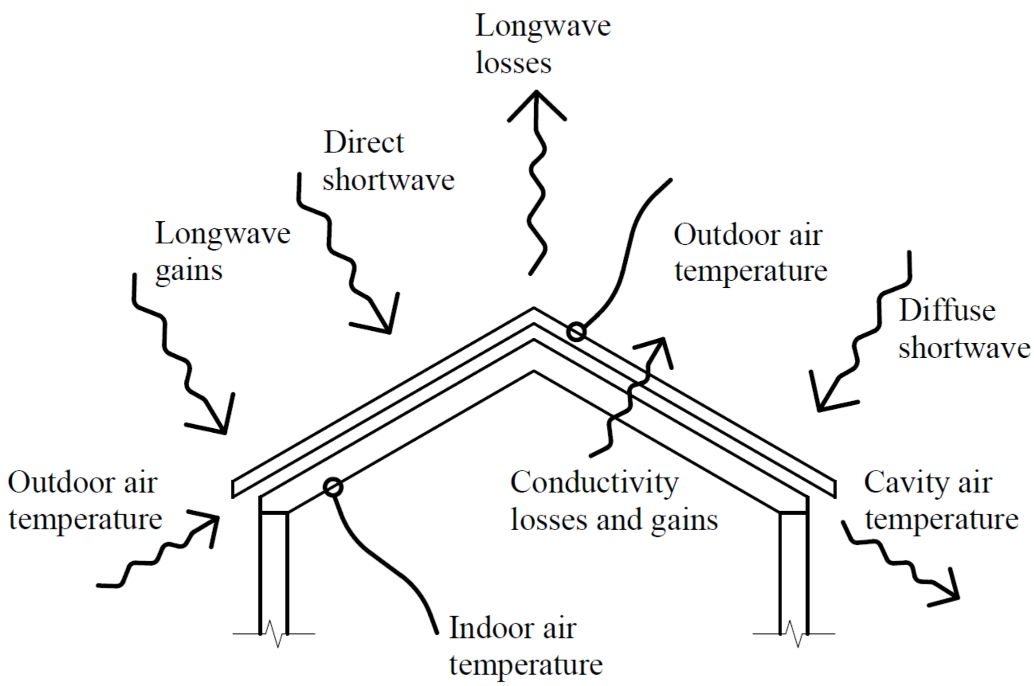

Figure 3. 3. *Heat Gains and Losses to a Ventilated Parallel Roof*

Note: In a ventilated parallel roof, in this study, heat is transported through the roof due to temperature differences between indoor and outdoor climates. The surface is heated and cooled due to radiation. The air entering the cavity through ventilation of outdoor air is either heating or cooling the construction and air in the cavity is also ventilated away.

A non-ventilated roof is also called a massive roof, figure 3.1. Massive roofs are fulfilling the following functions: tightness, structural bearing, thermal insulating as well as fire protection and more. The normal procedure is to build a massive structure of concrete or light concrete. The main issue of the roof due to moisture safety is to make sure the moisture from the construction phase is dried out (Arvidsson et al., 2017). A faulty construction may result in corrosion and condensation in the structure which might result in drips of water from the roof (Arvidsson et al., 2017).

As seen in figure 3.4, there are many types of roof types. The three most common types in Sweden are the due-pitched roof, the mono-pitched roof, and the flat roof. The due-pitched roof is commonly known as the saddle roof. A mono-pitched roof is easily ventilated by wind and stack effect, a due-pitched roof often needs a ventilation outlet at the ridge, on flat roofs, the main hazard is to remove precipitation on the roof (Arvidsson et al., 2017).

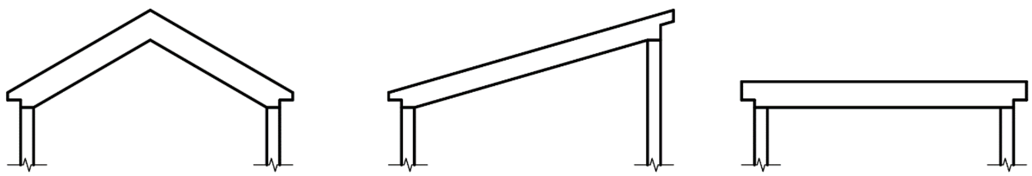

Figure 3. 4. *Different Types of Inclined Roofs*

Note: From left to right: A due-pitched roof (saddle roof), a mono-pitched roof and a flat roof.

From here on the study, only research due-pitched ventilated parallel roofs.

3.1 The Purpose of the Air Cavity

Originally the development of parallel ventilated roofs was to make the exterior surface of the roof cold in winter avoiding snow melting on the roof forming icicles at the eaves. The function of cooling the exterior roof could be used for cooling solar photovoltaic panels (Gullbrekken, 2018). But the main purpose today is to remove moisture by ventilation (Petersson, 2009).

Moisture in the cavity comes from (Petersson, 2009):

- Condensation: Due to moist air entering the cavity and condensing on the inner surface of the exterior roof if the roof is too cold.
- Infiltration: Due to moist air infiltrating from indoors to outdoors through a leakage in the interior vapour barrier and because of an indoor overpressure.
- Driving rain: Due to leakages in the exterior roof in combination with driving rain.
- Built-in moisture: Due to high moisture content in the building materials used in the construction.

3.2 Design

The conventional way of constructing a ventilated parallel roof in Sweden today is presented in figure 3.5.

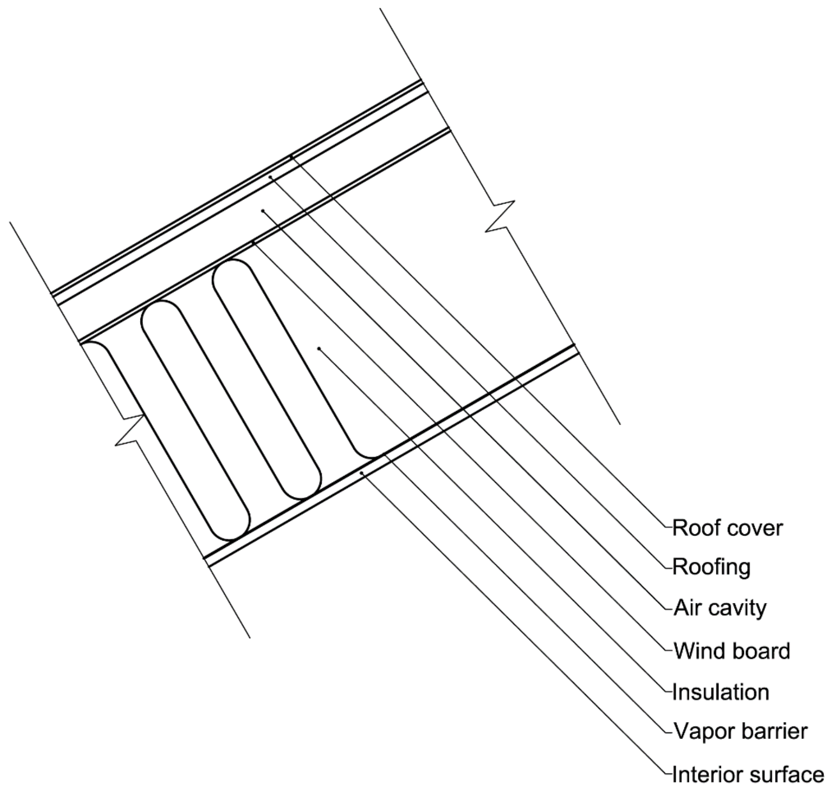

Figure 3. 5. *Detail of a Parallel Ventilated Roof*

Note: A ventilated parallel roof is normally constructed with an interior surface (gypsum), vapour barrier, insulation, windboard, air cavity, roofing (wood) and roof cover (bitumen, titles or steel sheets).

According to Arvidsson et al. (2017) a few pieces of advice is to be followed to ensure the moisture safety of the construction:

- The air cavity must be at least 50 mm high.
- A vapour barrier is mounted, and the joints are sealed by tape or similar.
- No beams or rules, perpendicular to the roof angle interrupts the air cavity.
- The insulation is by some means held down from the air cavity.

In current Swedish guidelines, there are no recommended dimensions of the air cavity. The guidelines state that the roof should be designed in a way that no moisture damage will occur (Boverket, 2018). There are some suggestions of how this should be done: airtightness from the interior and assuring rainwater leaves the roof.

In other countries, there are more detailed national guidelines for air cavities in roofs. The guidelines have recommendations dependent on roof length, and roof inclinations and have different inlet designs (Gullbrekken, 2018).

Månhardt and Odén (2020) show that the parameter that has the largest impact on the construction is the outdoor climate in combination with the roof's tightness to penetration of rain and moisture infiltration from indoors to outdoors. If an air cavity is included, different designs are only making a small difference to the moisture safety of the roof. In normal design today is to use an air cavity of 45 mm, which is reasonable because that is a common dimension on studs, and 50 mm is not.

Arvidsson et al. (2017) notify that with increased insulation, the construction becomes more prone to moisture damage, and therefore must be more carefully designed.

3.3 Validation Object

The numerical model of this study is based on an existing building. Moisture safety was measured and evaluated in this building by Månhardt and Odén (2020) in their master thesis. In this chapter, roof construction is presented. Figures and tables are based on the study of Månhardt and Odén (2020).

3.3.1 Geometry and Materials

It is a parallel roof ventilated by a cavity. As seen in figure 3.6 there are two different roof heights and inclinations: 62° and 45°. The structure is made of two separated wooden frame systems to minimize thermal bridges. The height of the air cavity is 45 mm, and it is ventilated with outdoor air. The roof is well-insulated as is presented in table 3.2 (Månhardt and Odén, 2020).

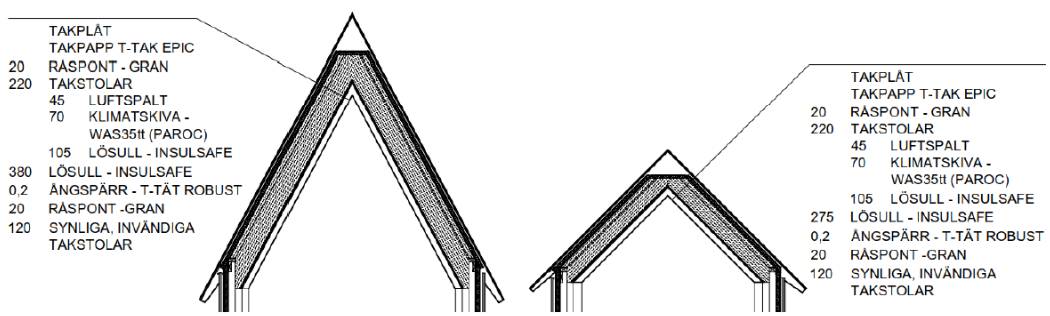

Figure 3. 6. *Cross-section of the Validation Object*

Note: The validation object has two roof inclinations: 62°and 45°. From outside to inside the materials are: steel sheets, roofing felt, wooden board, air cavity, climate board (insulation), mineral wool, vapour barrier, and a wooden board. The figure is used with permission from Månhardt and Odén, *Fuktsäkerhet i ventilerade parallelltak. Fallstudie med blinda beräkningar och utveckling av luftflödesmodell* (p.24), 2020, University of Lund, Copyright 2020 Gustaf Månhardt and Gabriel Odén.

In figure 3.7 red stripes show the cross-sections shown in figure 3.6. The cross-section in the south-north direction has a roof inclination of 62°and a ridge height of 8 m. The cross-section in the east-west-east direction has a roof inclination of 45°and a ridge height of 6 m. The geometry of the air cavity is presented in table 3.1 (Månhardt and Odén, 2020) and in figure 3.8.

Table 3. 1. *The Geometry of the Cavity of the Validation Object.*

Orientation	Roof inclination [°]	Width [mm]	Height [mm]	Length [mm]
South-North	62°	356	45	4000
West-East	45°	360	45	4000

Note: The geometry of the cavity in the study object.

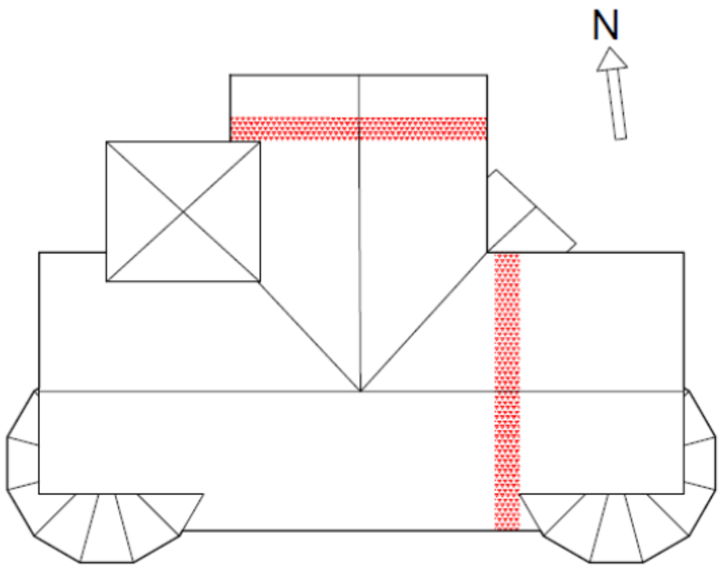

Figure 3. 7. *Orientation of the Roofs of the Validation Object.*

Note: The south-north oriented roof has the inclination 62° and the west-east oriented roof has the inclination 45°. The figure is used with permission from Månhardt and Odén, *Fuktsäkerhet i ventilerade parallelltak. Fallstudie med blinda beräkningar och utveckling av luftflödesmodell* (p.23), 2020, University of Lund, Copyright 2020 Gustaf Månhardt and Gabriel Odén.

The materials and geometrical dimensions of the cross-sections are presented in table 3.2 (Månhardt and Odén, 2020).

Table 3. 2. *Materials of the Roof of the Validation Object*

Building component	**Thickness [mm]**	**Product**	**Material parameters**
Exterior climate			
Roofing sheet	-	-	-
Roof underlayment	-	T-Tak Epic	Water resistance = 0.2 mvp
Wooden layer	20	Spruce	-
Air Cavity	45	-	-
Climate board	70	Paroc WAS 35	Conductivity = 0.033 W/mK Diffusion resistance = 1
Mineral wool	380-485	ISOVER InsulSafe	Conductivity = 0.034 W/mK Density = 30 kg/m^3
Vapor barrier	0.2	T-Tät Robust	Vapor resistance = $3 \cdot 10^6$ s/m
Wooden layer	20	Spruce	-
Interior climate			

Note: The position of materials in the table relates to the position of the material in the cross-section, where the uppermost material is towards the exterior.

The properties of the validation object are later in this study used for validating the numerical model.

3.3.2 Moisture Safety

In the study of Månhardt and Odén (2020), it was studied how different parameters affect the mean air exchange rate and mould growth. They used a mould growth index called MRD, where a higher value indicates a higher risk for mould growth. The effect of the studied parameters is shown in table 3.3.

Table 3. 3. *Parameters Affecting the Validation Object*

Parameter	**Mean Air Exchange Rate**	**Mould Growth MRD**
Increased cavity length	Lowered	At smaller lengths lowered At large lengths constant
Increased cavity height	Slightly increased	Increased
Increased inclination	Marginally affecting	Increased
Increased flow resistance	Slightly lowered	Lowered

Note: Geometrical parameters of the cavity affects the mean air exchange rate and the mould growth MRD differently according to the table.

The cavity length and inclination are often depending on each other, at least as long as the building width is the same.

Increasing the flow resistance could be done by different means: adding an insect net to the inlet and outlet, changing the size and design of the inlet and outlets, and other design changes in the cavity, and, bends in the cavity.

The parameter that affected the cavity the most was the outdoor climate. Different orientations also had a huge impact on the performance of the cavity and if there was a substantial rain leakage (which is not studied in this study).

It was concluded that a very low air exchange rate (10 air exchanges per hour) the MDR got drastically very high, but already at the air exchange rate of 20 per hour the MDR becomes lower, and at 25 air exchanges per hour the lowest possible value is found. With the increasing air exchange rate from 25 up to 350 1/hr, the MDR was slowly increasing linearly. In the study, a comparison between a varying air exchange rate according to the model used was more accurately describing the relative humidity and the temperature in the cavity than a low constant air exchange rate of 30 1/hr.

As long as the roof continued to be well-insulated different thicknesses on the insulation were only marginally affecting the conditions in the cavity.

The study concludes that the geometry of the cavity is not as important as it is that the cavity exists.

3.4 Study Object

The study object is a well-insulated ventilated parallel roof construction. The construction is based on the validation object but adjusted to be more like a standard contemporary Swedish roof construction. A construction from Träguiden (2020) has been regarded as a standard roof construction. The difference between the validation object and the study object is the total thickness of insulation, where the prior has 450 mm insulation in the east-west direction, 555 mm insulation in the south-north, and the latter has 405 mm insulation in all directions. In table 3.4 the building components are listed from the exterior side to the interior side.

Table 3. 4. *Materials of the Roof of the Study Object*

Building component	**Thickness [mm]**	**Product**	**Material parameters**
Exterior climate			
Roofing sheet	1	-	-
Roof underlayment	1	T-Tak Epic	Water resistance = 0.2 mvp
Wooden layer	22	Spruce	-

Air Cavity	45	-	-
Mineral wool	360	ISOVER InsulSafe	Conductivity = 0.034 W/mK Density = 30 kg/m^3
Vapor barrier	1	T-Tät Robust	Vapor resistance = $3 \cdot 10^6$ s/m
Mineral wool	45	ISOVER InsulSafe	Conductivity = 0.034 W/mK Density = 30 kg/m^3
Wooden layer	22	Spruce	-
Interior climate			

Note: The position of materials in the table relates to the position of the material in the cross-section, where the uppermost material is towards the exterior.

In the study, a few parameters of the roofs are varied to simulate different building physic scenarios. The parameters that vary are:

- Location: Lund, Gothenburg, Stockholm and Östersund
- Orientation of the roof: south, north, east, west
- The inclination of the roof: 15°, 30° and 45°
- Colour of the roof: dark and mate metal sheets, and bright and reflective metal sheets
- Insulation on the exterior side of the cavity: none or 100 mm

The geometry of the building is presented in table 3.5 and in figure 3.8. The length of the building is irrelevant for the study and is therefore not used. The height of the roof and the length of the cavity are varying with the inclination. Because the roof is a saddle roof, it has two cavities, one on each side. In table 3.5 of one cavity is presented. The length of the roof is divided by cavities separated by wooden studs. In the study, only one cavity between two wooden studs is considered. In Sweden, a common centrum to centrum distance between studs is 600 mm, which is used in the study. The studs are 45 mm in width, which means that the width of the cavity is 555 mm.

Table 3. 5. *The Geometry of the Cavity of the Study Object.*

Building width [mm]	**Roof inclination [°]**	**Width [mm]**	**Height [mm]**	**Length [mm]**
10000	30°	555	45	5774
10000	45°	555	45	7071

Note: The geometry of the cavity in the study object.

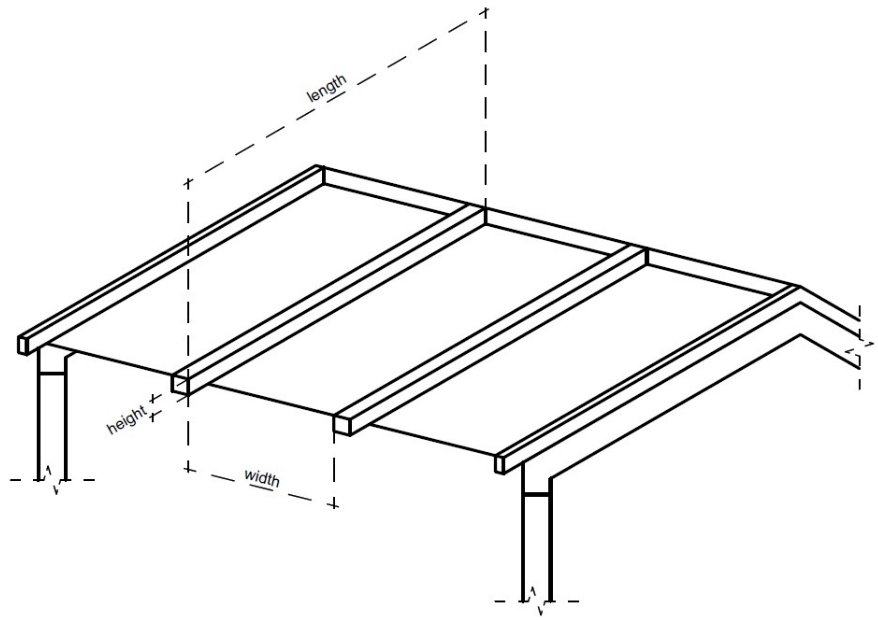

Figure 3. 8. *A Sketch of the Cavity of a Ventilated Parallel Roof*

Note: A sketch of the ventilated parallel roof including three air cavity sections defining the length, height and width.

4
Physical Models

In this chapter, the mould growth in a naturally ventilated air cavity is described through four physical models. Firstly, in section 4.1, an airflow model is describing the quantity of the airflow through the cavity dependent on driving forces. Secondly, in section 4.2, the moisture gains in the air cavity due to moisture infiltration from indoors to outdoors. Thirdly, in section 4.3, the coupled heat and moisture transport equations are used by the numerical software. Finally, in section 4.4, a model describes the risk of developing mould growth on the surface.

4.1 Airflow Model

When calculating moisture transport through an air cavity, the standard procedure is to assume an air exchange rate. In this model, the air exchange rate is calculated by solving balance equations for pressure differences. The air exchange rate is given by equation 4.1 (Hagentoft, 2001):

$$n = \frac{\dot{V}_{cav}}{V_{cav}} \tag{4.1}$$

Where:

n	is the air exchange rate [1/hr]
V_{cav}	is the volume of air that is exchanged [m^3]

The airflow rate expresses the velocity of the air that passes a cross-section in the cavity:

$$\dot{V}_{cav} = u_{cav} A_{cav} \tag{4.2}$$

Where:

u_{cav}	is the velocity of air in the cavity [m/s]
A_{cav}	is the cross-section area of the cavity [m2]

The velocity of air in the cavity is achieved by solving the pressure balance of the cavity. The driving force for the air is the pressure difference between the inlet and the outlet of air in the cavity. Air resistance in the cavity causes the airflow to slow down according to equation 4.3 (Hagentoft, 2001):

$$\dot{V}_{cav} = \frac{C \cdot \Delta P^{n}_{driving\ forces}}{\sum S_{cav}} \tag{4.3}$$

Where:

$\dot{V}_{cav}$	is the airflow rate in the cavity [m^3/s]
C	is the flow coefficient depending on the characteristic of the cavity, such as shape, size, surface [m^3/(sPa)]
$\Delta P_{driving\ forces}$	is the pressure difference between inlet and outlet [Pa]
n	is an exponent which normally is between 0.5 and 0.7 [-]
$\sum S_{cav}$	is the airflow resistance in the cavity [Pa/(m^3/s)]

The pressure difference occurs due to the impact of the outdoor climate. In equation 4.4, the pressure difference is divided into its two components: ΔP_{wind}, pressure difference due to wind, and $\Delta P_{thermal\ bouyance}$, pressure difference due to thermal buoyance (Hagentoft, 2001).

$$\Delta P_{driving\ forces} = \Delta P_{wind} + \Delta P_{thermal\ bouyance} \tag{4.4}$$

A pressure-loss balance similar to equation 4.3 can be applied to the cavity, and the air resistance can therefore be expressed as pressure differences due to pressure drop in the cavity, expressed in equation 4.5:

$$\sum S_{cav} = \frac{\Delta P_{pressure\ drop}}{\dot{V}_{cav}} \tag{4.5}$$

This means that according to (Falk, 2010):

$$\Delta P_{driving\ forces} = \Delta P_{pressure\ drop} \tag{4.6}$$

The pressure drop in the cavity occurs due to friction between the air and the cavity walls, and due to local losses in the design of bends, inlets, outlets, or other geometrical characteristics (Falk, 2010):

$$\Delta P_{pressure\ drop} = \Delta P_{frictional\ loss} + \sum \Delta P_{local\ losses} \tag{4.7}$$

All the equations combined to give the expression in equation 4.8:

$$\Delta P_{wind} + \Delta P_{thermal\ Bouyance} = \Delta P_{frictional\ loss} + \sum \Delta P_{local\ losses} \tag{4.8}$$

In the following chapter, all the parts of the equation will be explained further.

4.1.1 Driving Force due to Wind

Wind induces a pressure difference between the windward side and the leeward side of a roof. The pressure difference between the inlet and the outlet is the source of the driving force due to wind. This is expressed with equation 4.9 (Arvidsson et al., 2017):

$$\Delta P_{wind} = \Delta c_p \frac{\rho_{a,ext} u_{w,10}^2}{2} \tag{4.9}$$

Where:

ΔP_{wind}	is the pressure difference due to wind [Pa]
Δc_p	is the difference in wind pressure coefficient between windward and leeward sides [-]
$\rho_{a,ext}$	is the density of outdoor air [kg/m^3]
$u_{w,10}$	is the wind speed at the measurement station height of 10 m [m/s]

The pressure difference coefficient is affected by the local wind, which has a complex relation to the surroundings and the building's geometry and height. Gullbrekken et al. (2018) as well as Arfvidsson et al. (2017) suggest the use of $c_p = 0.7$ in engineering evaluations for wind-driven ventilations of pitched roofs and eaves-to-eaves ventilation.

Månhardt and Odén (2020) defined equation 4.10 for deciding the wind pressure coefficient when the wind direction is at an angle φ in relation to the inlet:

$$\Delta c_p(\varphi) = 0.48\,cos(1.3\varphi) + 0.22 \tag{4.10}$$

The density of humid air, $\rho_{a,hum}$ is used and can be calculated by equation 4.11 complemented by equation 4.12 for the density of the moist (Arfvidsson et al., 2017).

$$\rho_{a,hum} = \frac{p_a}{R_a T_K} + \frac{p_v}{R_v T_K} \tag{4.11}$$

$$p_v = \varphi 6.1078 \cdot 10^{\frac{7.5 T_C}{T_K}} \tag{4.12}$$

Where:

p_a	is the partial pressure of dry air, which is 100352 at ground level [Pa]
R_a	is the specific gas constant of dry air, which is 287.0058 [J/(kgK)]

p_v	is the pressure of water vapour [Pa]
R_v	is the specific gas constant of water vapour [J/(kgK)]
φ	is the relative humidity [-]
T_K	is the air temperature in Kelvin [K]
T_C	is the air temperature in Celsius [°C]

4.1.2 Driving Force due to Thermal Buoyance

Thermal buoyance is an airflow driven by a temperature gradient. Expressed as pressure differences due to different densities of air at different temperatures, the thermal buoyance originates from the stack effect according to equation 4.13 (Hagentoft, 2001).

$$\Delta P_{stack\ effect} = (\rho_{a,ext} - \rho_{a,cav}) g H_{in-out} \tag{4.13}$$

Where:

$\rho_{a,cav}$	is the density of the air in the cavity [kg/m^3]
g	is the gravity constant [m/s^2]
H_{in-out}	is the vertical height between the inlet and the outlet [m]

The stack effect can also be expressed as dependent on the temperature differences at different heights (Hagentoft, 1991):

$$\Delta P_{stack\ effect} = g\beta_{exp}\rho_{a,ext} \int_0^{H_{in-out}} (T_{a,cav} - T_{ext})\, dz \tag{4.14}$$

Where:

β_{exp}	is the coefficient of thermal expansion [1/K]
$T_{a,cav}$	is the temperature of the air in the cavity [K]
T_{ext}	is the temperature of outdoor air [K]

Equation 4.14 is only valid for mono-pitched roofs where the inlet and outlet are on different heights. Månhardt and Odén (2020) developed the equation to be applicable on a duo-pitched roof with an inlet and outlet on the same heights, but on different sides of the roof. Equation 4.15 is describing the stack effect considering the length of the cavity L, and the inclination θ of the roof:

$$\Delta P_{stack\ effect} = \\ = g\rho_{a,ext} sin\,(\theta_r) T_{ext} \int_0^{L_{cav}} \left(\frac{1}{T_{a,cav1}\,(l)} - \frac{1}{T_{a,cav2}\,(l)} \right) d\theta_r \tag{4.15}$$

Where:

θ_r is the inclination of the roof [°]
L_{cav} is the length of one cavity [m]
l is the length variable [m]
$T_{a,cav}\,(l)$ is the temperature of one cavity as a function of the length variable [K]

The air temperature in the cavity is dependent on the thermal balance of the cavity. Svantesson and Säwén (2019) did a thermal balance for a ventilated cavity, which is presented in figure 4.1. The driving forces that are affecting the air temperature in the cavity are the external climate, including the temperature of outdoor air, the direct shortwave radiation reaching the roof surface, the longwave radiation reaching the roof surface, and the temperature of indoor air. By thermal conductivity, the cavity's surfaces are changed, and by a radiative and convective thermal balance in the cavity, the temperature of the air in the cavity is achieved. Svantesson and Säwén (2019) also reduced the thermal network to an effective temperature and an effective heat transfer coefficient, for calculation reasons.

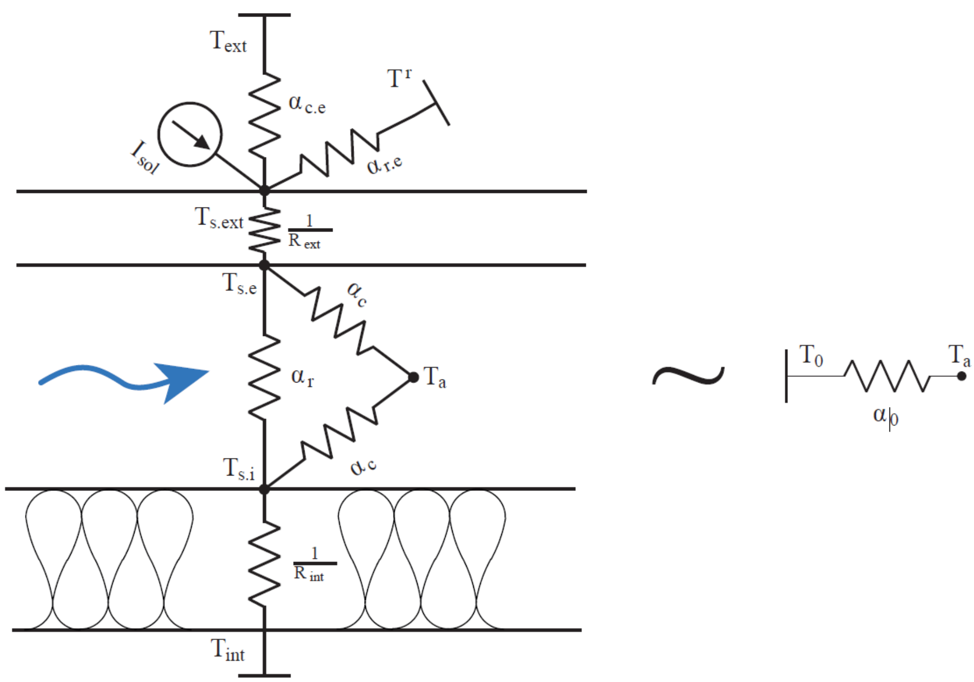

Figure 4. 1. *Thermal Network of the Cavity.*

Note: On the left: A thermal network of the ventilated parallel roof. On the exterior (top) outdoor air temperature T_{ext}, the equivalent temperature of the sky T^r, and solar heat load I_{sol} are affecting the exterior roof which has the thermal resistance R_{ext}. The convective $\alpha_{c,e}$ and the radiative $\alpha_{r,e}$ heat transfer coefficient are describing the relation between the temperatures and the surfaces. The temperature T_{int} of surroundings facing the interior roof, which is a thermal resistance R_{int}. The temperature $T_{s,e}$ on the inside of the exterior roof affects the air temperature T_a in the cavity due to the convective heat coefficient α_c. The temperature $T_{s,e}$ on the inside of the internal roof affects the air temperature T_a in the cavity due to the convective heat coefficient α_c. The insides of the cavity affect each other due to radiation depending on the radiative heat coefficient α_r. On the right: The same network but condensated to an effective temperature T_0 and an effective heat transfer coefficient. The figure is used with permission from

Where:

T_a	is the temperature of the air in the cavity [°C]
T_{ext}	is the temperature of outdoor air [°C]
T_{int}	is the temperature of surroundings facing the roof surface [°C]
T^r	is the equivalent temperature of the sky [°C]
I_{sol}	is the solar heat load acting horizontally on the roof surface [W/m^2]
α_r	is the radiant surface heat transfer coefficient in the cavity [W/m^{2}K]
α_c	is the convective surface heat transfer coefficient in the cavity [W/m^{2}K]
$\alpha_{r,e}$	is the radiant surface heat transfer coefficient of the external roof surface [W/m^{2}K]
$\alpha_{c,e}$	is the convective surface heat transfer coefficient of the external roof surface [W/m^{2}K]
R_{ext}	is the thermal resistance of the external roof structure [m^{2}K/W]
R_{int}	is the thermal resistance of the internal roof structure [m^{2}K/W]
T_0	is the effective temperature of the condensate thermal network [°C]
α_0	is the effective heat transfer coefficient of the condensate thermal network [W/m^{2}K]

The air temperature in the cavity will change along the path. At the inlet, the air temperature in the cavity is equal to the temperature of the outdoor air. Along the path, the temperature of the air will be dependent on the effective temperature T_0, the temperature of the air at the inlet T_{inlet}, the distance x from the inlet, and the characteristic length L_0, according to equation 4.16 (Arvidsson et al., 2017).

$$T_a = T_0 - (T_0 - T_{inlet})e^{-x/L_0} \tag{4.16}$$

The characteristic length L_0 is a variable of how fast the temperature of the air T_a, in the cavity reaches a steady-state temperature. The smaller L_0 is, the faster T_a will reach a steady state. Arfvidsson et al. (2017) provides equation 4.17 for deciding L_0:

$$L_0 = \rho_{a,cav} c_a h_{cav} u_{cav} \frac{1}{\alpha_0} \tag{4.17}$$

Where:

c_a	is the specific heat capacity of air [J/(KgK)]
h_{cav}	is the height of the cavity [m]
u_{cav}	is the airspeed in the cavity [m/s]
α_0	is the effective heat transfer coefficient of the condensate thermal network in figure 4.1 [W/m^{2}K]

The specific heat capacity is a property of how much heat is needed to increase the air temperature by one degree.

4.1.3 Pressure Drop Due to Friction

Pressure drop due to friction in the cavity is dependent on the length of the cavity, as well as the geometry of the cross-section. The pressure drop can be calculated with the Darcy-Weisbachs equation (Kronvall, 1980):

$$\Delta P_{frictional\ loss} = \lambda_{cav} \frac{L_{cav}}{d_H} \frac{\rho_{a,ext} u_{cav,m}^2}{2} \tag{4.18}$$

Where:

$\Delta P_{frictional\ loss}$	is the pressure drop due to friction [Pa]
λ_{cav}	is the frictional factor of the cavity [-]
L_{cav}	is the length of the cavity [m]
d_H	is the hydraulic diameter [m]
$u_{cav,m}$	is the mean velocity of the airflow in the cavity [m/s]

In cavities, the flow conditions are affecting the variables. In a cavity, the flow can be laminar, turbulent, or in between, which is also called transitional. Reynolds number is used to determine the condition of the flow (Kronvall, 1980).

Laminar flow:	if Re < 2300
Transitional flow:	if 2300 < Re < 4000
Turbulent flow:	if 4000 < Re

The Reynolds number can be calculated with equation 4.19 (Kronvall, 1980):

$$Re = \frac{d_H u_{cav,m}}{v_{kin,a}} \tag{4.19}$$

Where:

Re	is the Reynolds number [-]
$v_{kin,a}$	is the kinematic viscosity of air [m^2/s]

Most of the models are describing airflow conditions in a circular cross-section. The hydraulic diameter d_H [m] is the factor making it possible to use other than circular cross-sections. For a rectangular cross-section, h_{cav} is the height of the cross-section, and b_{cav} is the width of the cross-section according to equation 4.20 (Kronvall, 1980):

$$d_H = \frac{2h_{cav}b_{cav}}{h_{cav} + b_{cav}} \tag{4.20}$$

The frictional factor λ_{cav} [-] is dependent on the Reynolds number, not strictly on the airflow conditions. The first condition used is laminar flow, but the second condition used is transitional to turbulent flow. According to Kronvall (1980) the frictional factor λ_{cav} is:

$$\lambda_{cav} = \begin{cases} \frac{Re}{64} & \text{if Re} < 2300 \\ (2\,log(\frac{-4.793}{Re}\,log(\frac{10}{Re}+0.2\frac{\kappa}{d_H})+0.2698\frac{\kappa}{d_H}))^{-2} & \text{if Re} > 3500 \end{cases} \tag{4.21}$$

Where:

κ	is the relative roughness of the cavity's surfaces [m]

4.1.4 Pressure Drop Due to Local Losses

Local pressure drops occur due to local changes in the airflow cross-section area. At inlets, outlets, bends or other changes in the cross-section area. Kronvall (1980) expresses the local pressure drops at the inlet and outlet according to equations 4.22 and 4.23, and for the bend of 90° Idelchick (1960) presents equation 4.24:

$$\Delta P_{inlet,loss} = \xi_{in}\frac{\rho_{a,cav}u_{inlet,m}^2}{2} \tag{4.22}$$

$$\Delta P_{outlet,loss} = \xi_{out}\frac{\rho_{a,cav}u_{outlet,m}^2}{2} \tag{4.23}$$

$$\Delta P_{90,loss} = \xi_{90}\frac{\rho_{a,cav}u_{90,m}^2}{2} \tag{4.24}$$

Where:

ξ	is a loss coefficient, depending on the inlet, outlet or 90° bend [-]
$u_{inlet,m}$	is the mean velocity of the airflow right after the inlet [m/s]
$u_{outlet,m}$	is the mean velocity of the airflow right before the outlet [m/s]
$u_{90,m}$	is the mean velocity of the airflow at the 90° bend [m/s]

If the inlet and outlet are connected to the outdoor Kronvall (1980) presents the loss coefficient for inlet and outlet to equations 4.25 and 4.26 and Idelchik (1960) loss coefficient for bends in equation 4.27:

$$\xi_{inlet} = 1 + K_c \tag{4.25}$$

$$\xi_{outlet} = 0 \tag{4.26}$$

$$\xi_{90} = 45\lambda_{90}\xi_{sur90} \tag{4.27}$$

Where:

λ_{90}	is the frictional factor before the 90° bend, treated in section 4.1.3 [-]
$\xi_{sur90} = 0.8$	is a geometrical factor of the design of the cross-section before and after the 90° bend. Månhardt and Odén (2020) used this value for the reference case based on figure 2.3.2.4.1 in *Air Flows in Building Components* (Kronvall, 1980) [-]

The contraction factor K_c depends on the flow conditions, and has a weak dependence on the Reynolds number:

$$K_c = \begin{cases} 0.98Re^{-0.03} & \text{if Re < 1000} \quad \text{Laminar flow} \\ 10.59Re^{-0.374} & \text{if 1000 < Re < 3000} \quad \text{Transitional flow} \\ 0.57Re^{-0.01} & \text{if 3000 < Re < 40000} \quad \text{Turbulent flow} \end{cases} \tag{4.28}$$

4.2 Moisture Infiltration Model

Pressure differences between different sides of a solid material induce infiltration of air through the layer. The air contains a certain amount of vapour which also is transported through the layer. All solid material has different resistance against air infiltration, as well as different resistance to vapour infiltration, because, in some materials, the air infiltration and the vapour infiltration are not the same.

4.2.1 Infiltration Through Air-Open Layers

When the vapour is transported by the air it is called moisture convection. This happens in cavities, holes and small air cells of a porous material. The convection can be described as an airflow rate. For a roof that is open to infiltration the airflow through the roof can be expressed by equation 4.29 (Arfvidsson, 2017).

$$q_{inf} = q_{50}\left(\frac{\Delta P_{roof}}{50}\right)^{\beta} \tag{4.29}$$

Where:

q_{inf}	is the leakage through the roof [l/(sm^2)]
q_{50}	is the leakage through the roof at 50 Pa pressure difference [l/(sm^2)]
$\beta = 0.7$	is an exponent dependent on the flow resistance. The normal value used in engineering calculations is 0.7 [-]

ΔP_{roof}	is the total pressure difference over the roof [Pa]

The validation object (Månhardt & Odén, 2020) uses $q_{50} = 0.3$ l/(sm^2) which is a standard demand on buildings according to the certificate FEBY 18.

The total pressure difference over the roof consists of three components, the pressure difference due to the stack effect, $\Delta P_{stack\ effect}$, the pressure difference due to wind, ΔP_{wind} (equation), and pressure difference due to fans, ΔP_{fans}. Which is described by the equation (Arvidsson et al., 2017):

$$\Delta P_{roof} = \Delta P_{stack\ effect} + \Delta P_{wind} + \Delta P_{fans} \tag{4.30}$$

Calculating the stack effect $\Delta P_{stack\ effect}$ is done with the same equation as in equation 4.13, but with a few small changes:

$$\Delta P_{stack\ effect} = (\rho_{a,ext} - \rho_{a,int})gH_{np} \tag{4.31}$$

Where:

$\rho_{a,int}$	is the density of indoor air, equation [kg/m^3]
H_{np}	is the vertical distance between the neutral pressure plane and the inlet of the cavity [m]

For the validation object Oden and Månhardt (2020) presume that the infiltration was equally allocated on all of the roofs, which results in that the neutral pressure plane is located at half the height of the roof, which is used for H_{np}.

The pressure difference due to wind ΔP_{wind} uses equation 4.9, but with a different wind pressure coefficient Δc_p.

$$\Delta c_p = c_{p,ext} - c_{p,int} \tag{4.32}$$

The exterior wind pressure coefficient $c_{p,ext} = 0.5$ according to Arfvidsson et al. (2017). For dimensioning from a structural point of view the worst case should be used, meaning an indoor pressure coefficient of either +0.2 or -0.3 (Isaksson & Mårtensson, 2017). Månhardt and Odén (2020) assumed the reference case is not a dimensioning scenario regarding wind. Therefore, a standard value between the two worst-case values can be used, where the interior pressure coefficient is $c_{p,int} = 0$.

In the model, the ventilation system is assumed to be in balance, and therefore no pressure difference occurs due to fans, which means $\Delta P_{fans} = 0$ Pa.

4.2.2 Moisture Source

Moisture is added as the difference in vapour content between the indoor air and the outdoor air according to equation 4.33. The airflow rate through the construction explains how much moisture is transported through the construction (Wallentén, 2018).

$$G_{inf} = (v_{a,int} - v_{a,ext,sat})q_{inf} \tag{4.33}$$

Where:

G_{inf}	is the moisture source, which is the amount of moisture accumulated in the structure per time [kg/s]
$v_{a,int}$	is the moisture content in the indoor air [kg/m^3)]
$v_{a,ext,sat}$	is the moisture content at 100 % relative humidity in the outdoor air [kg/m^3]

The equation assumes that the air on the exterior of the construction will become saturated. Because the outdoor air can not have a higher moisture content, the difference between the indoor moisture content and the moisture content of saturated outdoor air is assumed to be accumulated as a moisture source in the structure. The outdoor air is not always saturated, which means that more moisture could be accumulated in the construction (Wallentén, 2018).

4.2.3 Saturated Vapour Content

The saturated vapour content $v_{a,s}$ is calculated with a formula from the German DIN-standard (4108) in equation 4.34 (Hagentoft, 2001).

$$v_{a,s} = \frac{a\left(b + \frac{T_C}{100}\right)^n}{461.4(T_C + 273.15)} \tag{4.34}$$

Where:

$0 \leq T_C \leq 30$ $a = 288.68$ Pa, $b = 1.098$, and $n = 8.02$

$-20 \leq T_C \leq 0$ $a = 4.689$ Pa, $b = 1.486$, and $n = 12.3$

The relative humidity φ is calculated by equation 4.35 (Hagentoft, 2001).

$$\varphi = \frac{v_a}{v_{a,s}} \tag{4.35}$$

Where:

v_a	is vapour content [kg/m^3]

4.3 Coupled Heat and Moisture Transport

Heat and moisture transport through a building can be described by two coupled equations 4.36-4.37. Several different models exist because all the physics is not yet known, especially for moisture transport (Wallentén, 2018). The following equations are used in the numerical software WUFI (section 5.3).

For heat transport:

$$c\rho_m \frac{\partial T}{\partial t} = \frac{\partial}{\partial x}\left(\lambda_m \frac{\partial T}{\partial x}\right) + h_e \frac{\partial}{\partial x}\left(\delta_v \frac{\partial}{\partial x}\left(\varphi v_{m,s}\right)\right) \tag{4.36}$$

For moisture transport:

$$\frac{\partial w}{\partial \varphi}\frac{\partial \varphi}{\partial t} = \frac{\partial}{\partial x}\left(D_w \frac{\partial w}{\partial x}\right) + \frac{\partial}{\partial x}\left(\delta_v \frac{\partial}{\partial x}\left(\varphi v_{m,s}\right)\right) \tag{4.37}$$

Where:

T	is the temperature of the material [°C]
t	is the time [s]
x	is the position in the material [m]
h_e	is the evaporation enthalpy of water [J/kg]
λ_m	is the heat conductivity of the material, dependent on the moisture content [W/mK]
c	is the specific heat capacity of the material (including the moisture content) [W/m^{2}K]
ρ_m	is the density of the material (including moisture content) [kg/m^3]
φ	is the relative humidity of the air in the material [%]
$v_{m,s}$	is the saturated vapour content of the air in the material [kg/m^3]
w	is the moisture content of the material [kg/m^3]
D_w	is the liquid transport coefficient [m^2/s]
δ_v	is the vapour permeability [m^2/s]
v_m	is the vapour content of the air in the material [kg/m^3]
$\frac{\partial w}{\partial \varphi}$	is the moisture capacity [kg/m^3 %]

In physics, the properties of the equations happen constantly and parallelly. The heat transport equation consists of three parts, on the left side is the heat storage depending on both the dry material and the water content of the material. On the right side, the first term is the moisture dependent thermal conductivity, and the second term is the vapour enthalpy flow, meaning water evaporating in one place and condensing in another place. The moisture transport equations also consist of three parts: moisture storage on the left, and the right: liquid transport and vapour diffusion. The vapour diffusion is strongly temperature-dependent (Fraunhofer IPB, 2009a).

The equations are simplified, and the most important simplifications and assumptions according to Wallentén (2018) are:

- There is no air convection
- The moisture transport is divided into two parts: liquid transport and vapour transport. No detailed research supports this assumption.
- The moisture capacity is not temperature-dependent.
- The liquid transport coefficient is not temperature-dependent.
- There is no gravitation

4.4 Mould Growth Index

The risk of mould fungi growth on wooden materials can be simulated by a mathematical model. Several different models exist, and in this study, the MGI (mould growth index) model will be used (Hukka & Vittanen, 1999). The model is not predicting the biological growth and number of mould fungi cells, but the possible activity of mould growth present on the surface of wooden materials depending on two parameters: temperature and humidity.

The model presupposes a few assumptions:

- The mould growth only happens on the surfaces of the material, and therefore only surface temperature and humidity are of interest.
- The mould fungi do not affect the behaviour of the material when it comes to transport mechanisms.

The mould growth index consists of a 7-grade scale (table 4.1):

Table 4. 1. The 7-grades of MGI.

MGI	Growth
0	no growth
1	some growth, but only seen in microscopy
2	moderate growth with more than 10% coverage, but only seen in microscopy
3	some growth which is detectible visually
4	growth covers more than 10%, detectible visually
5	growth covers more than 50%, detectible visually
6	growth coverage 100%, detectible visually

In the model, the mould growth index always starts at 0, if the conditions are favourable for mould growth, the growth will be initiated. Favourable conditions for mould growth are between 0-50 °C. If the temperature differs from this span, no mould growth will occur in the model. At different temperatures, the level of relative humidity decides if mould growth will be initiated. The critical relative humidity, at which mould growth will be initiated is (Hukka & Vittanen, 1999):

$$RH_{crit} = \begin{cases} -0.00267T_s^3 + 0.160T_s^2 - 3.13T_s + 100.0, & when\ T_s \leq 20 \\ 80\%, & when\ T_s > 20 \end{cases} \tag{4.38}$$

Where:

RH_{crit}	is the critical relative humidity [%]
T_s	is the surface temperature of the exposed material [°C]

The relations of equation 4.38 are shown in figure 4.2.

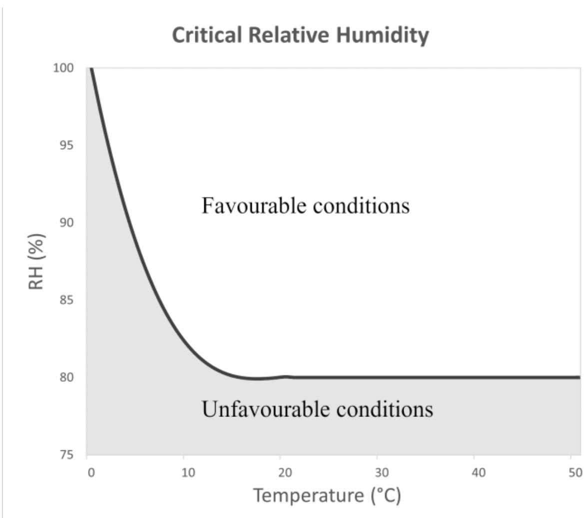

Figure 4. 2. *Critical Relative Humidity of MGI.*

Note: A curve describing the critical relative humidity. If the conditions of RH and Temperature are on or above the line it is favourable for mould to start growing.

When mould growth is initiated, it will continue growing until its maximum coverage at the specific level of relative humidity and temperature, or until the temperature and relative humidity will change. The maximum mould growth, M_{max} [-] that a certain combination of relative humidity and temperature can be described by equation 4.39 (Hukka & Vittanen, 1999).

$$M_{max} = 1 + 7\frac{RH_{crit} - RH}{RH_{crit} - 100} - 2\left(\frac{RH_{crit} - RH}{RH_{crit} - 100}\right)^2 \tag{4.39}$$

When conditions are favourable and M_{max} is not reached it will take some response time (weeks) in favourable conditions before the growth begins. The response time when $M < 1$ can be described by equation 4.40 (Hukka & Vittanen, 1999):

$$t_m = exp(-0.68\, ln\, T_s - 13.9\, ln\, RH + 0.14W - 0.33SQ + 66.02) \qquad (4.40)$$

If the mould growth index M is assumed to be linearly in time equation 4.41 can be expressed as the following differential equation describing the mould growth change per time (Hukka & Vittanen, 1999).

$$\frac{dM}{dt} = \frac{1}{7exp(-0.68\, ln\, T_s - 13.9\, ln\, RH + 0.14W - 0.33SQ + 66.02)} k_1 k_2 \qquad (4.41)$$

$$k_1 = \begin{cases} 1, & when\ M < 1 \\ \dfrac{2}{t_v/t_m - 1}, & when\ M \geq 1 \end{cases} \qquad (4.42)$$

The correction factor k_1(equation 4.42) are used when $M \geq 1$, and the correction factor k_2 are used when the mould growth is fluctuating. The response time until the mould becomes visual is described by equation 4.43 (Hukka & Vittanen, 1999):

$$t_v = exp(-0.74\, ln\, T_s - 12.72\, ln\, RH + 0.06W + 61.06) \qquad (4.43)$$

In dry periods the mould will not stay active, instead, in the model, it declines already after 6 hours. Visible mould will not disappear, but the growing part will. The decline is affected by how long time has passed since the dry period started. The decline rate can be expressed in relation to the start of the dry period (Hukka & Vittanen, 1999):

$$\frac{dM}{dt} = \begin{cases} -0.032, & when\ t - t_1 \leq 6\ h \\ 0, & when\ 6\ h < \ t - t_1 \leq 24\ h \\ -0.016, & when\ t - t_1 > 24\ h \end{cases} \qquad (4.44)$$

5
Method

This chapter is separated into different parts explaining different steps of the study. The first step is to convert the weather data into input data for the numerical simulations. The input needed is:

- Outdoor climate
- Indoor climate
- Air exchange rate in the ventilated cavity
- Infiltration of moisture from indoors to outdoors due to air leakage

These steps are explained in section 5.1.

The second step is to effectively handle large data sets. Because of the size of the data, it is impossible to handle it by hand, and therefore programming must be used. In section 5.2 the principles of how the large data sets were handled, are explained.

The third step is to build the numerical model. The first challenge was to adjust the study model to fit the validation model. The second challenge was to solve numerical problems that occurred. This is explained in section 5.3.

In the fourth step, the results from the numerical model were transformed into a mould growth index, which is explained in section 5.4.

Finally, in the fifth step, it is presented which parameters the study is evaluating, which is explained in section 5.5.

5.1 Input for the Numerical Simulations

Four different data sets are needed as input for the numerical simulations: Outdoor climate; Indoor climate; Air exchange rate in the ventilated cavity; and Infiltration from indoors to outdoors.

Raw data from SMHI has been processed by Nik (2010). From his licentiate, weather data for building physics were available according to table 5.1. The data are further explained in chapter 2. In sections 5.1.1 to 5.1.4, the data are processed to fit the purpose of this study.

Table 5. 1. *Climate Data for the Study.*

Parameter	**Unit**
Outdoor Air Temperature	[°C]
Outdoor Relative Humidity	[%]
Global Shortwave Radiation	[W/m^2]
Diffuse Shortwave Radiation	[W/m^2]
Direct Shortwave Radiation	[W/m^2]
Longwave Sky Radiation	[W/m^2]
Wind Direction	[°]
Wind Speed	[m/s]
Precipitation	[mm/s]

Note: In the table, the weather parameter needed for the study and their units are presented.

5.1.1 Outdoor Climate

In the data from Nik (2010) the air temperature and wind speed have been enlarged by the power of 10 to avoid decimals in the calculations. In this study, these data sets are restored to their original power of 10. The relative humidity is converted from percentage to decimals. The precipitation is converted from [mm/s] to [mm/hr]. Precipitation is only available for scenarios A1B, not for A2 and B1. All radiation data used as a part of the outdoor climate is defined as horizontal radiation, which is when the radiation strikes the surface at the angle of its normal, meaning the maximum amount of radiation reaches the surface.

5.1.2 Indoor Climate

The indoor climate is based on the standard EN 13877 which is a European Standard. This is the same as Månhardt and Odén (2020) used in their study. The indoor air temperature and relative humidity are calculated by WUFI, according to the plots in figure 5.1) when the outdoor climate is imported. The indoor temperature is 20 °C all the year. The indoor humidity is dependent on the outdoor temperature. When the outdoor temperature is ≤ 0 °C the internal moisture gain is 2 g/m^3 and when the outdoor temperature is ≥ 20 °C the internal moisture gain is 0 g/m^3. At outdoor temperatures between 0 °C and 20 °C, the internal moisture gain is linearly varying between 2 and 0 g/m^3.

.

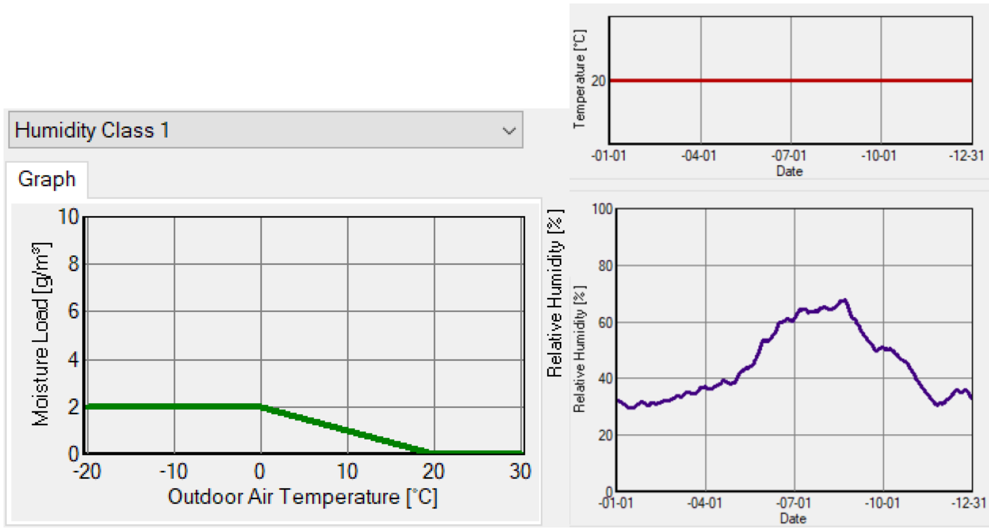

Figure 5. 1. *The European Standard EN 13877 for indoor climate.*

Note: The plot on the left shows the moisture gain to the indoor air depending on the outdoor temperature in humidity class 1. The plot on top to the right shows the constant indoor temperature of 20°C. The plot to the bottom right shows the indoor relative humidity depending on the moisture gain depending on the outdoor temperature.

5.1.3 Air Exchange Rate in Ventilated Cavity

Modelling a ventilated air cavity in WUFI is done by defining a cell with the properties of air, and then adding an air exchange source to the cell. A text file (.txt) must be imported to WUFI including the air exchange rate for each hour.

The air exchange rate per hour is solved by a Matlab program according to the physics in section 4.1. Equations 4.1-4.8 are used for achieving the air exchange rate per hour based on a pressure balance of the cavity. Wind (section 4.1.1) and thermal buoyance (section 4.1.2) creates a pressure difference between the inlet and outlet of the cavity. The pressure balance is depending on the direction of wind towards the studied roof according to equation 4.10. Because of the dependency of wind direction, the flow direction can become negative, then reversed wind direction is tested, and if that also produces a negative result, then the result is assumed to be zero in the model.

In the cavity, pressure drops occur at inlets, outlets and bends (section 4.1.4). The roof in the study model has a pressure drop at the inlet assumed to be equivalent to an insect net and specified in equation 4.25, at the bend on the edge it is assumed that it represents the air leaving and then entering the second cavity, therefore the bend can be regarded as equivalent as two inlet pressure drops. It is assumed that there is no pressure drop at the outlet according to equation 4.26. There are pressure losses due to friction along the cavity walls (section 4.1.3). The calculations are depending on emissivity, absorptivity, and heat transfer coefficients, according to table 5.2. The standard in the study is to use values for the dark-coloured roof. The values for the bright-coloured roof are only used in study G, where it is compared with the dark-coloured roof.

Table 5. 2. Transfer Parameters for the Airflow Model.

Parameter	Value	Reference
Emissivity dark-coloured roof	0.9	Steel sheet, black and mate according to WUFI 2D (2022)
Emissivity bright-coloured roof	0.27	Steel sheet, steel polished (Hagentoft, 2001)
Absorptivity dark-coloured roof	0.87	Steel sheet, black and mate according to WUFI 2D (2022)
Emissivity bright-coloured roof	0.5	Light colours, polished aluminium (Hagentoft, 2001)
Emissivity wood	0.9	Wood (Hagentoft, 2001)
Emissivity insulation	0.9	Assumed same as wood
Thermal resistance to indoor air	0.1 m^2K/W	Roof according to SS-EN ISO 6946 (2017)

Note: Values on emissivity, absorptivity, convective heat transfer coefficient and thermal resistance for the airflow model.

In study F, additional external insulation of 100 mm was added above the cavity in the airflow model.

In study E, the variable air exchange rate is compared to a constant air exchange rate of 25 1/hr.

5.1.4 Moisture Infiltration

The resulting moisture gain due to infiltration from indoors to outdoors is added in WUFI as a moisture source. According to Wallentén (2018), it is normal practice to add the moisture source in the outer layer of the vulnerable construction, in this case, in the wood. Because there is a cavity, the moisture source must be put on the inner side of the cavity. Calculating infiltration is normally done for each square meter. Using these values based on the square meter demands that the WUFI model is 1000 mm in width. Otherwise, some scale effects occur due to differences between 1D and 2D.

The driving force for the infiltration is the pressure difference between indoors and outdoors, which is calculated by equation 4.30. The flow rate is calculated by equation 4.29 and the moisture gain by equation 4.33. The principle is that the difference between the indoor vapour content and the exterior saturated vapour content is added to the construction as a moisture gain. The pressure difference is the driving force.

Negative infiltration is neglected, meaning that no moisture is removed from the construction due to infiltration.

The infiltration uses the same $q_{50} = 0.3$ l/(sm^2) as in the validation object (Månhardt & Odén, 2020).

5.2 Programming Large Data Sets

Data used in this study is variated by the following parameters

- 3 scenarios
- 4 locations
- 4 roof orientations
- 2 roof inclinations
- 2 roof colours
- 2 different sizes of external insulation
- Variable and constant air exchange rate in the cavity

Testing all parameters towards each other would mean 384 different combinations. Each of these combinations consists of around 20 different parameters with hourly values for 140 years (1227240 hours). This means about $1.9 \cdot 10^{10}$ values which must be in the correct location in the data sets. Processing large sets of data demand a powerful computer, and even then, it takes a long time to process all the data.

5.2.1 The Matlab Software

The software used for handling and programming the data sets is MATLAB R2020b (version 9.9.0.1467703 for win64). It is a matrix-based language designed for engineers and scientists (MathWorks, 2022a).

5.2.2 Large Data Sets

Working with large data sets requires a systematic way of not mixing the data. Human mistakes must be prevented. Naming and structuring of the data must be logical, trackable and provide a control function. Because of the great size of the data sets, it is of great importance to reduce the calculation time. Some calculations are heavy for the computer. These calculations must be reduced to a minimum and are only executed when necessary.

5.2.3 Structure of the Data

The data available from Nik (2010) and Rossby Centre was provided in .mat-files in a desktop file structure. .mat-files are binary MATLAB files for storage. There are different versions of the .mat-files, where some of the data produced had to use the latest version 7.3 which allows more than 2 GB for each variable (MathWorks, 2022b).

In the .mat-files the data are stored in a *structure array* (MathWorks, 2022c). In a structure array, data is stored in different fields. One array consists of different fields, and each field consists of any kind of data. These structures can be nested in levels. Imagine a structure of all the weeks (52) of the year, and each week is a field of days (7). To access the third day in week 40 one type:

week(40).dayOfWeek (3)

Where the *week* is the name of the structure array, and *dayOfWeek* is the name of the field.

5.2.4 Exporting Data Sets to Numerical Simulations

Three different files had to be exported for each numerical simulation:

- Outdoor climate
- Air exchange rate in the ventilated cavity
- Moisture infiltration from indoors to outdoors.

5.2.4.1 Export of Outdoor Climate

The data is exported to a .wac-file. The file includes a heading: WUFI®_WAC_02, which is read by WUFI when importing. The following rows include meta-data that does not affect the calculations: location, project name, longitude, latitude, height above the sea, time zone, time step, number of data lines, and number of data columns. Then comes a row explaining which data is included in the file. The parameters are:

- WD: Wind direction
- WS: Wind speed
- RN: Precipitation
- PSTA: Pressure
- TA: Air Temperature
- HREL: Relative humidity
- ISGH: Horizontal global shortwave radiation
- ISD: Horizontal diffuse shortwave radiation
- ISDH: Horizontal direct shortwave radiation
- ILAH: Horizontal longwave atmospheric counter-tradition

.wac-files allows WUFI to load other weather parameters as well.

This row is followed by all hourly data which is shown in figure 5.2.

wufi_WAC_stockholm_north_1991-2001 - Notepad

File Edit Format View Help

```
WUFI®_WAC_02
10      Line Offset to 'Number of Data Columns'
Stockholm, North, Scenario: A1B, Inclination: 45, Cavity length: 4 [m], Cavit
FutureClimate_Execute.m
18.06   Longitude [Â°]; East is positive
59.33   Latitude [Â°]; North is positive
10      HeightAMSL [m]
1.0     Time Zone [h from UTC]; East is positive
1       Time Step [h]
96433   Number of DataLines
10      Number of DataColumns
WD      WS      RN      PSTA    TA      HREL    ISGH    ISD     ISDH    ILAH
19      6.1317  0.0000  1013.25 -7.463  0.7894  0       0       0       261
18      6.0243  0.0000  1013.25 -7.510  0.7871  0       0       0       258
17      5.9182  0.0000  1013.25 -7.553  0.7870  0       0       0       256
16      5.8136  0.0026  1013.25 -7.597  0.7868  0       0       0       253
15      5.7105  0.0146  1013.25 -7.640  0.7867  0       0       0       250
14      5.6019  0.0103  1013.25 -7.697  0.7892  0       0       0       248
13      5.4945  0.0043  1013.25 -7.753  0.7918  0       0       0       257
13      5.3886  0.0000  1013.25 -7.810  0.7945  0       0       0       250
11      5.3161  0.0000  1013.25 -7.807  0.7957  0       0       0       246
10      5.2462  0.0000  1013.25 -7.803  0.7969  5       5       0       245
9       5.1791  0.0000  1013.25 -7.800  0.7980  51      51      0       245
8       5.2130  0.0000  1013.25 -7.593  0.7889  92      92      0       240
7       5.2485  0.0000  1013.25 -7.387  0.7798  104     104     0       241
6       5.2856  0.0000  1013.25 -7.180  0.7708  78      78      0       247
```

Figure 5. 2. *The Appearance of a .wac-file.*

Note: Weather data are imported to WUFI preferable by .wac-files. The first side of the file is shown in the figure.

5.2.4.2 Export of Air Exchange Rate

The data is exported to a .txt-file with only two columns. In the first column, each hour is exported, starting on the first hour. In the second column, the air exchange rate per hour of the cross-section of the roof is exported.

5.2.4.3 Export of Moisture Infiltration

The data is exported to a .txt-file with only two columns. In the first column, the last hour of each day is exported, and in the second column, the daily mean value of moisture infiltration from indoors to outdoors is given, adjusted according to the size of the WUFI-model (5.3.5).

5.2.4.4 WUFI Reading Source Files

When WUFI reads a source file, in this study the air exchange rate and the moisture infiltrations, it starts checking the first column, which hour to start applying a source to. The source value on the same row will be applied for every stated hour until the next specified hour in the first column. Therefore, values are only needed when changes in the sources happen (Fraunhofer IBF, 2008).

5.3 Numerical Simulations

The two coupled equations 4.36-4.37 describing the heat transport and the moisture transport cannot be solved analytically. A common engineering solution is to use a numerical method where computer software divides the actual construction into small elements, making calculations for each element, and then repeating this for every time step of the period of interest.

5.3.1 The WUFI Software

In Sweden, both in industry and academy WUFI (Wärme- Und Feuchtetransport Instationär) is a widespread software for doing non-steady moisture transport assessments. The widespreadness of the program as well as the high reliability due to different validating experiments makes it a reasonable choice for this study. There are a few different versions of WUFI. The Chalmers University of Technology has a license on WUFI 2D (version 3.4.2.181.181.DB.24.78), and therefore the 2D version is used in this study. The models can be simplified to 1D calculations which are needed in this study (Fraunhofer IBF, 2018).

The calculation core of WUFI is based on two non-steady coupled differential equations 4.36-4.37. The equations are solved iteratively through the discretization of the implicit finite volume method (Fraunhofer IBF, 2009).

5.3.2 Calculations Procedure in WUFI

Numerical calculations are done implicitly in WUFI, which means that when each calculation is done, one criterion is that equations 4.36 and 4.37 are already fulfilled for the next time step. This means that the length of the time step can be chosen freely, a drawback is that because equations 4.36 and 4.37 already are fulfilled, the solution might become false at the used time step. A way of avoiding false results is to try different time steps in a convergence study (which is done in section 5.3.7). The smaller the time step, the more accurate the result, but below a certain length of the time step, the results will not change.

Using a numerical method, both time and space are discretised. The materials are divided into several cells, and the time is divided into several time steps. Both equations must be solved for each cell and each time step. In figure 5.3 the calculation procedure is presented: The solver first guesses the initial values based on the initial conditions (Step A), then solves the heat transport equation 4.36 (step B), followed by solving the moisture transport equation 4.37 (Step C). To be sure that the solution is good enough, the solver must redo (Step D and E) the calculations until the difference between different solutions (ψ for the heat equation and θ for the moisture equation) is small enough, fulfilling the convergence criterium ε (Wallentén, 2018). There could be thousands of calculations for each cell in each time step.

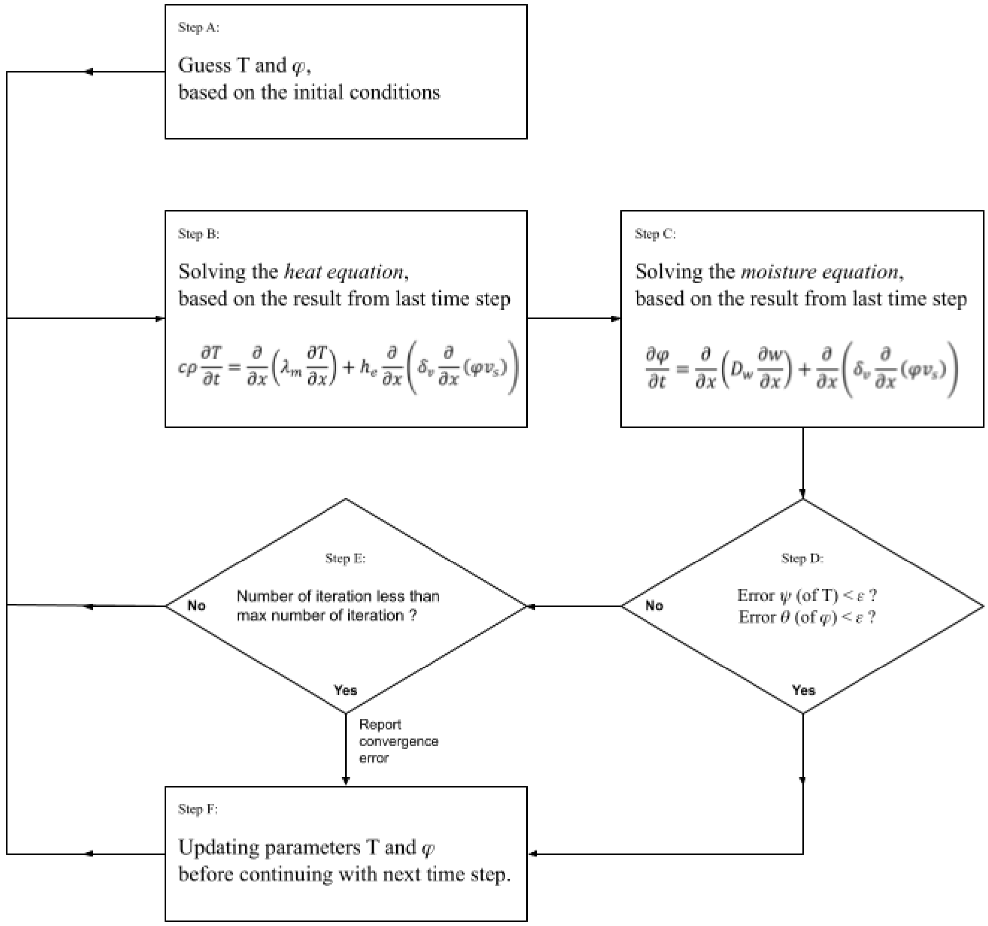

Figure 5. 3. *The Calculation Scheme of WUFI.*

Note: The calculation starts with guessing the temperature, T and the relative humidity, φ. Then the heat transport is calculated and after that the moisture transport. If the error Ψ of T or the error θ of φ are larger than the criterium ε, the iteration is done again, otherwise, the calculated T and φ are used for the next calculation step.

5.3.3 Water Content in WUFI

The water content, of material in WUFI, is defined by a moisture storage function, which is represented by a table of relative humidity and their corresponding water content. The moisture storage function includes three thresholds: Firstly, the *maximum water content* w_{max} which is defined by the porosity of the material. At w_{max} the material is supersaturated, and condensation might occur. At a relative humidity of 100% in the material, it is called that *free saturation*, w_f is reached. Because w_f includes air pockets in the material, it has less water content than in w_{max}. The value w_{80} is the *practical moisture content*, and it corresponds to the equilibrium at a relative humidity of 80 %. Both w_f and w_{80} are empirically known for many materials and are implemented in the WUFI material database. WUFI does not consider hysteresis and is only calculated with an average moisture storage function (Fraunhofer IBF, 2013).

Below the value of w_f, relative humidity is the driving force for moisture calculations in WUFI. For each step, first, the temperature is calculated based on the previous step, then the relative humidity is calculated, and after that, the water content is calculated, as a secondary property. When a material approaches 100% relative humidity the inclination of the graph becomes very steep, and very small differences in relative humidity result in very large differences in water content. Doing calculations in that region may result in numerical problems. The system becomes more stable with more points in sensitive regions (Fraunhofer IBF, 2013).

At w_f and above, the relative humidity is always 100% and the water content can therefore not be dependent on the relative humidity. Instead, the water content is determined by the boundary conditions, which are either condensation or evaporation, increasing or decreasing (Fraunhofer IBF, 2013).

For some materials, a fine and researched moisture storage function are used for the material, but for some materials, a simplified moisture storage function is used. A material that does not have an accurate moisture storage function is air (Fraunhofer IBF, 2013).

5.3.4 Numerical Problems

A numerical problem is when the calculation fails due to some reason. It is often a combination of different aspects that make the numerical problem occur. The consequence is that the calculations stop, either the difference ε of ψ and θ never reaches an accepted value, or the results might become physically impossible, with temperatures of several billion degrees, and water content of more than 1000 kg/m^3, regardless of material (Fraunhofer IBF, 2001).

To address numerical problems in this study, several adjustments have been tried to improve the stability, increase reliability, and shorten the computing time.

Cells of deep materials, the insulation, were divided into several similar-sized cells. Using too large cells of insulation might result in very steep changes between neighbouring values, which might lead to numerical failure.

The elements in areas of high moisture, close to and in the air cavity, have small elements. The elements where moisture sources are present need small elements.

The air cell in the cavity has been divided into three cells, where the cell in the middle is the place for the source of the air exchange rate. In this cell, an air material in WUFI is used which enables a low w_f of 0.017 g/kg. In the air cells in contact with the wood smaller elements are used with changed moisture properties, w_f of 47 g/kg. The reason for this is that WUFI has no realistic way of handling condensation, by introducing a small layer of air that can hold more water than normal at w_f a condensation layer is created (Wallentén, 2018).

When numerical problems were encountered, the following actions were used to find a solution:

- Checking the water content for the whole construction, and for elements exposed to high moisture load. This is done by analysing the water content plots in WUFI (figure 5.4). The values has to variate in a reasonable span with no extrem values.
- Troubleshooting for faults in the input values and settings in WUFI
- Checking the convergence by the WUFI motion tool
- Changing the grid, often to smaller elements in positions with high moisture content and large fluctuations in moisture content or relative humidity.
- Changing the computational parameters: Convergence criterium ε and the maximum number of iterations (MAXIT)
- Excluding one of the sources, troubleshooting where the problem lies

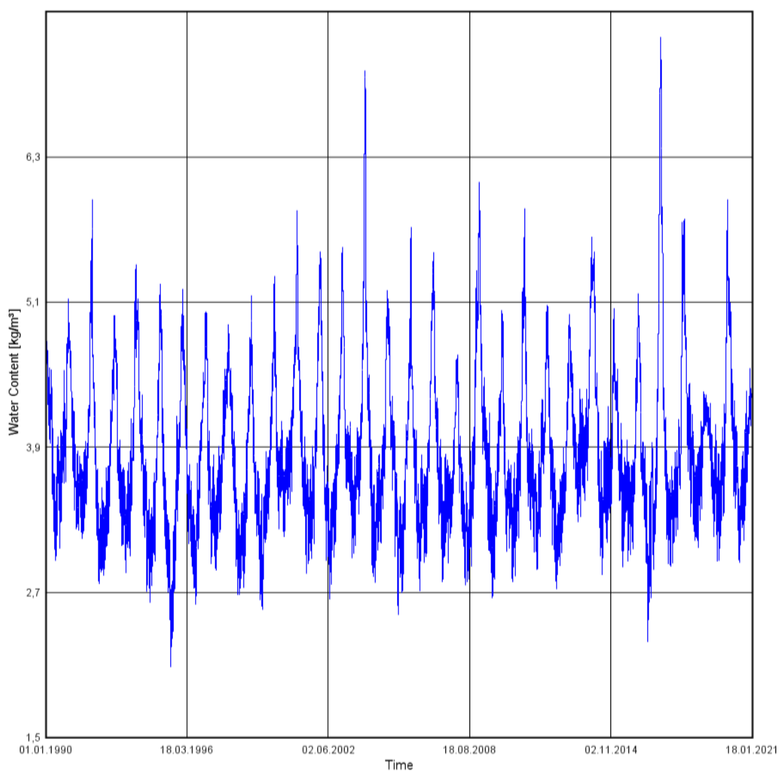

Figure 5. 4. *Water Content of a Simulation*

Note: The Water Content of a simulation should vary without too large peaks. In this 30-year simulation two peaks standing out, but the plot later returns to the normal amplitude .

Other measurements have had a positive impact on the calculations, like changing the moisture storage function and adding a moisture buffering layer, but no possible motivation for such changes has been found.

5.3.5 WUFI-Model

The numerical model in WUFI is based on a WUFI-model created by Månhardt and Odén (2020). Their model is based on an existing building, which is presented in section 3.3, as the validation object. The model of the validation object was validated with measurements of relative humidity and temperature of the air in the cavity of the existing building.

In the following headings 5.3.5.1-5.3.5.7, the construction of the WUFI-model for this study is presented, also called the Study Model.

The model has been adjusted to avoid numerical problems (5.3.4), it has been optimized by convergence studies (5.3.7) to work as efficient as possible, and it has been validated (5.3.6) by the model of Månhardt and Odén (2020).

5.3.1 Geometry

The top surface in the WUFI model is representing the boundary to the outdoor climate, and the bottom surface in the model is representing the boundary to the indoor climate. The vertical sides of the model are adiabatic boundaries, which means there are no heat or moisture fluxes through these sides. This is a standard setup for solving 1D problems in a 2D program. In WUFI, the geometry is defined in cells, each cell is given the properties of a material, and each cell consists of elements, which are defined in the Grid section (5.3.5.2). In the study, only 1D transports are studied. All 2D and horizontal effects are neglected. In the vertical direction (y-direction in WUFI) the materials are defined with the correct size according to the study object in section 3.4. In the horizontal direction (x-direction in WUFI) the cells of the model measure 1000 mm, to make sure the model fits the size of the sources from the 1D model. Deep materials like insulation, are split into several different cells with the same material properties. The air cavity must be separated into smaller cells. These cells have different properties when it comes to moisture storage, to avoid numerical problems. More about the material properties in section 5.3.5.3, and numerical problems in section 5.3.4.

5.3.1.5 Grid

The model of Månhardt and Odén (2020) is created in WUFI Pro and is therefore in 1D. Because this study is executed in WUFI 2D, the 2D behaviour of the model must be simplified to the behaviour of a 1D model. The solution for this was to make the model with as few horizontal elements as possible (in the current WUFI version that means two elements). The grid in the vertical direction is built to be a copy of the grid of the validation model. Månhardt and Odén (2020) used 100 elements automatically generated as a "fine" grid, which means that the size of the cells becomes smaller closer to the border of the elements. When this is done in WUFI 2D a completely different grid is produced. Therefore, the grid in this study had to be adjusted manually for every cell to be as similar as possible to the grid of the validation model. The grid is presented in figure 5.5 wherein reversed order where the exterior part is at the bottom of the list. Every cell is composed of two parts, a and b. Therefore, the minimum size of a cell is two elements, both in the x- and y-direction. The exponential factor (Exp. Fac) expresses if the size of elements in the cell is increasing, decreasing or are kept the same. The two last columns show the size of the first and last element of the current half-cell.

Min. # of elements: x: 2 y: 2 Max. # of Elements: x: 3 y: 100 Total # of Elements: x: **2** y: **90**

ID	Width	No. El.	Exp. Fac.	First El.	Last El.
X-1a	500	1	1	500	500
X-1b	500	1	1	500	500
Y-1a	6.25	1	1	6.25	6.25
Y-1b	6.25	1	1	6.25	6.25
Y-2a	22.5	4	0,9	6.5426	4.7696
Y-2b	22.5	14	0,9	2.9174	0.7416
Y-3a	0.5	1	1	0.5	0.5
Y-3b	0.5	1	1	0.5	0.5
Y-4a	45	14	1,1	1.6086	5.5533
Y-4b	45	4	1,1	9.6962	12.9056
Y-5a	45	2	1	22.5	22.5
Y-5b	45	2	1	22.5	22.5
Y-6a	45	2	1	22.5	22.5
Y-6b	45	2	1	22.5	22.5
Y-7a	45	4	0.9	13.0852	9.5391
Y-7b	45	7	0.8	11.3883	2.9854
Y-8a	0.5	1	1	0.5	0.5
Y-8b	0.5	1	1	0.5	0.5
Y-9a	22.5	5	1.3	2.4881	7.1062
Y-9b	22.5	5	0.7	8.1137	1.9481
Y-10a	0.5	1	1	0.5	0.5
Y-10b	0.5	1	1	0.5	0.5
Y-11a	11	4	0.9	3.1986	2.3318
Y-11b	11	9	0.9	1.7957	0.773
Y-12a	0.5	1	1	0.5	0.5
Y-12b	0.5	1	1	0.5	0.5
Y-13a	0.5	1	1	0.5	0.5
Y-13b	0.5	1	1	0.5	0.5

Figure 5.5. *The Grid in WUFI 2D.*

Note: The grid of the model is WUFI. The first column expresses which cell. All cells are divided into 2 half-cells: X-1 are divided into X-1a and X-1b. The second column expresses the width of the half-cell. The third column expresses the number of elements the half-cell is built of. The fourth column expresses if the size of the elements is increasing in size (>1), decreasing in size (<1) or is all the same in size (=1). The two last columns show the size of the first and the last element of the half-cell.

5.3.1.6 Materials

The main principle of defining the materials of the model is to use the same properties Månhardt and Odén (2020) used in their study. The materials are presented in table 5.3.

Table 5.3. *The Material Parameters of the Study Model.*

Building component	**Name of material in the WUFI database**	**Thickness [mm]**	**Changed properties (new values)**
Roofing sheet	Roof Membrane V13	1	-
Roof underlayment	Weather resistive barrier (sd=0.2m)	1	-
Wooden board	Spruce, radial	22	-
Condensation layer	Air layer 50 mm	1	-
Air Cavity	Air layer 50 mm, without additional moisture capacity	45	Diffusion resistance: $\mu = 0.1$
Condensation layer	Air layer 50 mm	1	-
Insulation: Mineral wool	ISOVER ULTIMATE Klemmfilz - 035	80 80 80 80	Heat conductivity: $\lambda = 0.034$ W/mK Density: $\rho = 30$ kg/m^3
Vapour barrier	Vapour barrier (sd=100m)	1	Diffusion resistance: $\mu = 75000$
Insulation: Mineral wool	ISOVER ULTIMATE Klemmfilz - 035	45	$\lambda = 0.034$ W/mK $\rho = 30$ kg/m^3
Wooden board	Spruce	22	-

Note: The position of materials in the table relates to the position of the material in the cross-section, where the uppermost material is towards the exterior.

The insulation is divided into 4 layers with the same material properties. The reason for this is to avoid numerical problems. The air cavity is divided into 3 layers, where the middle layer is the thickest. This layer represents the air mass that is often exchanged for outdoor air. In WUFI this material can only store very little moisture. The two outer condensation layers have higher moisture storage capacity, which is needed if condensation would take place at the surface of the cavity. All the air layers must be chosen with the name-ending '50 mm' because this gives the correct heat conductivity and diffusion resistance for an cavity with of 50 mm stagnantly air. The changes done to the material properties are the same that Månhardt and Odén (2020) did to adjust the validation model to the validation object. In reality, air in a ventilated cavity is not stagnant, and can not be separated into distinct layers, it is more like a gradient. Therefore, a smaller diffusion resistance is used in the middle air layer to allow easier transport of moisture to the outer layers.

5.3.1.7 Initial Conditions

Initial values of temperature and relative humidity are needed for every cell in the model before the simulation can start. The initial values used are the same as in the study of Månhardt and Odén (2020). The temperature of all materials was 18 °C and for relative humidity, 80% was used for all materials.

The tons of calculations required for a 90-year-WUFI-simulation demand a lot of computer power. In this study, a calculation computer with a lot of memory has been used. Still, the maximum length of simulations in WUFI with this model is 30 or 40 years depending on the case. Therefore, three separated simulations must be executed to simulate 90 years, and three sets of initial values are needed. The solution to this is to start the next simulation period one year earlier, making the first and last years of the two simulations overlap. This will make the model reach a periodical steady-state with its environment. For example: Simulation 1: 2010-2040; Simulation 2: 2040-2070. This means that calculations are done for the year 2040 in both simulation 1 and simulation 2, but in the latter, the data from that year will not be used. It is only needed to make the model adjust itself.

5.3.1.8 Surface and Climate

The vertical sides of the model are defined as adiabatic because no transport is considered in this direction. On the top of the model, the outdoor climate is defined, and on the bottom of the model, the indoor climate is defined.

The outdoor climate is imported as a climate file (.wac) which has been created by the data from Nik (2010) by a Matlab code (5.2.4.1). The radiation data of the climate file is all defined as the normal vector to a horizontal roof. WUFI will calculate the amount of radiation on the roof according to the inclination and orientation that is entered into the software. The heat transfer coefficient is defined as wind dependent. The shortwave radiation absorption (0.87) and longwave radiation emission (0.9) are defined the same as Månhardt and Odén (2020) did in their study. These represent the radiative properties of the surface's material and colour. Explicit Radiative Balance was used which is shown in figure 5.6. This is the most advanced calculation mode in WUFI for calculating radiative balances. The reason for using this mode is that it will calculate the radiative transfer coefficient for each step depending on the longwave counter-radiation, the reflection of longwave radiation and shortwave radiation on the ground and a cloud index. The values are almost the same as the default setup off WUFI 2D with small changes in ground shortwave reflectivity (from WUFI standard 0.20 to 0.26) according to the setup of Månhardt and Odén (2020). If this mode is not used, WUFI would use a standard value of 6.5 W/m^2K as the radiative transfer coefficient.

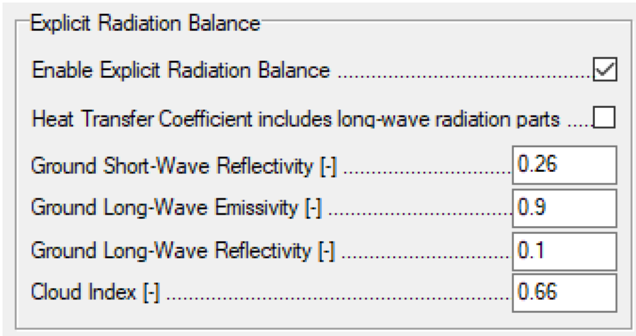

Figure 5. 6. *The Numerical Settings for Radiation Balance.*

Note: When using WUFI's advanced mode for calculating radiation balance the ground reflectivity for shortwave and longwave radiation must be added, as well as the ground emissivity of the longwave radiation. For cloud index, a standard value is used.

The orientation of the roof must be defined if the roof is inclined, according to table 5.4.

Table 5. 4. *The Setup for Orientations in WUFI.*

	South	West	North	East
Orientation in WUFI	0°	90°/-270°	-180°/180°	-90°/270°

Orientation and inclination are affecting the amount of global shortwave radiation and direct shortwave radiation hitting the roof. The inclination of the roof will also affect the effect of rain on the roof. The adhering fraction of rain uses the standard value for the inclined roof (0.7) because the roof is not flat (1) and not vertical (0). The driving rain coefficient used is according to WUFI's pre-defined setting because rain is considered to only hit the roof from above (figure 5.7).

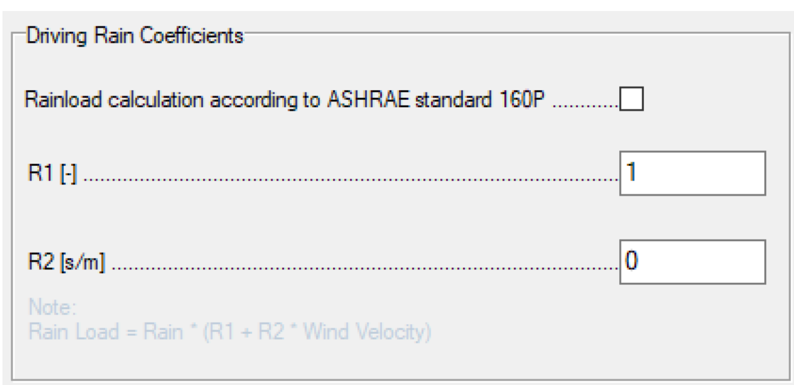

Figure 5.7. *The Driving Rain Coefficients.*

Note: Driving rain setup in WUFI

5.3.1.9 Sources

Three gains and losses are added as sources in the model:

- Leakage from rain as a moisture source
- Air Exchange Rate of outdoor air in the cavity as an air change source
- Infiltration of moisture from indoors to outdoors as a moisture source.

The source for moisture gains from leakage of rain is placed in the element closest to the cavity on the exterior side, the blue area in figure 5.8. The sources have the same width as the model (1000 mm) but only 1 mm in height or one element in size. The percentage of driving rain that reaches the sources is set at 0.1 % according to Wallentén (2018). If rain leakage is not the actual topic, a value between 0.1-0.5% is recommended for roofs. The value is arbritary, but adds some leakage to the construction. The relating boundary of the source is the outdoor climate. The driving rain coefficient is defined according to the standard procedure of WUFI 2D shown in figure 5.7.

The source for the air exchange rate is entered by the exported file of the air exchange rate (5.2.4.2). The relating boundary of the source is the outdoor climate. The source is applied to the air material without extra moisture capacity. It is therefore 45 mm in height. The width of the source is the same as the model (1000 mm) and is applied as the turquoise area in figure 5.8. According to The Wufi-Team (2014), the sources are equally distributed in proportion to the area.

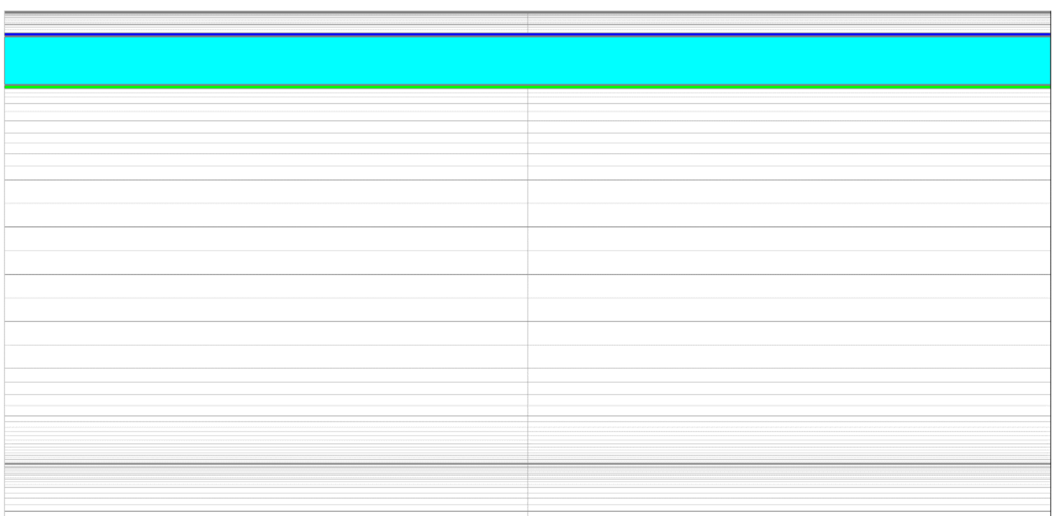

Figure 5.8. *The Sources in The Grid of The Model.*

Note: The source for driving rain is dark blue and is added in the wood right above the air cavity. The source for air exchange rate is turquoise and is added to the air cavity of 45 mm height. The source for moisture infiltration is green and is added to the climate board right below the air cavity. Between all the sources there is a condensation layer of 1 mm without an added source.

The source for infiltration is entered by the exported file of moisture infiltration from indoors to outdoors (5.2.4.3). No relating boundary is needed. The source is applied to the element closest to the cavity on the interior side. The sources have the same width as the model (1000 mm) but only 1 mm in height or one element in size and is applied as the green area in figure 5.8.

5.3.1.10 Computational Parameters

The standard choice of settings for WUFI 2D had to be adjusted to fit the validation model which used WUFI Pro. On the advanced settings, the maximum number of iterations MAXIT was changed from 1500 to 500, and the convergence criterium ε was changed from 5e-3 to 5e-6. The reason for this is that WUFI 2D and WUFI Pro use different standard settings.

5.3.2 Validation of the WUFI-model

The study model was validated by comparing results with the validation model of Månhardt and Odén (2020).

The following validations were carried out:

- Comparing results from the airflow model of Månhardt and Odén (2020) with the modified model used in this study.
- Comparing results from the moisture infiltration model of Månhardt and Odén (2020) with the new model used in this study.
- Comparing results from the WUFI model of Månhardt and Odén (2020) with the validation model of this study.

The airflow model and the moisture infiltration model show the same results for the same indata.

Comparing the WUFI models on the other hand did not give completely consentient results as shown in figures 5.9-5.12. The process of validating the model is shown in figure 5.8. Available data was input data for WUFI and output data from WUFI. The principle of the validation was that the input data from Månhardt and Odén (2020) was used in the validation model of this study. The mould growth index was used on the WUFI output data from the validation model and the WUFI output data from Månhardt and Odén (2020). The mould growth index from the two different models was compared.

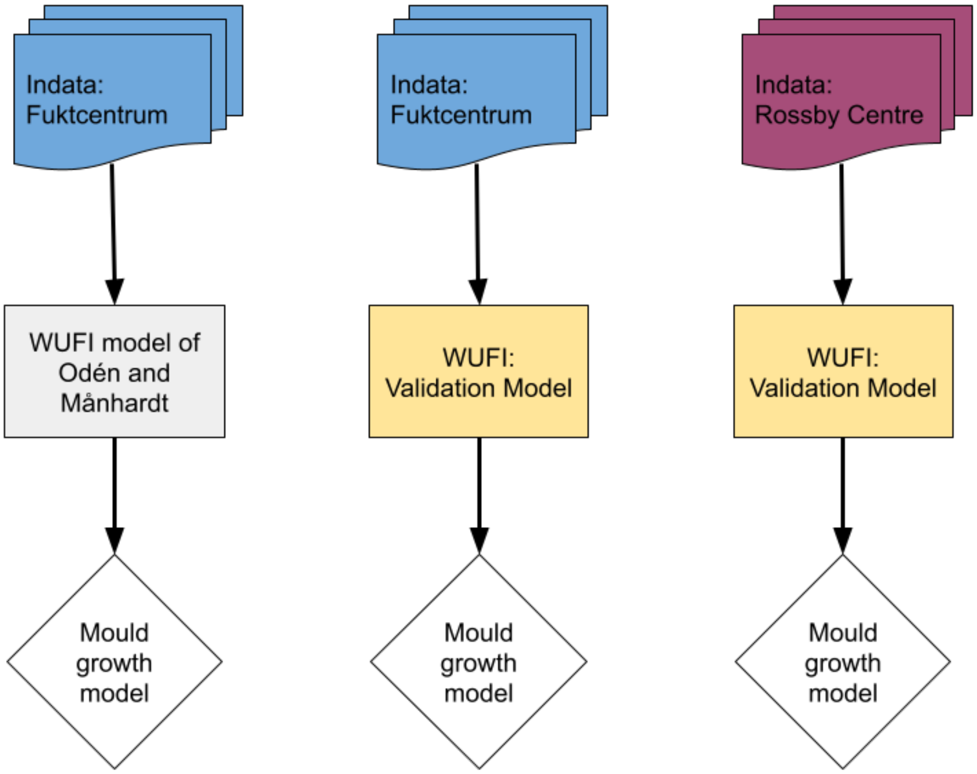

Figure 5. 9. The Process Of Validating The Model

Note: The left pipe shows how data from Fuktcentrum was used by Månhardt and Odén (2020) in WUFI for calculating T and RH. The middle pipe shows how data from Fuktcenturm was used with the validation model developed in this study to achieve T and RH. The right pipe shows how data from Rossby Centre was used with the validation model to achieve T and RH. The mould growth model was used to compare the MGI of all the three simulations resulting in the comparison in figures 5.10-5.12.

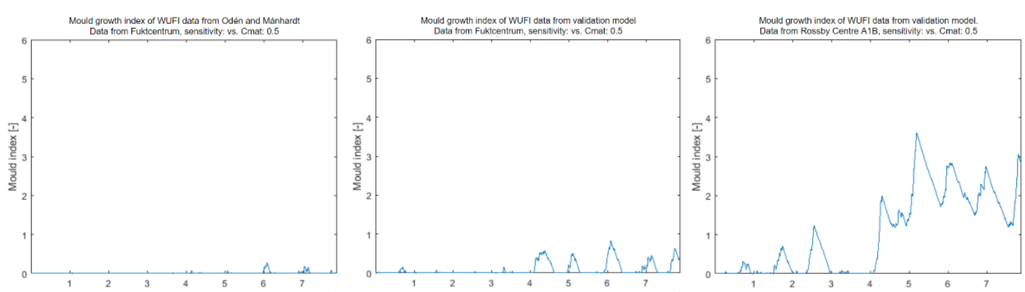

Figure 5. 10, Figure 5. 11 & 5. 12 Comparison of the Model of Månhardt and Odéns and the Validation Model.

Note: The left plot shows the mould growth of the results from WUFI Pro simulations of Månhardt and Odén *(2020)* with weather data from Fuktcentrum. The middle plot shows the mould growth of results from WUFI 2D simulations of the validation model with weather data from Fuktcentrum. The right plot shows the mould growth of results from WUFI 2D simulations of the validation model with weather data from Rossby Centre. All data in the figures are for the same time period, year 1990 to year 1998.

The reason why the results were not the same is that there are some differences between WUFI 2D and WUFI Pro. Firstly, they are not generating the grids in the same way. This was solved by generating the 2D grid manually. Secondly, some settings exist in WUFI 2D that do not exist in WUFI Pro and the other way around. The absence of a comprehensive manual of the software makes it very hard to know what setting the software uses when the setting is missing. Settings that may have affected the results are:

- In the explicit radiation balance of WUFI 2D, there is a setting called *longwave radiation is a part of the heat transfer coefficient* (figure 5.6). This setting is missing in WUFI Pro. The assumption is that if the setting is used, the longwave radiation is not calculated, and is accounted for as a part of the heat transfer coefficient which is specified in the program. By unchecking the setting, it is assumed that the longwave radiation is calculated separately from the convective part of the heat transfer coefficient. This is also which is assumed to be done in WUFI Pro, and which is used in this study.
- Secondly, the sources are defined in another way in WUFI 2D than in WUFI Pro. Different units are used for the data. In WUFI Pro there are settings defining how the sources are distributed on the elements to which it is applied. These settings are not available in WUFI 2D. According to The WUFI-Team (2014), sources are always distributed evenly in proportion to the areas of the elements. Because of the confusion with the different units, it is assumed that the source is applied most realistically on a model that has a width of 1000 mm because in WUFI Pro the source units are by m2, but this is hard to verify.
- Thirdly, there are many more advanced computational settings in WUFI 2D than in WUFI Pro. By reading on forums and using a trial and error procedure it was found that the MAXIT has to be 500 and the convergence criterium 5e-6 (section 5.3.5.7). The difference between figure 5.11 and 5.12 is reasonable because different data sets are used and both are validated (chapter 2).

The construction of the study model in section 3.4 is based on the validation model (section 3.3). The construction is slightly different. The main difference is that the study model has a lower amount of insulation. In table 5.5 the material properties used in validating the model are presented. The difference from the materials presented in section 3.4 is that the two condensation layers in the air cavity are 2 mm each instead of 1 mm, additional insulation called Climate Board has been added right inside of the cavity and the insulation has changed size from 380 mm to 485 mm.

Table 5. 5. *The Material Parameters for the Roof in the Validation Model.*

Building component	**WUFI material**	**Layer thickness [mm]**	**Changed properties (new values)**
Roofing sheet	Roof Membrane V13	1	-
Roof underlayment	Weather resistive barrier (sd=0.2m)	1	-
Wooden board	Spruce, radial	22	-

Condensation layer	Air layer 50 mm	2	-
Air Cavity	Air layer 50 mm, without additional moisture capacity	45	Diffusion resistance: $\mu = 0.1$
Condensation layer	Air layer 50 mm	2	-
Climate board	ISOVER INTEGRA AP Supra - 035	70	Heat conductivity: $\lambda = 0.033$ W/mK
Insulation: Mineral wool	ISOVER ULTIMATE Klemmfilz - 035	97 97 97 97 97	Heat conductivity: $\lambda = 0.034$ W/mK Density: $\rho = 30$ kg/m^3
Vapour barrier	Vapour barrier (sd=100m)	1	Diffusion resistance: $\mu = 75000$
Insulation: Mineral wool	ISOVER ULTIMATE Klemmfilz - 035	45	$\lambda = 0.034$ W/mK $\rho = 30$ kg/m^3
Wooden board	Spruce	22	-

Note: The position of materials in the table relates to the position of the material in the cross-section, where the uppermost material is towards the exterior.

5.3.3 Convergence of the WUFI-model

A numerical model gets more accurate results when the time step is smaller, when the elements are smaller, and the number of iterations is greater. But every extra calculation takes time and computer power to execute. Therefore, the convergence of different parameters must be found. This means that when the parameter is changed to a more computational have parameter, the results are still the same, for example, Doing the same calculations for the time step of 30 minutes instead of 60 minutes. If the results are almost the same, the time step of 60 minutes can be used, and the calculation time can be cut by half.

Convergence studies have been performed on the models with satisfying results. In some cases, studies had to be done again to ensure the result is reliable.

5.4 Mould Growth Index

A mould growth index is used for evaluating the risk of moisture-related damage in the construction. The actual growth cannot be calculated or predicted, but the possibility of growth can be calculated by a mould growth index.

The mould growth index is evaluated with a Matlab code following the equations in section 4.4. The input needed is the temperature of the evaluated surface and relative humidity at the surface. With these parameters, the mould growth index is calculated as a 7-graded scale where values below 3 mean that the mould growth is only visible in a microscope.

5.5 Parameters to Study

A parameter study was performed to get an understanding of what measures affect the future mould growth index. The number of cases to evaluate had to be limited with the time of the project in consideration. Therefore, the focus has been on the worst cases and the cases that differ the most from each other. Focus has also been on Stockholm as the standard case with which all other cases have been compared to. The reason for this is to decrease the number of simulations and calculation that has to be done, but also because Stockholm is the only case that has been validated in the study of Månhardt and Odén (2020).

Firstly, a comparison between the emission scenarios A1B, A2 and B1 are performed.

Secondly, four orientations are studied: South, north, east, and west. Already before the study, some knowledge is known about the weather data. Shortwave radiation is always the most in the south and the least in the north. At night, the north-facing surface surfer the most from longwave radiation cooling because the roof gets less heated by shortwave radiation in the daytime than in the other orientations.

Thirdly, different locations are studied: Lund, Gothenburg, Stockholm and Östersund. Knowledge before the study is that the more southern the higher the mean outdoor air temperature is, which means that the temperatures decrease in the following order Lund, Gothenburg, Stockholm and Östersund. In the study of locations, only three orientations are compared: south, east and north. They were chosen before the west because the west has similar results to the east but with a lower mould growth index.

Fourthly, the inclination of the roof is studied: 30° and 45°. In all other studies, 30° is used. Changing the roof inclination will change the airflow in the cavity as well as the view factor of the roof, resulting in a different amount of radiation striking the roof. The inclinations of 30° and 45° are considered commonly used in Sweden. The north and south directions are studied because the north is considered the worst case, and the south is the case heated the most with shortwave radiation.

Fifthly, a constant airflow in the cavity is compared with variable airflow. In Swedish literature, a low and constant value of the air exchange rate is recommended. A value of constant low airflow is therefore compared to the variable airflow rate to understand differences. The east orientation is compared because it has a worse mould growth index than the west, and there is more wind from the east than from the north.

Sixthly, in the case of moisture damage relating to a large longwave night cooling, it is of interest to evaluate the effect of adding additional insulation on the exterior side of the cavity. The inside of the cavity will thereby not be cooled or heated at the same magnitude, by radiation, as if there was no external insulation. The north orientation is studied because that is where the most severe night cooling occurs.

At last, the colour of the roof is affecting the properties of absorption and reflection which is affecting the temperature of the construction. The dark-coloured roof used in the other studies is compared with a reflective bright-coloured steel roof.

6
Result

In this chapter, the results are presented. There are a few different results:

- Outdoor climate data, which is achieved from Rossby Centre. The data presented are properties of the outdoor air: temperature, vapour content and relative humidity.
- Exposed surface climate data which consists of temperatures and relative humidity of the exposed surface is calculated by numerical simulations in WUFI. The data is complemented by data on the air exchange rate in the cavity and the moisture infiltration rate from indoors to outdoors.
- Mould growth index, which is calculated based on the temperature and relative humidity of the surface of the exposed material.

A few different scenarios have been tested in the study. The study uses Stockholm as the standard and makes a parametric study concerning a standard case called STO STD.

STO STD is the following:

- Emission scenario: A1B
- Period: the year 2010-2100
- Location: Stockholm
- Inclination: 30°
- Colour: Dark and mate metal sheets
- Variable air exchanges rate based on the airflow model

To understand the effect of different parameters a parametric study is performed by trying the following parameters according to section 5.5:

Study A: Comparing the emission scenarios A1B, A2 and B1 for orientation south, north, west, and east in Stockholm year 2010-2100.

Study B: Roof orientations: south, north, west, and east in Stockholm year 1980-2100.

Study C: Locations with different climates: comparing Gothenburg, Lund, Stockholm and Östersund for the north and east orientations for Stockholm year 2010-2100.

Study D: Roof inclinations: comparing 30° and 45° for the south and north orientation in Stockholm year 2010-2100.

Study E: Constant Cavity Airflow: Comparing a constant air exchange rate of 25 1/hr with the varying air exchange rate achieved from the airflow model for the east-facing roof in Stockholm year 2010-2100.

Study F: Adding extra 100 mm insulation on the exterior side of the cavity for the south orientation in Stockholm year 2010-2100.

Study G: Changing the exterior colour on the roof from dark and mate to bright and reflective for the south, east and north orientations in Stockholm year 2010-2100.

- Dark-coloured roof longwave emissivity: 0.9; shortwave absorptivity: 0.87
- Bright-coloured roof longwave emissivity: 0.27; shortwave absorptivity: 0.5

6.1 The Outdoor Climate of Stockholm

In figures 6.1-6.3 the temperature, relative humidity, and vapour content of outdoor air for Stockholm are presented. The shaded grey lines represent the hourly fluctuations, the turquoise lines represent the variations of monthly mean values, and the blue line represents the yearly mean. In the long run, an increase in the yearly mean of the temperature and the vapour content occurs. Because the increase happens in both temperature and vapour content, it means that the relative humidity is relatively constant, or even increases slightly, otherwise, it would decrease according to section 4.2.3.

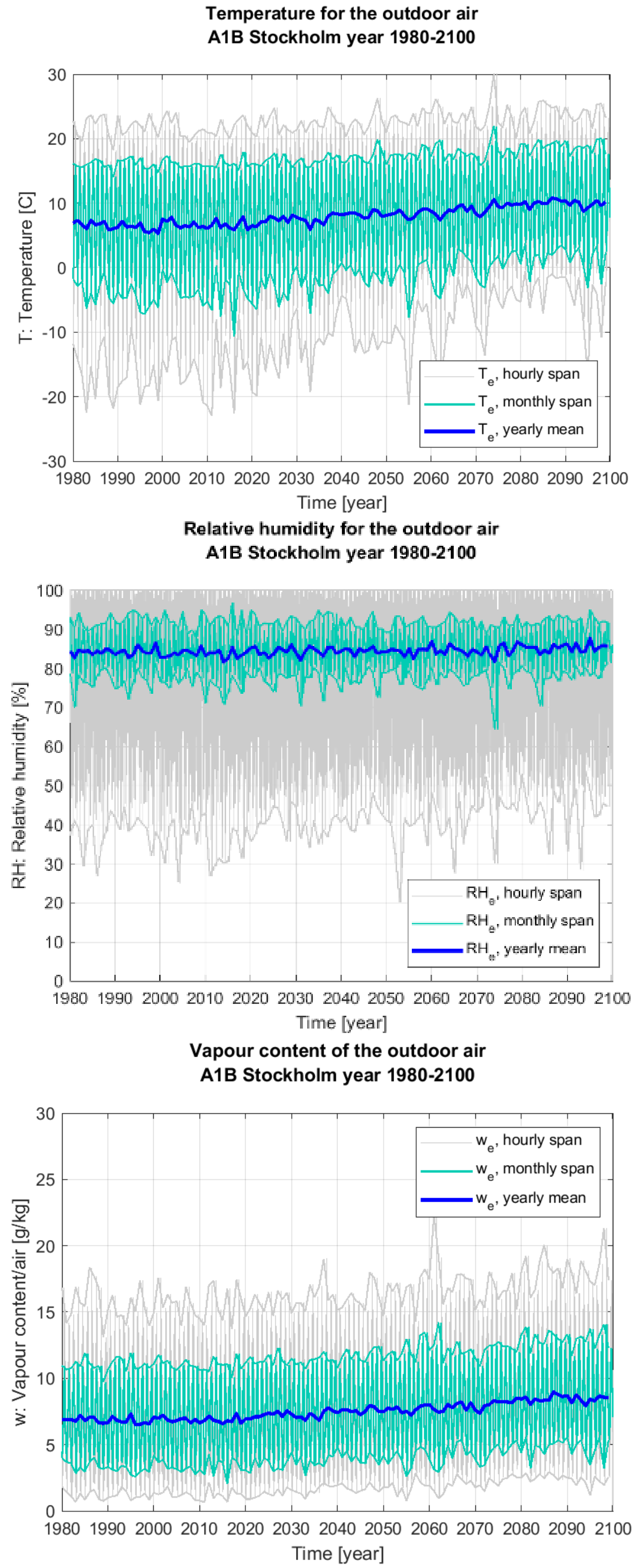

Figure 6.1, *6. 2* & 6. 3*. The Outdoor T of STO; The Outdoor RH of STO; The Outdoor w of STO*

Note: All the plots show data for the year 1980-2100 for Stockholm. The plot to the left shows outdoor air temperature. The plot in the middle shows the outdoor air's relative humidity. The plot to the right shows the vapour content of the outdoor air. The blue line represents the yearly mean, the turquoise represents the span of the monthly mean, and the grey lines are the span of hourly values.

6.2 Study A: Emission Scenarios

In this study, three emission scenarios, A1B, A2 and B1 are compared to each other. Scenario B1.

In figures 6.4 and 6.5, the temperature and relative humidity of an STO STD for emission scenarios A1B, A2 and B1 are compared. The yearly means of each scenario are plotted with differently coloured lines. A1B is dashed black, A2 is dashed orange and B1 is turquoise.

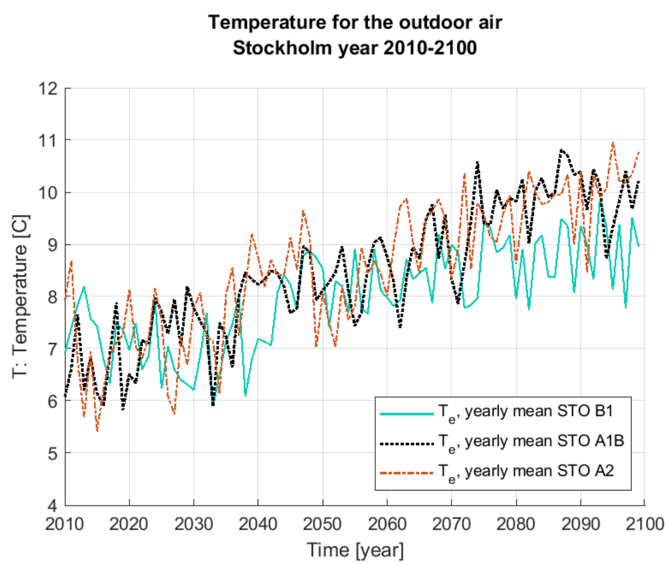

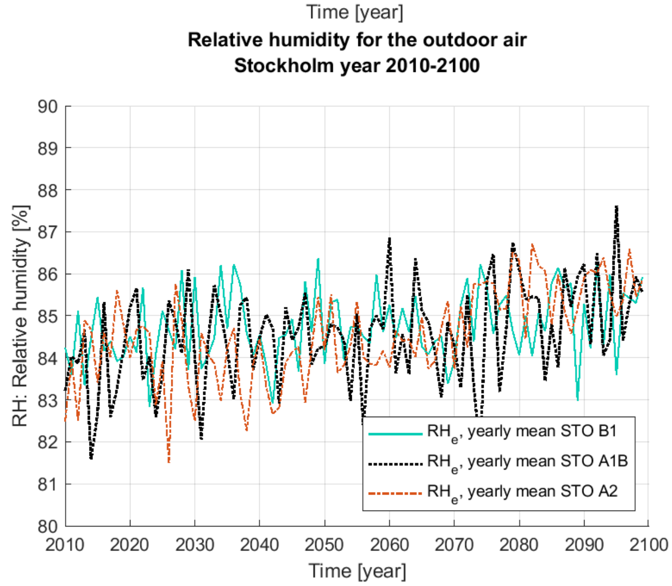

Figure 6.4-6.5. *The Outdoor T of A1B, A2 and B1 for STO; The Outdoor RH for A1B, B2 and B1 for STO*

Note: The plots show yearly mean values for the emission scenarios A1B, A2 and B1 for STO STD. The left plot shows outdoor air temperatures, and the right plot shows outdoor relative humidity.

When comparing scenarios A1B, A2 and B1 the increase in air temperature is greatest in A2 and the least in B1. The development is varying but is seemingly following a linear increase in all the scenarios to the end of the century where B1 stops at a mean value of 9 °C, A1B at 10.2° and A2 at 10.8 °C. The relative humidity is also increasing in all the scenarios but is not completely linear. The B1 increases more than the other scenarios at the beginning of the century, but after a while, all the scenarios are at similar levels at the end of the century. Because the relative humidity is exponential dependent on the temperature it means that A2 has a higher vapour content than A1B which has a higher vapour content than B1 when they have the same relative humidity. The temperature of B1 is slowly decreasing at the beginning of the century, which is probably one reason why B1 has higher relative humidity in the same period.

In figure 6.6 the infiltration of STO STD is compared for the emission scenarios A1B, A2 and B1.

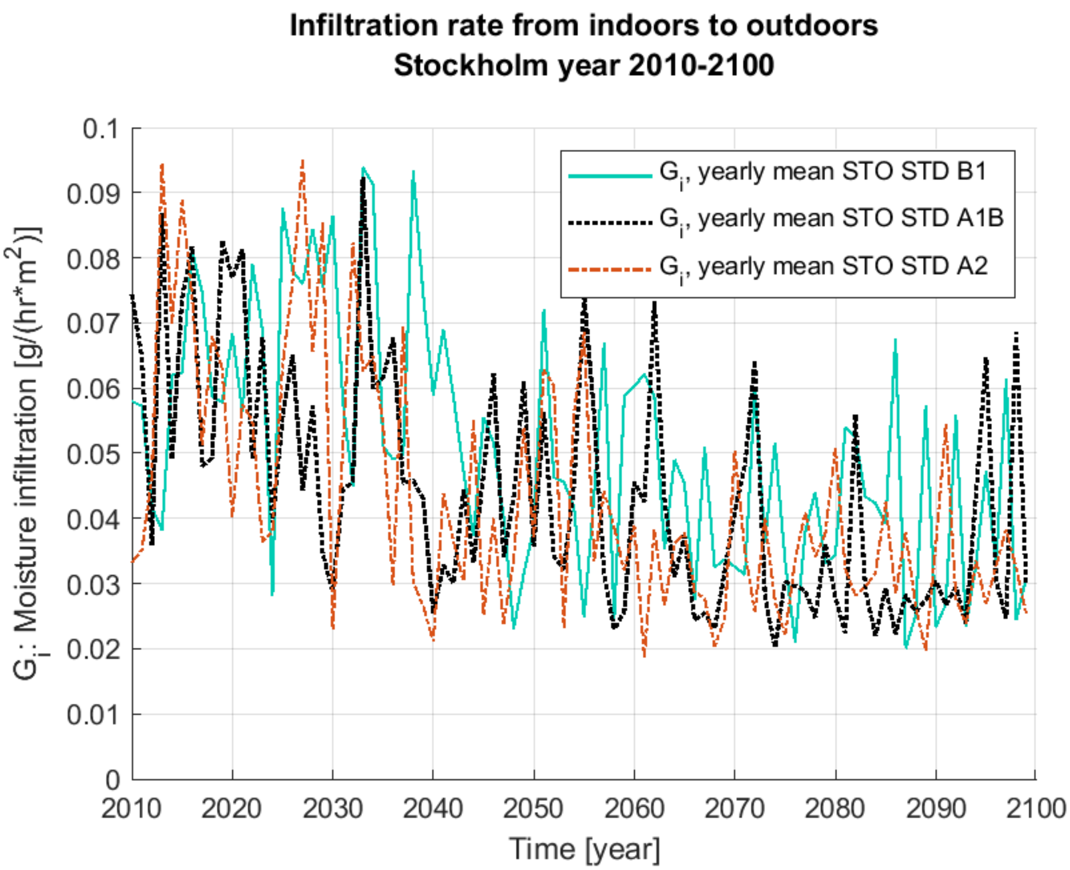

Figure 6.6. *The Moisture Infiltration Rate for A1B, A2 and B1 for STO*

Note: The plot shows the infiltration rate for emission scenarios A1B, A2 and B1 for STO STD.

In figures 6.7 and 6.8, the air exchange rate of STO STD for the emission scenarios A1B, A2 and B1 for the south- and east-facing roofs are compared.

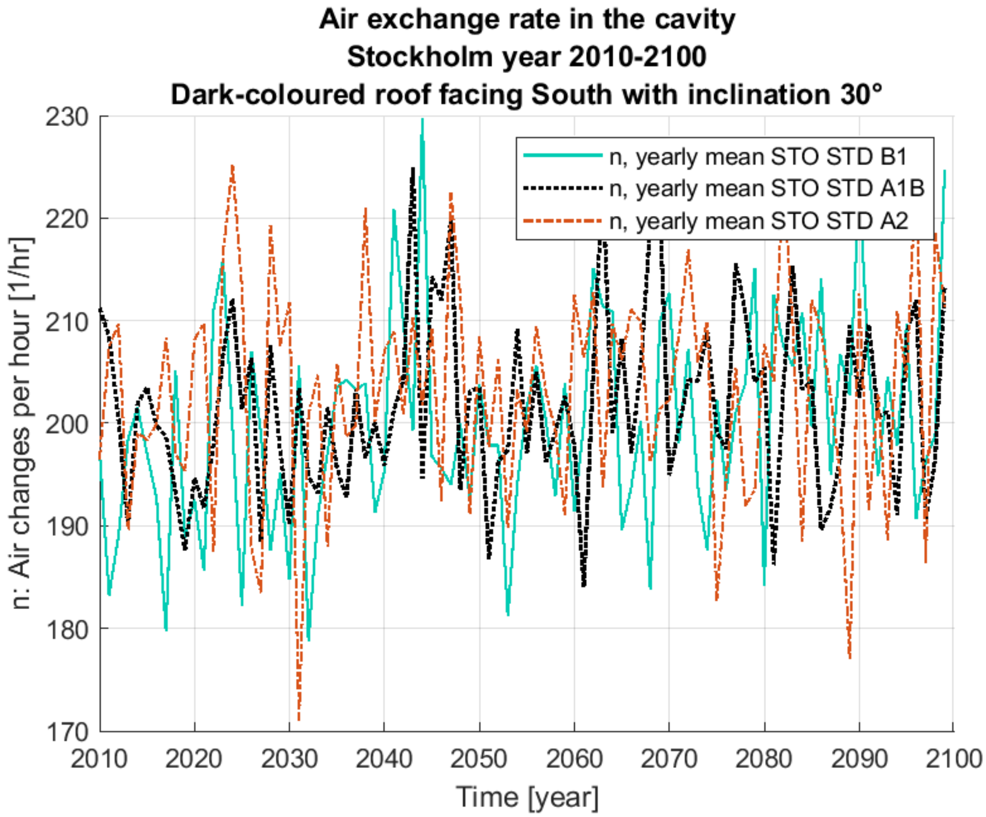

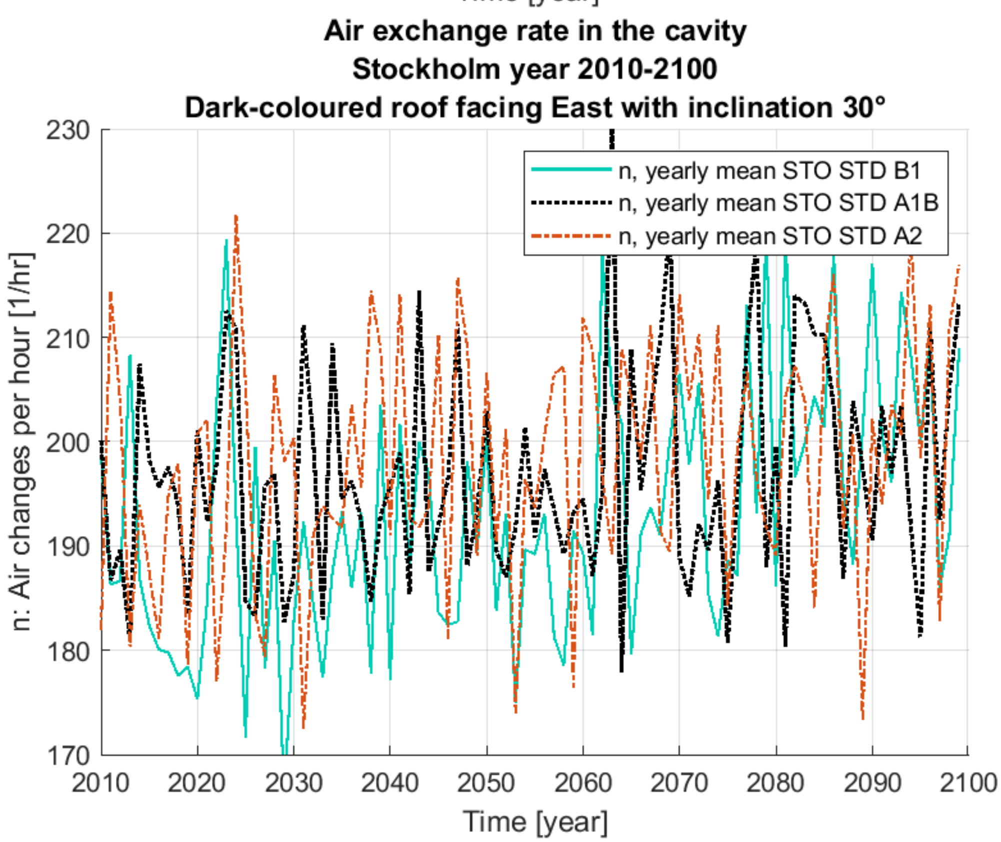

Figure 6.7-6.8. *The Air Exchange Rate for South and East, A1B, A2 and B1 for STO*

Note: The plot shows the air exchange rate for the emission scenarios A1B, A2 and B1 for STO STD. The left plot shows the south-facing roof and the right plot shows the east-facing roof.

In figures 6.9 and 6.10, the MGI of the south- and east-facing orientations for STO STD for emission scenarios A1B, A2 and B1 are compared. A1B and A2 are of the same magnitude and B1 has considerably lower MGI.

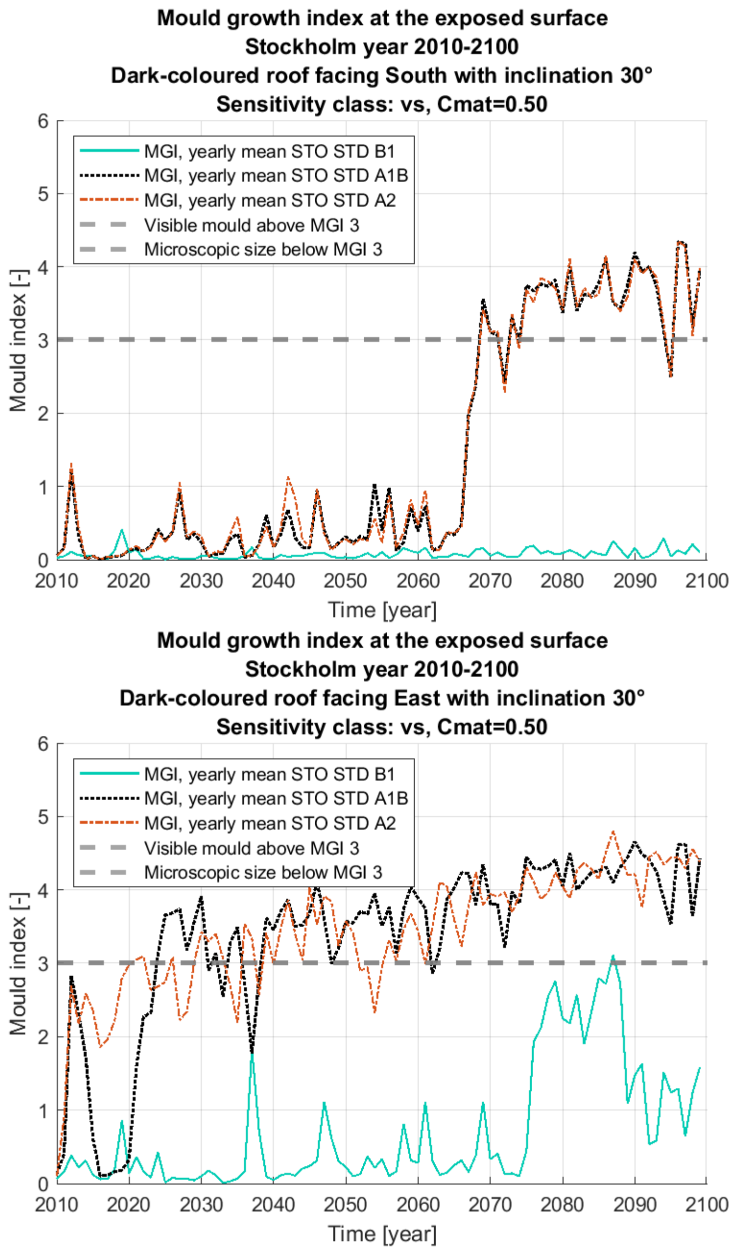

Figure 6.9-6.10. *The MGI for South and East, A1B, A2 and B1 for STO*

Note: MGI for the emission scenarios A1B, A2 and B1 for STO STD. The left plot shows the south-facing roof and the right plot shows the east-facing roof.

6.3 Study B: Orientation

Results for the four orientations south, north, west, and east are presented in this section. The moisture leakage is the same for all orientations and the air exchange rates are the same for south and north, and west and east. The STO STD is considered for the years 1980-2100.

6.3.1 South-facing Roof

The south-facing roof is exposed to more sun than the surfaces facing other orientations. In figures 6.11-6.14 the temperature and relative humidity of the exposed material is presented. In figure 6.11 the air exchange rate in the cavity is presented, and in figure 6.12 the rate of moisture infiltration is presented. The shaded grey lines represent the hourly fluctuations, the turquoise lines represent the variations of monthly mean values, and the blue line represents the yearly mean. The red line represents the yearly temperature and relative humidity of the outdoor air.

The temperature and relative humidity at the surface will result in an MGI which is presented in figure 6.15. The turquoise line represents the hourly fluctuations, and the blue line yearly mean. When the MGI has a value higher than the grey dashed line the mould is estimated to be visible, and if the MGI is below the grey dashed line, the mould is only at the microscopic size.

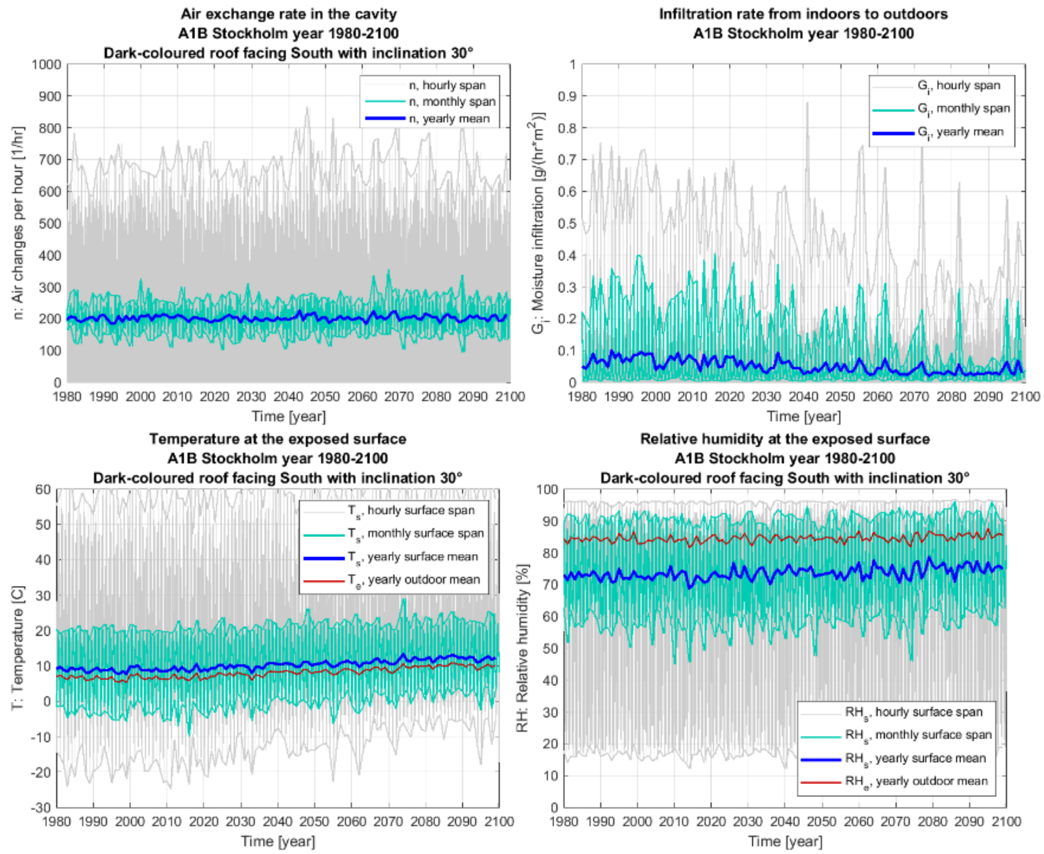

Figure 6.11, *6. 12, 6. 13 &* 6.14. *STO STD year 1980-2100 South: n, G, T and RH at the surface*

Note: The top left plot shows the air exchange rate. The top right plot shows the moisture infiltration rate. The bottom left plot shows the temperature at the exposed surface. The bottom right plot shows relative humidity at the exposed surface. The blue lines represent the yearly mean, the turquoise represents the span of the monthly mean, and the grey lines are the span of hourly values.

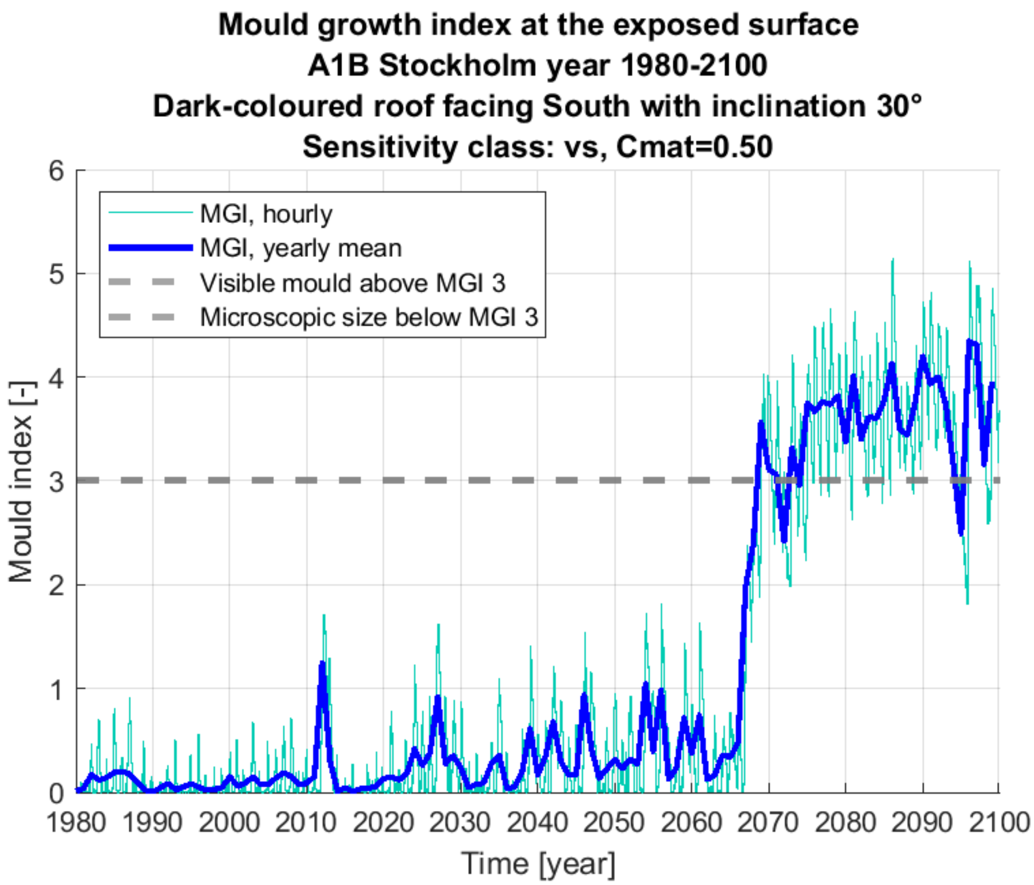

Figure 6.15. *STO STD year 1980-2100 South: MGI*

Note: The blue line represents the yearly mean, the turquoise represents the span of the monthly mean, and the grey lines are the span of hourly values. The dashed grey line of MGI 3 represents a threshold where the mould becomes visible.

6.3.2 North-facing Roof

The north-facing roof is exposed to less heating than the other orientations and is therefore cooled to lower temperatures at night. In figures 6.16-6.19 the temperature and relative humidity of the exposed material is presented. In figure 6.16 air exchange rate in the cavity is presented, and in figure 6.17 the rate of moisture infiltration is presented. The shaded grey lines represent the hourly fluctuations, the turquoise lines represent the variations of monthly mean values, and the blue line represents the yearly mean. The red line represents the yearly temperature and relative humidity of the outdoor air.

The temperature and relative humidity at the surface will result in an MGI which is presented in figure 6.20. The turquoise line represents the hourly fluctuations, and the blue line yearly mean. When the MGI has a value higher than the grey dashed line the mould is estimated to be visible, and if the MGI is below the grey dashed line, the mould is only at the microscopic size.

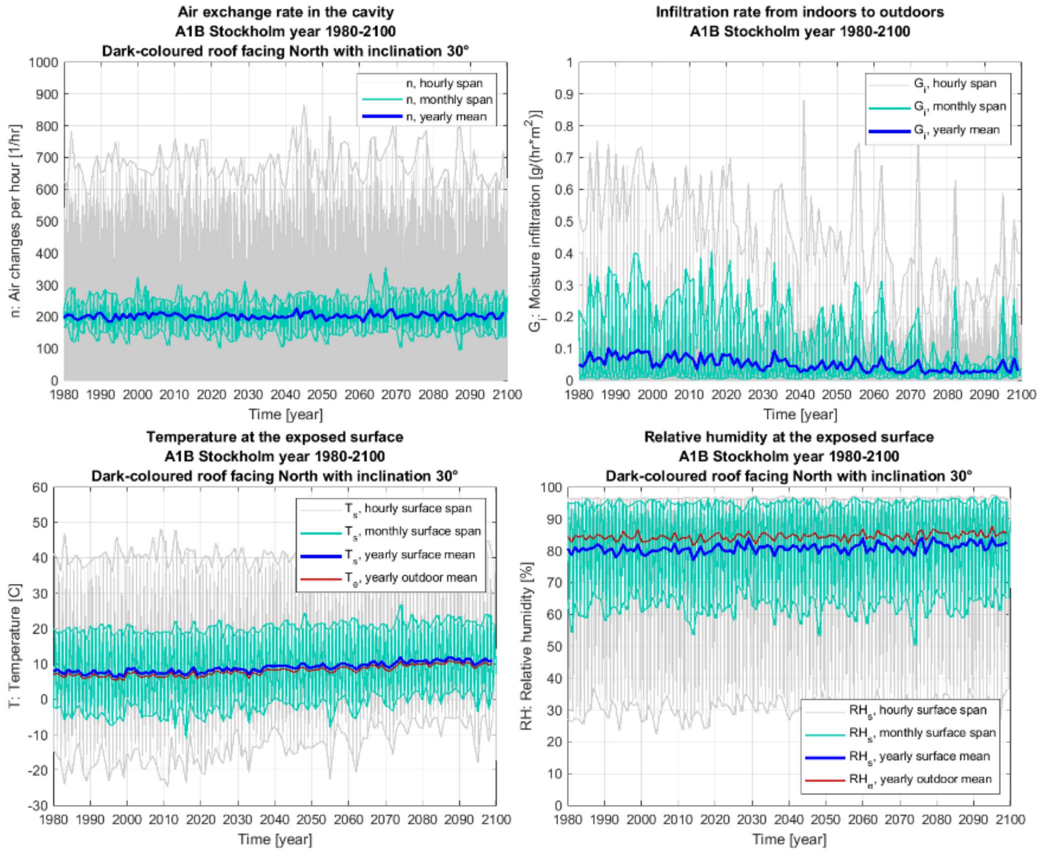

Figure 6.16, *6. 17, 6. 18 &* 6.19. *STO STD year 1980-2100 North: n, G, T and RH at the surface*

Note: The top left plot shows the air exchange rate. The top right plot shows the moisture infiltration rate. The bottom left plot shows the temperature at the exposed surface. The bottom right plot shows relative humidity at the exposed surface. The blue lines represent the yearly mean, the turquoise represents the span of the monthly mean, and the grey lines are the span of hourly values.

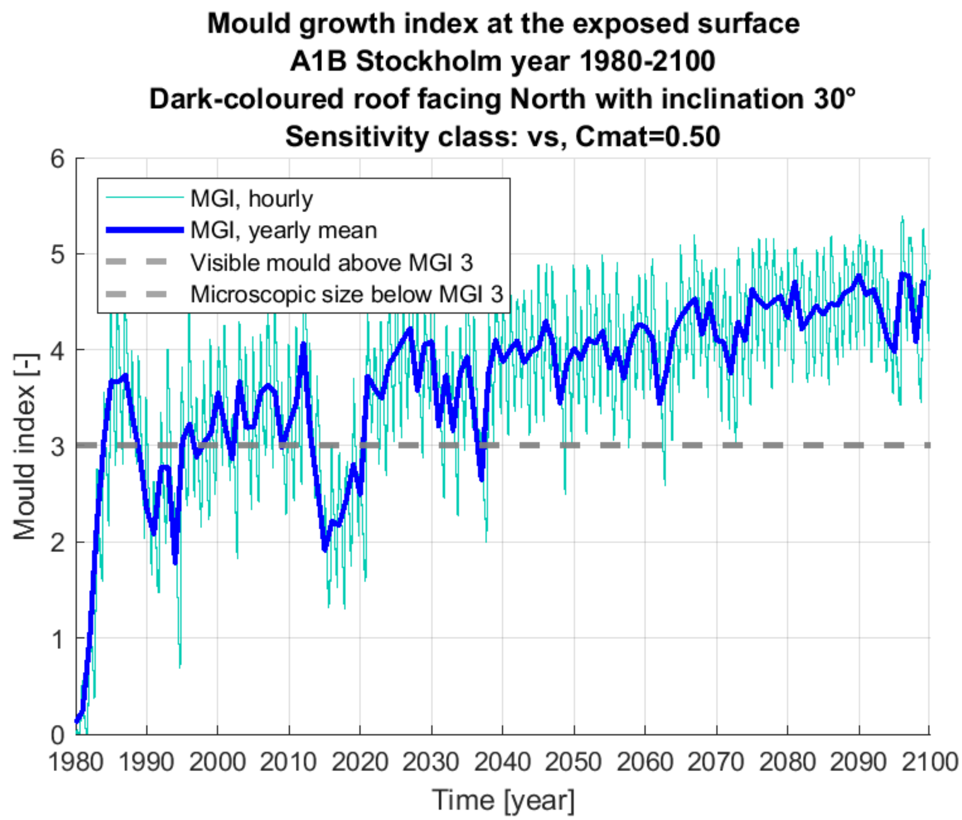

Figure 6.20. *STO STD year 1980-2100 North: MGI*

Note: The blue line represents the yearly mean, the turquoise represents the span of the monthly mean, and the grey lines are the span of hourly values. The dashed grey line of MGI 3 represents a threshold where the mould becomes visible.

6.3.3 West-facing Roof

The west-facing roof is exposed to more sun after midday than the surfaces facing other orientations. In figure 6.21-6.24 the temperature and relative humidity of the exposed material is presented. In figure 6.21 the air exchange rate in the cavity is presented, and in figure 6.22 the rate of moisture infiltration is presented. The shaded grey lines represent the hourly fluctuations, the turquoise lines represent the variations of monthly mean values, and the blue line represents the yearly mean. The red line represents the yearly temperature and relative humidity of the outdoor air.

The temperature and relative humidity at the surface will result in an MGI which is presented in figure 6.25. The turquoise line represents the hourly fluctuations, and the blue line yearly mean. When the MGI has a value higher than the grey dashed line the mould is estimated to be visible, and if the MGI is below the grey dashed line, the mould is only at the microscopic size.

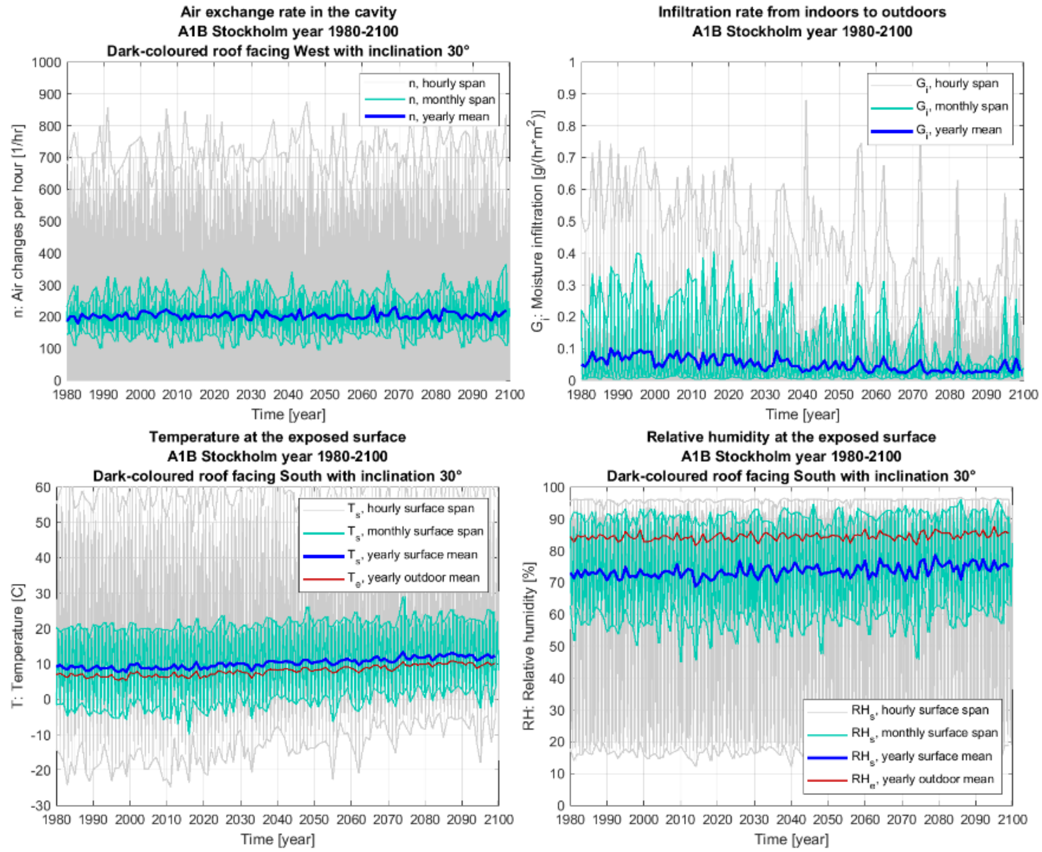

Figure 6.21, *6. 22, 6. 23* & 6.24. *STO STD year 1980-2100 West: n, G, T and RH at the surface*

Note: The top left plot shows the air exchange rate. The top right plot shows the moisture infiltration rate. The bottom left plot shows the temperature at the exposed surface. The bottom right plot shows relative humidity at the exposed surface. The blue lines represent the yearly mean, the turquoise represents the span of the monthly mean, and the grey lines are the span of hourly values.

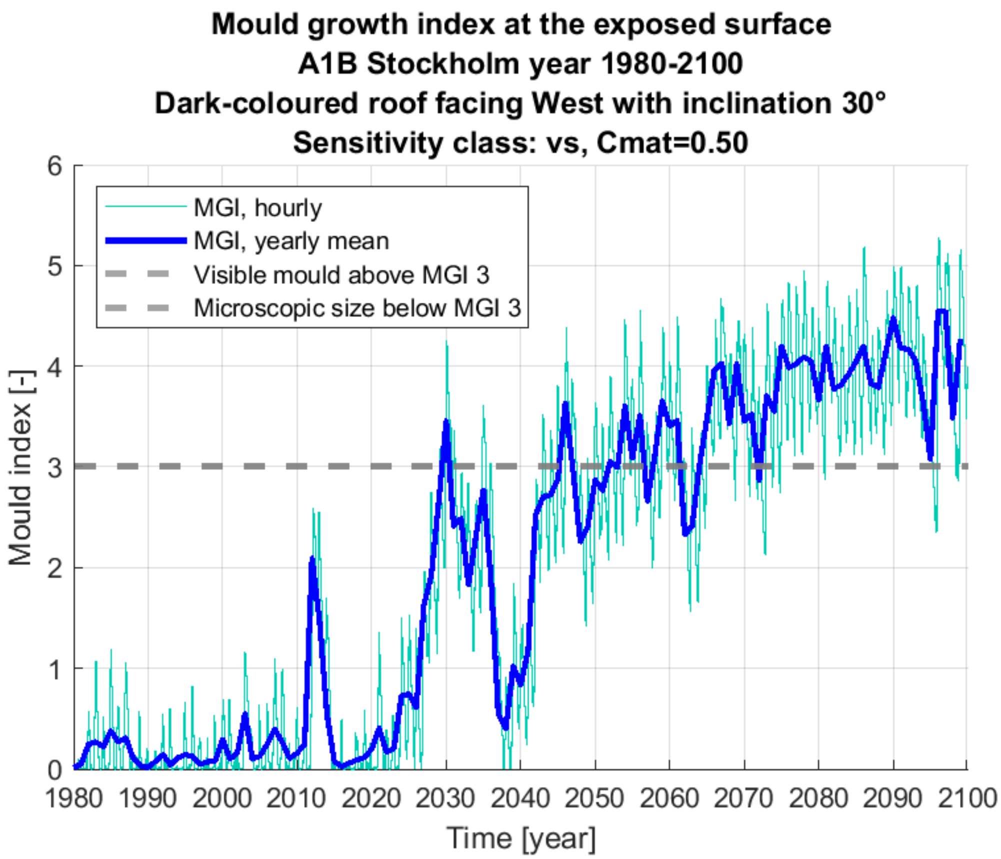

Figure 6.25. *STO STD year 1980-2100 West: MGI*

Note: The blue line represents the yearly mean, the turquoise represents the span of the monthly mean, and the grey lines are the span of hourly values. The dashed grey line of MGI 3 represents a threshold where the mould becomes visible.

6.3.4 East-facing Roof

The east-facing roof is exposed to more sun before midday than the surfaces facing other orientations. In figures 6.26-6.29 the temperature and relative humidity of the exposed material is presented. In figure 6.26 the air exchange rate in the cavity is presented, and in figure 6.27 the rate of moisture infiltration is presented. The shaded grey lines represent the hourly fluctuations, the turquoise lines represent the variations of monthly mean values, and the blue line represents the yearly mean. The red line represents the yearly temperature and relative humidity of the outdoor air.

The temperature and relative humidity at the surface will result in an MGI which is presented in figure 6.30. The turquoise line represents the hourly fluctuations, and the blue line yearly mean. When the MGI has a value higher than the grey dashed line the mould is estimated to be visible, and if the MGI is below the grey dashed line, the mould is only at the microscopic size.

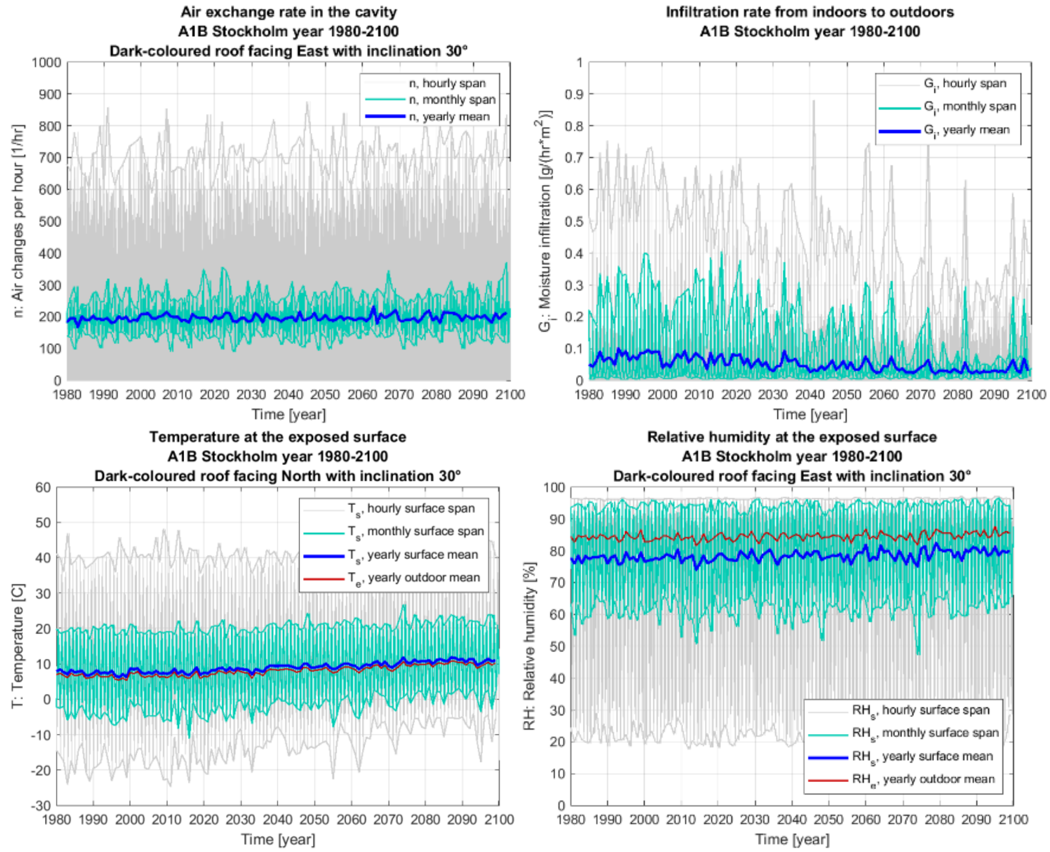

Figure 6.26, *6. 27, 6. 28 &* 6.29. *STO STD year 1980-2100 East: n, G, T and RH at the surface*

Note: All the plots show data for STO STD east for the year 1980-2100. The top left plot shows the air exchange rate. The top right plot shows the moisture infiltration rate. The bottom left plot shows the temperature at the exposed surface. The bottom right plot shows relative humidity at the exposed surface. The blue lines represent the yearly mean, the turquoise represents the span of the monthly mean, and the grey lines are the span of hourly values.

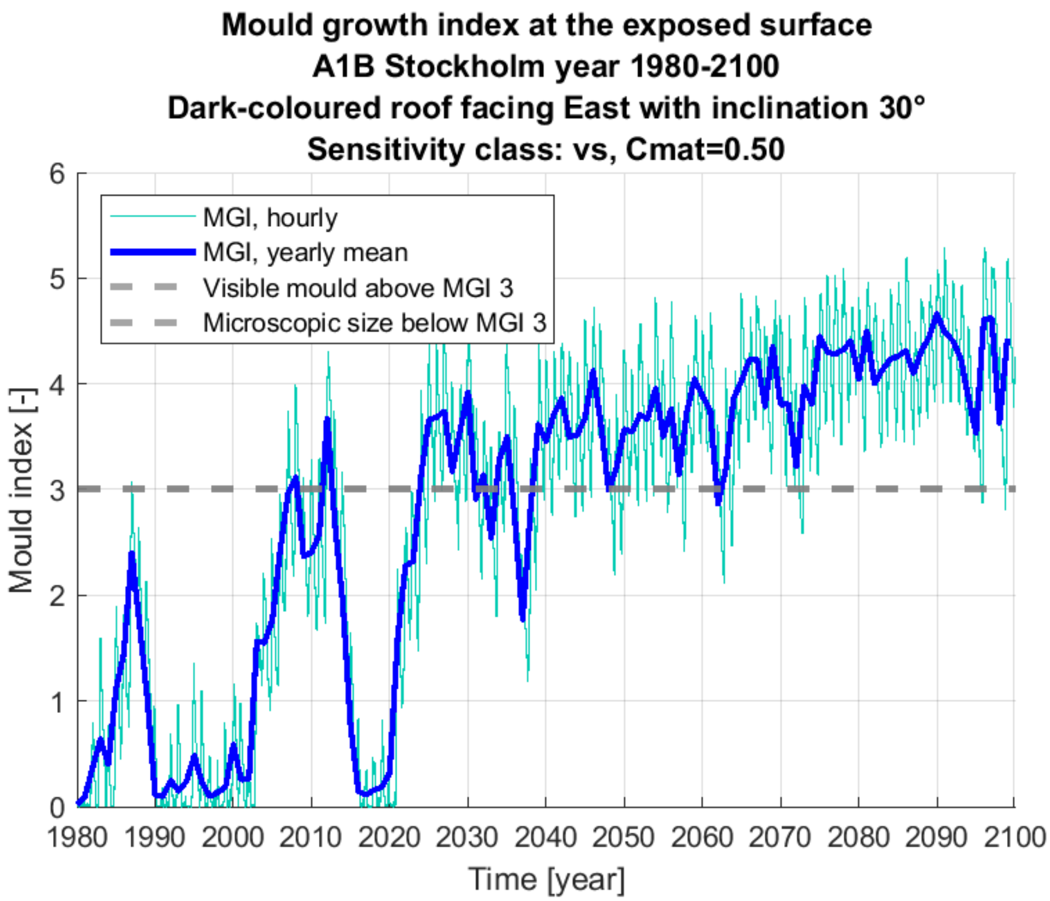

Figure 6.30. *STO STD year 1980-2100 East: MGI*

Note: The blue line represents the yearly mean, the turquoise represents the span of the monthly mean, and the grey lines are the span of hourly values. The dashed grey line of MGI 3 represents a threshold where the mould becomes visible.

6.3.5 Comparing Orientations

When comparing the different surfaces, the temperatures and the relative humidity at the exposed surfaces follow a similar curve but are offset from each other. In figure 6.31 the whole lines represent temperature, and the dotted lines represent relative humidity. The colour of the lines represents the different surfaces and the outdoor air. Notable is that of the exposed surfaces the north-facing surface has the highest relative humidity and the lowest temperatures. Only the outdoor air has higher outdoor temperatures and relative humidity.

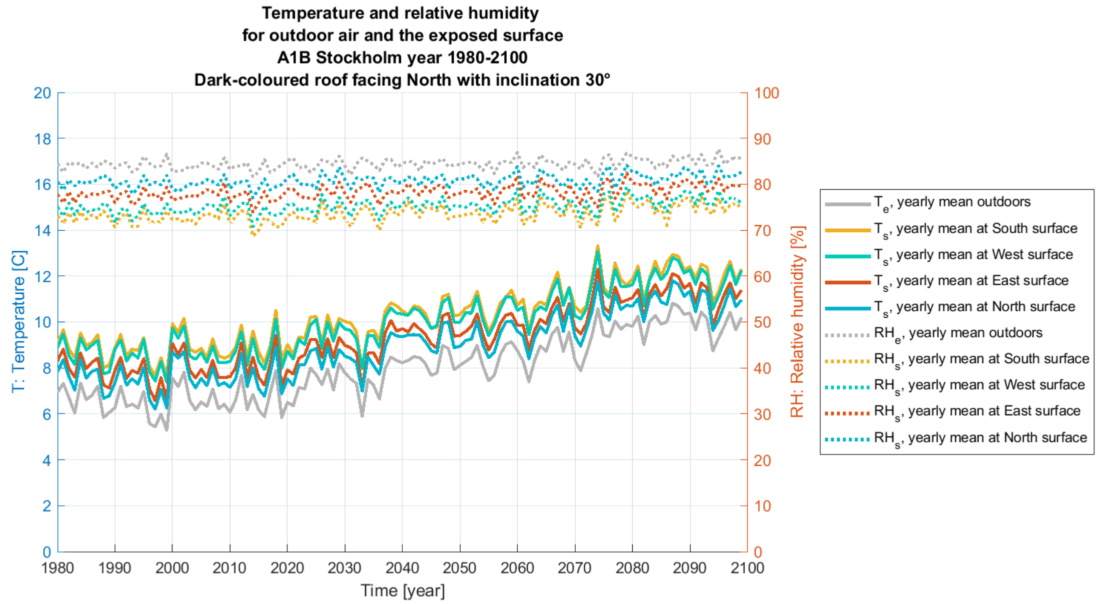

Figure 6.31. *T and RH for Air and Surfaces STO STD year 1980-2100*

Note: The whole lines represent yearly mean temperatures of outdoor air and surfaces in all orientations. The dotted lines represent the yearly mean relative humidity of outdoor air and at surfaces in all orientations.

In figure 6.32 MGI of four different orientations for STO STD for the year 1980-2100 is presented. The north-facing surface, the blue line, shows the highest MGI, and the south-facing surface, the yellow line, shows the lowest MGI.

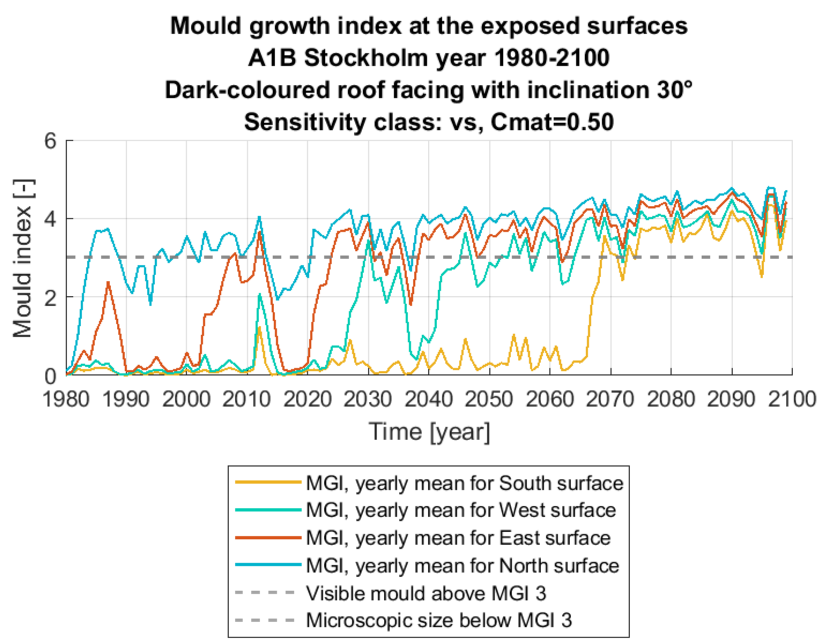

Figure 6.32. *MGI for All Orientations STO STD year 1980-2100*

Note: The different coloured lines represent MGI of differently oriented surfaces. The dashed grey line represents an MGI of 3 where the mould becomes visible.

6.4 Study C: Locations

The climate expressed in mean values of temperature (T) and relative humidity (RH) of outdoor air is shown in Figures 6.33 and 6.34. Östersund (OST), red line, shows the lowest T and the RH. Lund, turquoise line, shows the highest T and the lowest RH. Gothenburg (GOT), blue line, and Stockholm (STO), yellow line, show similar T and RH, but where Stockholm is a little lower in both parameters.

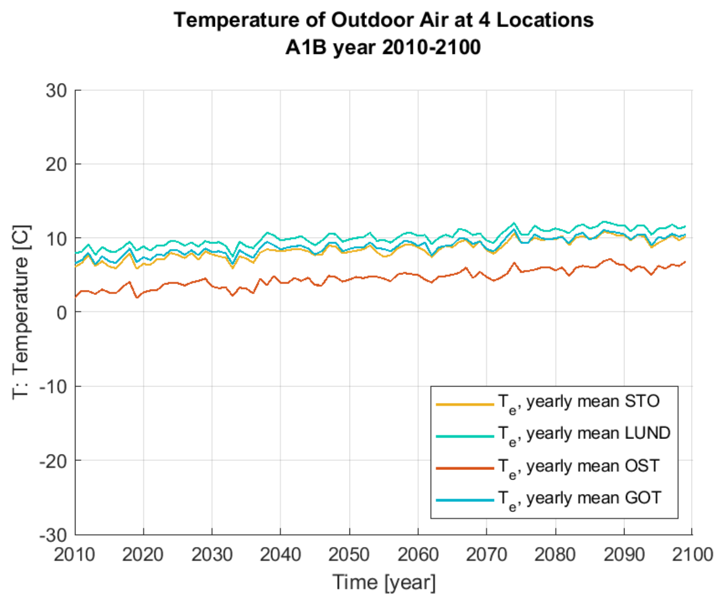

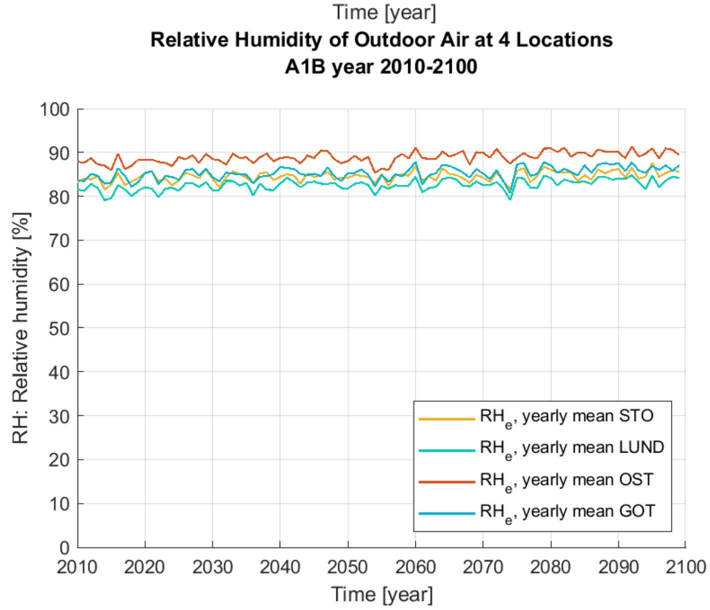

Figure 6.33-6.34. *Outdoor T and RH at Different Locations for the Year 2010-2100*

Note: The different coloured lines represent yearly mean values in different locations. The left plot shows temperatures, and the right plot shows relative humidity.

The two worst orientations in Stockholm are compared with Östersund, Lund and Gothenburg in figures 6.35-6.37. Most of the time Gothenburg has the highest MGI and Stockholm has the lowest.

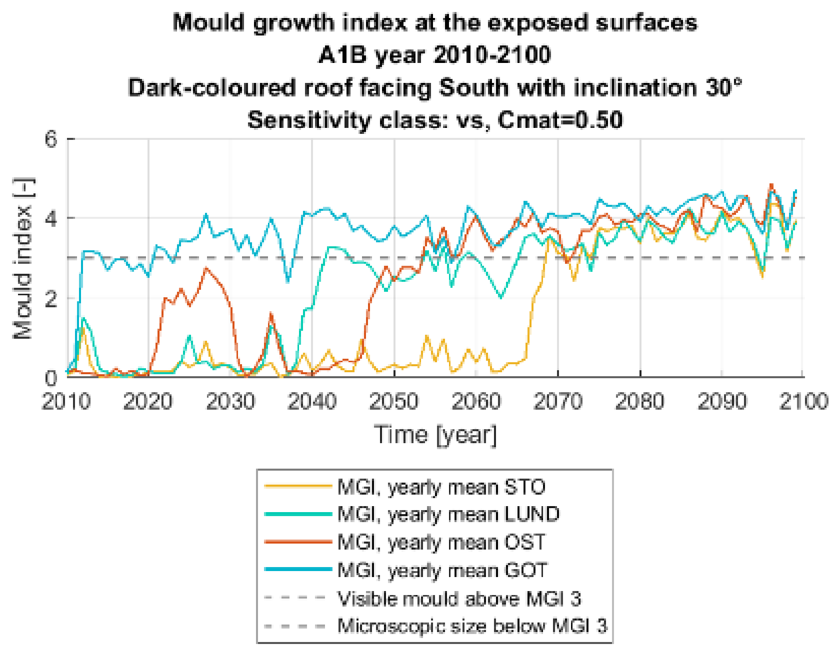

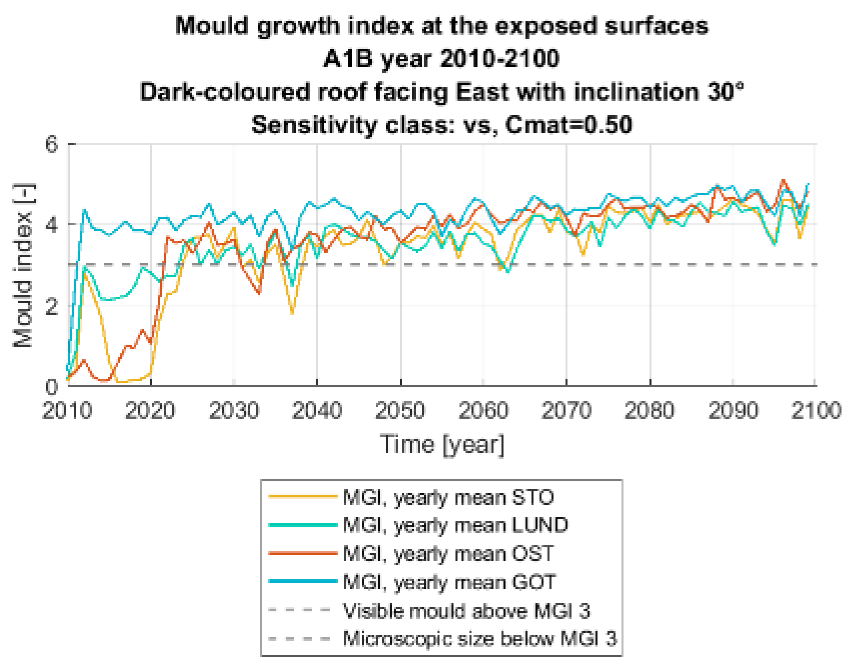

Figure 6.35-*6. 36. MGI at Different Locations for the Year 2010-2100*

Note: The different coloured lines represent MGI of the same oriented surfaces at different locations. The dashed grey line represents an MGI of 3 where the mould becomes visible.

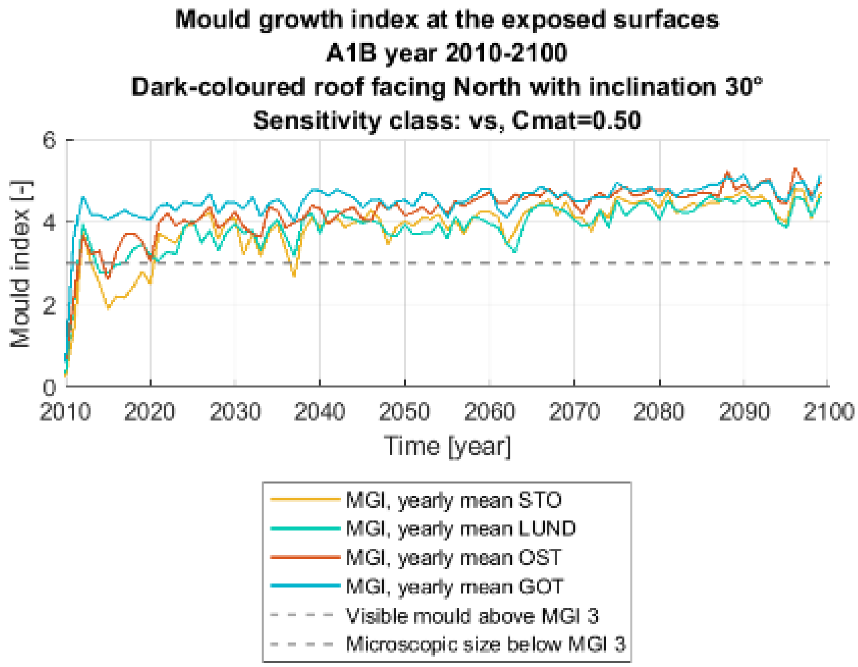

Figure 6.37. *MGI at Different Locations for the Year 2010-2100*

Note: The different coloured lines represent MGI of the same oriented surfaces at different locations. The dashed grey line represents an MGI of 3 where the mould becomes visible.

6.5 Study D: Inclinations

Two inclinations (30° and 45°) on roofs are compared for Stockholm. In figures 6.38 and 6.39 the air exchange rate of the cavity is shown for the 45°-roof. The shaded grey lines represent the hourly fluctuations, the turquoise lines represent the variations of monthly mean values, and the blue line represents the yearly mean. The red line represents the yearly mean of the 30°-roof. Figure 6.38 shows the east orientation, and figure 6.39 shows the north orientation. In both orientations, the yearly mean air exchange rate is lowered with a greater angle.

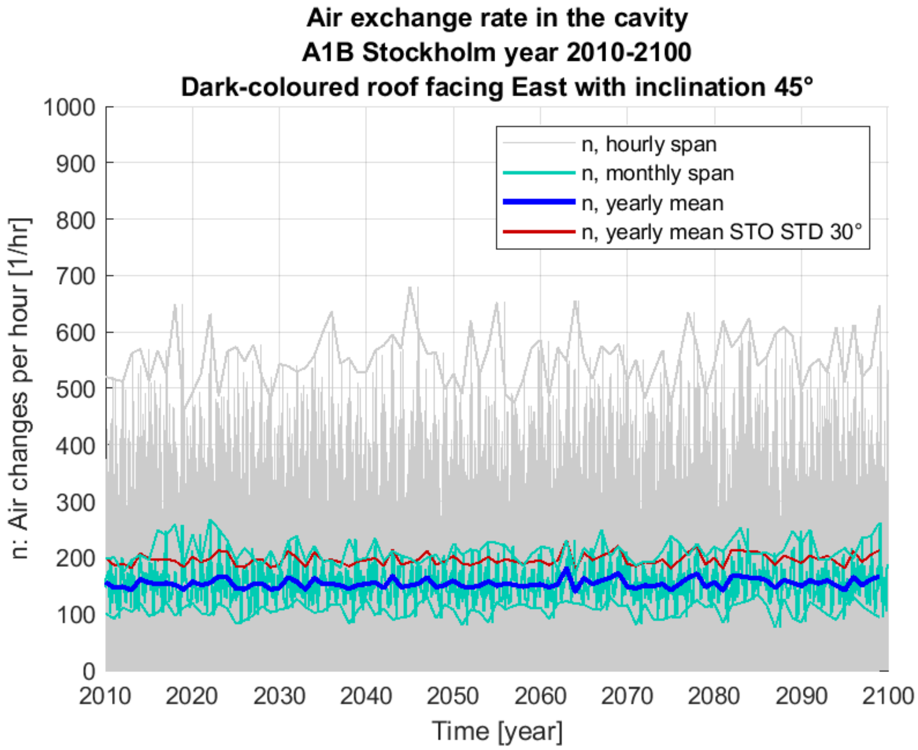

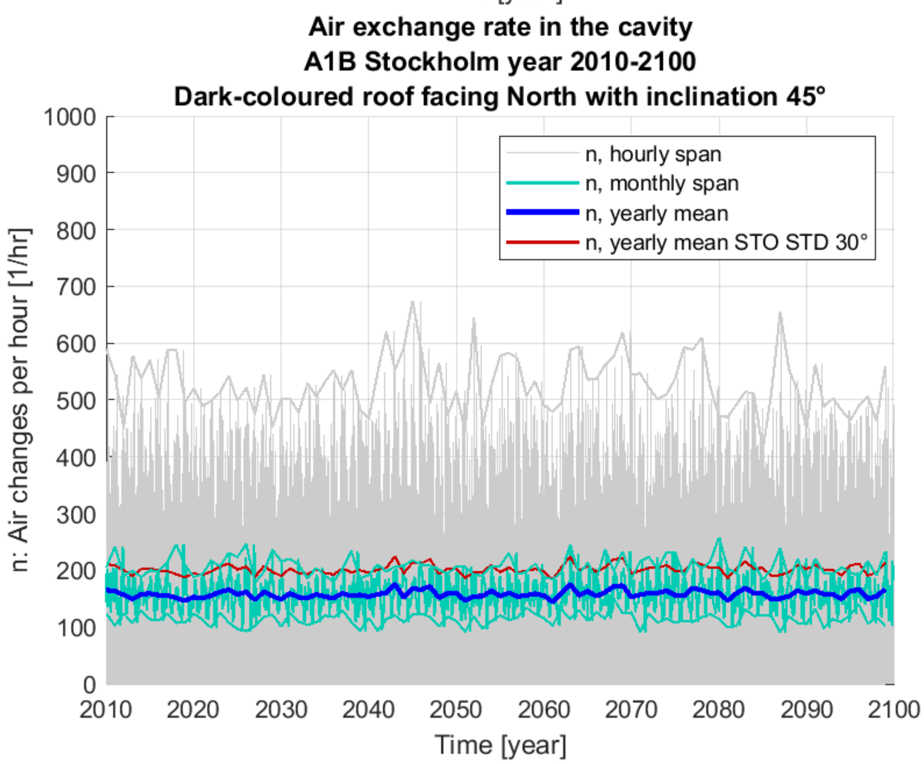

Figure 6.38-6.39. *Air Exchange Rate for Inclination 45° of STO STD East and North*

Note: The red line represents the yearly mean for STO STD with an inclination of 30°. The rest of the lines represent STO STD with an inclination of 45°. The blue lines represent the yearly mean, the turquoise represents the span of the monthly mean, and the grey lines are the span of hourly values. The left plot shows the east-facing surface, and the right plot shows the north-facing surface

The MGI is slightly affected by the lowered air exchange rate. In figures 6.40 and 6.41, the MGI for the north-facing and east-facing exposed surfaces are presented. The turquoise line represents the hourly fluctuations, the blue line the yearly mean, and the red line, the yearly mean for the MGI of the standard case of Stockholm (STO STD). The standard case is explained at the beginning of chapter 6.

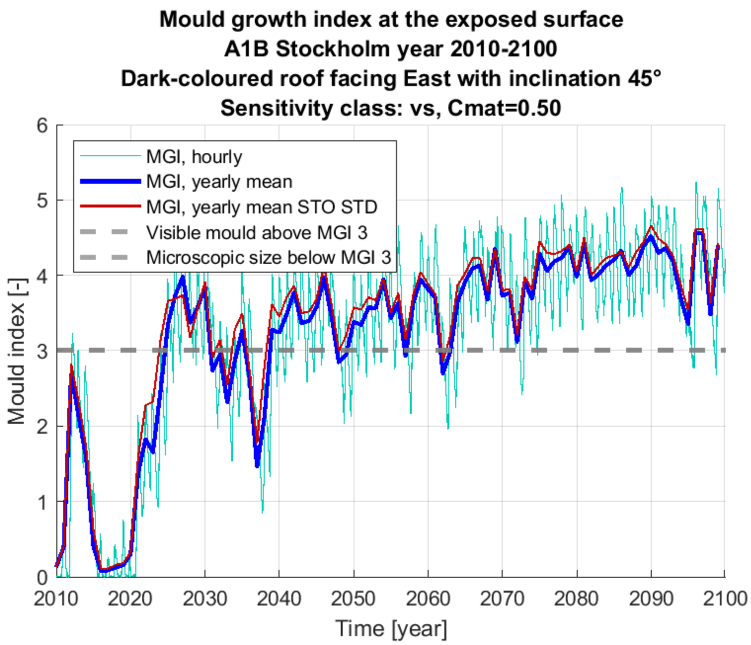

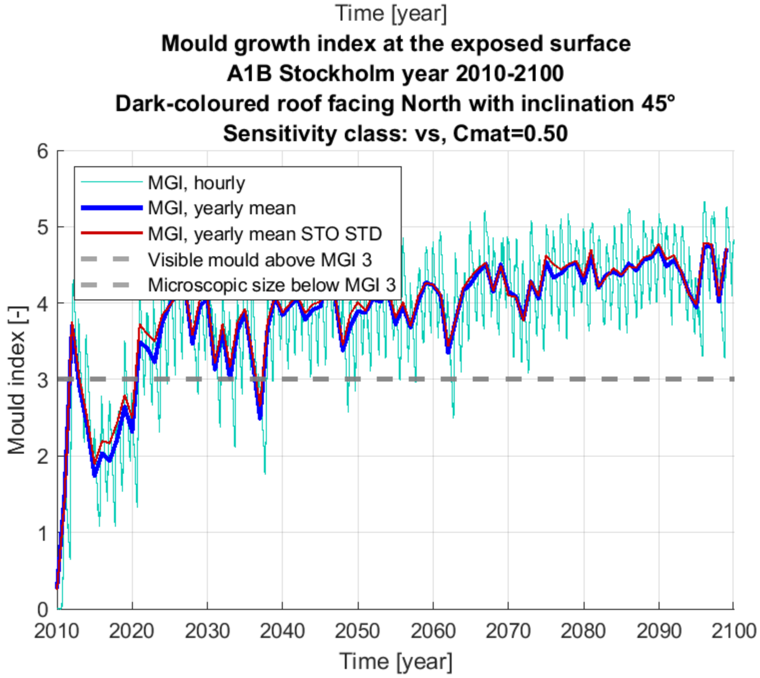

Figure 6.40-6.41. *MGI for Inclination 45° of STO STD East and North*

Note: The red line represents the yearly mean for STO STD with an inclination of 30°. The rest of the lines represent STO STD with an inclination of 45°. The blue lines represent the yearly mean, the turquoise represents hourly values. The left plot shows the east-facing surface, and the right plot shows the north-facing surface. *The dashed grey line represents an MGI of 3 where the mould becomes visible.*

6.6 Study E: Constant Cavity Airflow

In figure 6.42 the air exchange rate (blue line) of STO STD in the eastward direction is compared with a constant air exchange rate of 25 1/hr (red line). In figure 6.43 the resulting MGI of the 25 1/hr air exchange rate is compared with the STO STD. The red line represents the yearly mean of STO STD and the blue line the yearly mean of the 25-1/hr-case, and the turquoise line represents the hourly fluctuations. The constant airflow receives a considerably lower MGI for the years 2020-2050. In the other years, the MGI is slightly higher in STO STD.

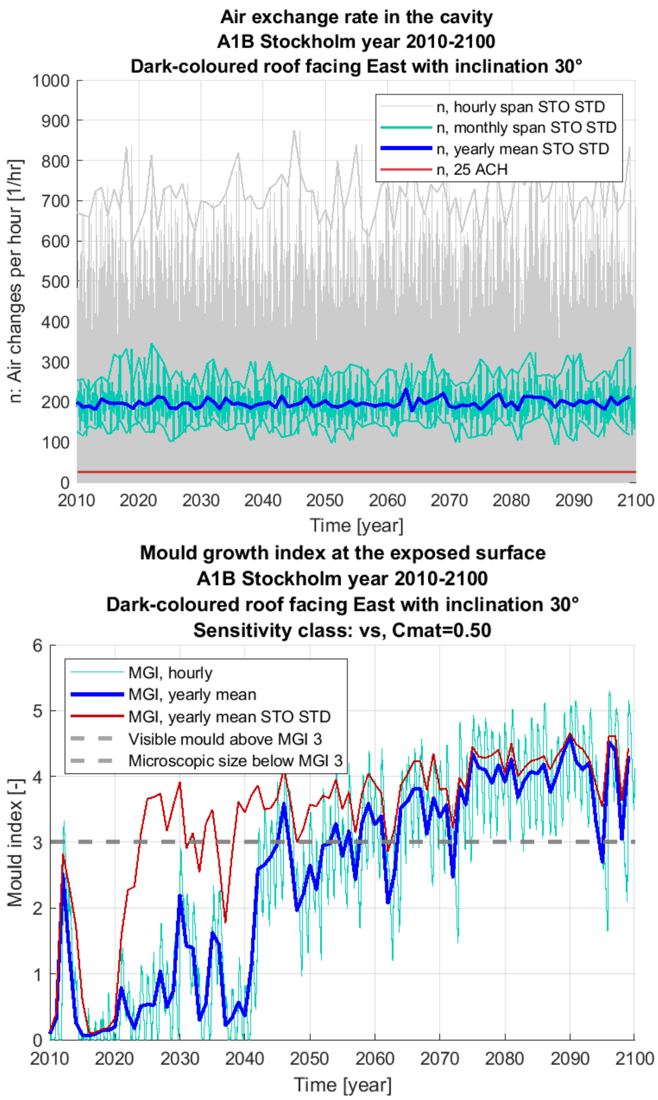

Figure 6.42-6.43. *Air Exchange Rate and MGI for Varied and Constant Ventilation of STO STD East*

Note: The left plot shows the air exchange rate. The red line represents the yearly mean values of a constant air exchange rate of 25 1/hr. The blue lines represent the yearly mean, the turquoise represents the span of the monthly mean, and the grey lines are the span of hourly values. The right plot shows MGI where the red line represents the yearly mean for STO STD and the blue line the yearly mean for constant ventilation. The turquoise represents hourly values. The dashed grey line represents an MGI of 3 where the mould becomes visible.

6.7 Study F: Additional External Insulation

In figure 6.44 the MGI for the case with additional exterior insulation is shown. The turquoise line represents the hourly fluctuations, the blue line the yearly mean, and the red line represents the yearly mean of STO STD. The MGI of STO STD is slightly higher than the case with the additional insulation.

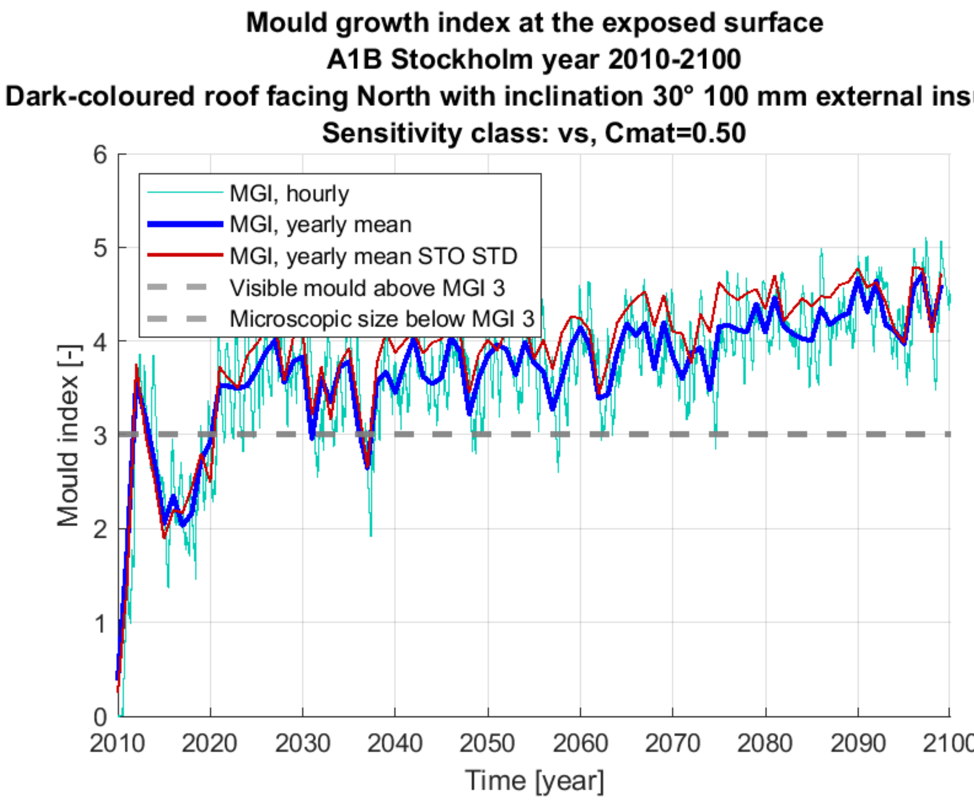

Figure 6.44. *MGI STO STD North Additional External Insulation*

Note: The red line represents the yearly mean for STO STD and the blue line the yearly mean with additional external insulation of 100 mm. The turquoise represents hourly values. The dashed grey line represents an MGI of 3 where the mould becomes visible.

6.8 Study G: Roof Colour

In figures 6.45 and 6.46 the surface temperature of the exposed surface in southward orientation for a bright-coloured surface is compared with the dark-coloured STO STD. The grey lines show the hourly fluctuations of the temperature. The roof with bright colours, figure 6.45, has smaller peaks (the grey lines) than the roof with dark colours, figure 6.46.

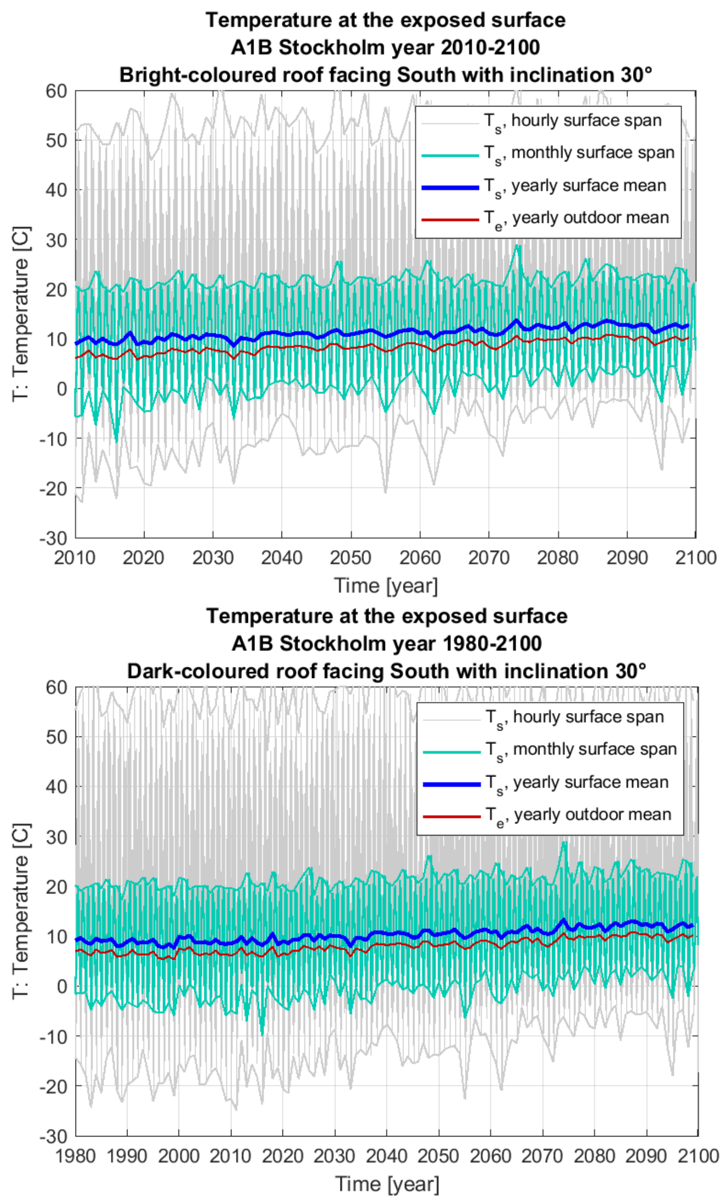

Figure 6.45-6.46. *Surface Temperature for STO STD Bright-coloured and Dark-coloured Roof.*

Note: The red line shows yearly mean values. The blue line represents the yearly mean at the surface, the turquoise represents the span of the monthly mean at the surface, and the grey lines are the span of hourly values at the surface. The left plot shows a bright-coloured roof, and the right plot shows a dark-coloured roof.

In figure 6.47 the MGI of different orientations of the bright coloured roof is compared to each other. In all directions, the MGI is higher on the dark roof, which is shown in a similar figure for the dark roof (figure 6.48).

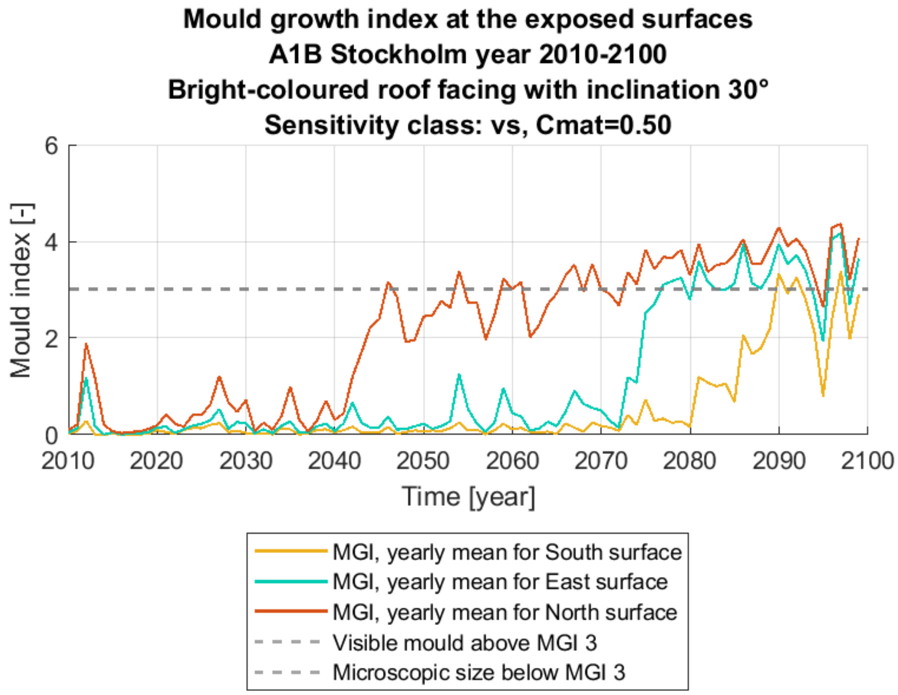

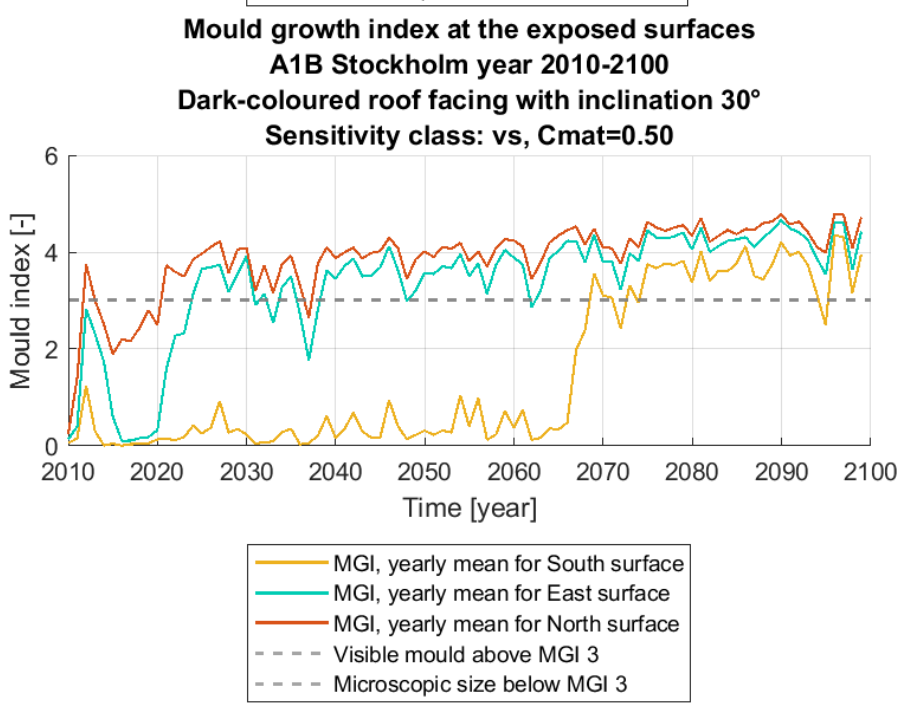

Figure 6.47-6.48. *Comparing MGI for STO STD South, East and North. Bright-coloured and Dark-coloured Roof.*

Note: The differently coloured lines represent different orientations. The dashed grey line represents an MGI of 3 where the mould becomes visible. The left plot shows the bright-coloured roof and the right plot shows the dark-coloured roof.

7
Discussion

In the discussion, it is important to understand the difference between Fuktcentrum data and the Rossby Centre data. The Rossby Centre data consists of the three data sets A1B, A2 and B1. Explanations of the different data sets are found in sections 2.3 and 2.4.

The A1B data has a more critical impact on moisture safety than the Fuktcentrum data. This is shown in the validation of the study model in Figures 5.9 and 5.10. Even though to the data from Fuktcentrum is measured data, the Rossby Centre data has been validated. The climate models cannot perfectly describe the climate. All models have their strengths and weaknesses and describe different parts of the climate with varying accuracy. Therefore, the most comprehensive study would use a variety of climate models and emission scenarios. The truth of the forecast would then likely be somewhere in between the results of all the models. Together the models make up a span of a likely future climate.

The mould growth index is an index that predicts if there are conditions for mould to start growing. Together with the future climate data, the mould growth index predicts the risk of mould growth in a possible future climate. The result in the study is therefore far from certain that they will become true, but they are likely.

When analysing the results, it is notable that there are threshold points in the different data sets. When a threshold point is passed it is unlikely that the mould growth will decline because of the continuously increasing favourable conditions for mould growth in the future weather data sets. In a few cases, there were peaks of mould growth, which later declined. For example, in figure 6.30 there are peaks that decline after 10-20 years, but later the mould growth index becomes even higher than the peaks earlier. The reason why there appear to be threshold points that make the mould growth index plots look like stairs is that the unique combination of temperature and relative humidity over a long period decides if the mould growth will decline. When the climate becomes more favourable for mould growth it will start to increase again.

When comparing A1B, A2 and B1, the main difference is a greater increase in outdoor air temperature of A2 than A1B, as well as a greater increase of A1B than B1. In combination with a varying air exchange rate and moisture infiltrations in all the scenarios, it is visible in the MGI that A1B and A2 are comparably critical and that B1 is more moderate. This differs from the study of attics with the same data sets done by Nik et al. (2012). It could be because of differences in geometry and volume of the attic and the ventilated parallel roof. The latter has a higher air exchange rate, which results in more conditions with a higher risk of mould growth in the roof construction. But this is not studied and has to be considered in future studies.

Comparing the different orientations: south, west, east, and north, their mould favourability is increasing in the same order. As seen in figures 6.11, 6.16, 6.21 and 6.26 the air exchange rate is the same in south and north orientations, and in east and west orientations. This is because they both are parts of the same saddle roof construction. The moisture infiltration is the same in all directions (6.12, 6.17, 6.22 and 6.27). In WUFI, the wind direction and speed also affect the transfer coefficient of the roof. The main difference between the orientations is the amount of radiation that strikes and leaves the surfaces and the wind speed and direction of the wind. Especially between south and north, and between east and west. The reason why the north is having a higher MGI than the south is that the net balance of radiation of the roof is lesser in the north resulting in a cooler roof which results in higher relative humidity and a more climate with a higher risk of mould growth (figure 6.31) for mould growth (figure 6.32), even if the temperature on the south side is higher.

The results of different locations show that Gothenburg is the location with the greatest risk for mould growth. Stockholm is the location with the least risk of mould growth for mould growth, especially on the south roof. The results corresponds quite good to the prior results on attics by Nik et al. (2012) where they concluded that the conditions in Gothenburg has the greatest risk for mould growth. In the study on attics, Östersund had the least risk for mould growth, but in this study, the risk of mould growth is greater (figure 6.35). The reasons for the difference between the two studies have to be investigated in detail in further studies. The reason for this could be that the air exchange rate is much higher in the ventilated parallel roof than in the attic resulting in that the mould-favourable outdoor climate entering the construction more often.

The larger inclination results in a slightly smaller yearly mean air exchange rate. In the study of Månhardt and Odén (2020) the air exchange rate was marginally affected by the inclination but was lowered by the increased length of the cavity. Because the geometry of the study case always was considered a building of 10 meters in width (section 3.4), the cavity of a roof with a larger inclination was longer than if the inclination were smaller. In the study of Månhardt and Odén (2020) the mould growth index is slightly decreasing with a lower air exchange rate. The same relationship is seen in figures 6.40 and 6.41. In the same reasoning, Månhardt and Odén (2020) concluded that lowering the air exchange rate lowers the risk of mould growth. In figure 6.43, the same result is seen when a variable air exchange rate is compared with a constant air exchange rate of 25 1/hr.

The north-facing exposed surface is in almost all studied cases the worst scenario. The reason for this is the high relative humidity, which is a result of lower temperatures than the other roofs in combination with a high air exchange rate which lets the outdoor air with high relative humidity enter the cavity. Especially on nights when the temperature gets lower due to longwave radiation the risk increase in relative humidity and condensation is the greatest. A solution to this problem is to add additional insulation on the exterior side of the cavity, which would lower the effect of longwave radiation cooling on the inside of the cavity. In study E the standard Stockholm north case is compared with the same case but with 100 mm additional insulation. The result is positive with a little decrease in MGI (figure 6.45). The small impact on the MGI may be because the main effect on the cavity is the high air exchange rate which both cools the inside of the cavity and lets humid outdoor air enter. Compared with the east orientation of the standard case, the MGI is only slightly lower, which indicates that small changes in the radiation gains and losses both from shortwave and longwave are only making a small difference or that the amount of insulation is too small relative to total insulation thickness.

Another way of decreasing the amount of radiation affecting the cavity is changing the colour of the roof. In the standard case, the roof is dark and mate, in study F it is compared with a bright-coloured and reflective steel sheet roof. In figures 6.47 and 6.48 the effect is great with a large decrease in MGI. The effect is greater in the east and north orientations than in the south. But on the other hand, the south orientation already had a low risk of mould growth, so conditions possibly can not decrease a lot more. Only at the end of the century, the MGI for the south bright-roof was increase. The reason for this may be that the climate conditions get worse around the year 2070. Standardly a dark roof means a higher temperature, and therefore a lower risk of mould growth because of the lower relative humidity. The reason why a very reflective steel sheet is getting a lower risk of mould growth is not completely examined.

Throughout all the results the MGI is quite high. Even for the results of today. This could have two different explanations. The first is that the conditions of parallel roofs in Sweden today are bad. Because the construction is not easy to examine, it is impossible to know in a lot of cases. The second is that compared to the validation study, the results are somewhat extravagated, giving a larger MGI than the real conditions actual suggests.

This could be the case because of the uncertainties of the way WUFI handles the cavity. The reasons for this are discussed in section 5.3.6.

At last, it is important to remember that the MGI just indicates the conditions of mould to grow and the actual mould growth. Therefore, high mould growth does not automatically lead to mould, but to a vulnerability to mould.

8
Conclusion

Considering different parameters affecting the risk of mould growth in a ventilated parallel roof, the outdoor climate conditions have the greatest impact, also the orientation of the roof has a large impact with north as dimensioning when not considering driving rain and rain leakage. The air tightness also makes a huge impact. The existence of a cavity is important, but the effect of different geometries compare to each other are small.

The only parameter that gives significantly better moisture safety is a brighter and more reflective colour on the exterior roof surface. But, this result has to be treated with forethought because it partially contradicts the normal relations between dark colour, high temperature and lower risk of mould growth.

Generally, the more potent climate scenarios A1B and A2 indicate increasingly favourable conditions for mould growth in the future. The B1 scenario, on the other hand, shows slightly more favourable conditions, and at the end of the century still below the visible level of mould growth.

The main conclusion of the study is that it is likely that ventilated parallel roofs in Sweden will be subjected to a higher risk of mould growth in the future.

8.1 Future Research

To understand how parallel ventilated roofs will operate in future climate precipitation and driving rain with leakage could be studied to understand other serious moisture loads. The drying out potentials of built-in moisture as a part of the moisture balance could also be studied.

The impact of additional insulation due to extra insulation and snow in winter on roofs in northern Sweden could be studied further.

A study could be investigating the future performance of a mechanically ventilated cavity in a future climate.

The results in this study for northern Sweden differed a lot from precedent studies on attics. Therefore, a detailed investigation concerning the differences between attics and ventilated parallel roofs would be useful for a deeper understanding of the subject.

Bibliography

Arfvidsson, J., Harderup, L.-E., & Samuelson, I. (2017). *Fukthandbok: Praktik och teori.* Stockholm: AB Svensk Byggtjänst.

ASHRAE. (2001). *Fundamentals.* Atlanta: American Society of Heating, Refrigeration and Air Conditioning Engineers.

Bjurström, P. G. (2007). *Byggnadsmaterial. Uppbyggnad, tillverkning och egenskaper.* Lund: Studentlitteratur AB.

Boverket. (2018). *Boverkets byggregler - föreskrifter och allmänna råd.*

Eriksson, O. (2017). *Fuktsäkra parallelltak: En studie av risken för mögepåväxt i parallelltak med variable ångbroms.* Lund: Lunds Tekniska Högskola.

Falk, J. (2010). *Ventilerad luftspalt i yttervägg : luftomsättningar och konvektiv fukttransport.* Lund: Lunds tekniska högskola.

Fraunhofer IBF. (den 29 3 2001). *WUFI's Perfromance and Limitations*. Hämtat från Wufi-wiki: https://www.wufi-wiki.com/mediawiki/index.php/Discussion:WUFI-Pro_PerformanceandLimitations

Fraunhofer IBF. (2008). *Hygrothermal Sources*. Hämtat från Wufi-wiki: https://www.wufi-wiki.com/mediawiki/index.php/1D:Dialog_EditHygrothermalSources

Fraunhofer IBF. (den 8 July 2009). *Details:Physics: Moisture Transport in Building Materials*. Hämtat från Wufi-Wiki: https://www.wufi-wiki.com/mediawiki/index.php/Details:Physics

Fraunhofer IBF. (den 13 6 2013). *Moisture Storage Function*. Hämtat från Wufi-wiki: https://www.wufi-wiki.com/mediawiki/index.php/Details:MoistureStorageFunction

Fraunhofer IBF. (den 19 December 2018). *Validation*. Hämtat från WUFI: http://wufi.de/en/software/validation/

Fraunhofer IBP. (den 30 September 2008). *Long-wave Radition Exchange*. Hämtat från Wufi-wiki: https://www.wufi-wiki.com/mediawiki/index.php/Details:LongWaveExchange

Fuktcentrum. (2018). *Description of data for Heat and Moisture Simulation in Sweden.* Hämtat från Fuktcentrum: https://www.fuktcentrum.lth.se/fileadmin/fuktcentrum/klimatdatafiler_4_staeder/Description_of_climate_data_from_LU_Building_Physics_.pdf

Gullbrekken, L. (2018). *Climate adaptation of pitched wooden roofs (Doctoral thesis).* Trondheim: NTNU.

Gullbrekken, L., Uvsloekk, S., Geving, S., & Kvande, T. (2018). Local loss coefficients inside air cavity of ventilated pitched roofs. *Journal of Building Physics*, Vol 42(3) 197-219.

Hagentoft, C.-E. (1991). Air convection coupled with heat conduction in a wall. A thermal analysis. Notes on Heat Transfer, 7. Lund: Building Physics.

Hagentoft, C.-E. (2001). *Introduction to Building Physics.* Lund: Studentlitteratur AB.

Hukka, A., & Vittanen, H. (1999). A mathematical model of mould growth on wooden material. *Wood Science and Technology 33*, ss. 475-485.

Hägerhed Engman, L., & Samuelsson, I. (2006). Kalla vindar: Problem och förbättringar. *Bygg & Teknik (4/06)*, 22-26.

Idelchik, I. E. (1960). *Translated: Handbook of hydraulic resistance. Coefficients of local resistance and of friction.* Moskva-Leningrad:: Gosudarstvennoe Energeticheskoe Izdatelstvo.

IEA. (1996). *IEA SHC Annual Report.*

Isaksson, T., & Mårtensson, A. (2017). *Byggkonstruktion - Regel och formelsamling (3 edition).* Lund: Studentlitteratur AB.

Kehrer, M. (2008). *WUFI® Workshop NTNU / SINTEF 2008: Heat and Moisture Sources.* Hämtat från wufi.no: http://www.wufi.no/workshop-08/SourcesAndSinks.pdf

Kjellström, E., Bärring, L., Gollvik, S., Hansson, U., Jones, C., Samuelsson, P., . . . Wyser, K. (2005). *A 140-year simulation of Europe climate with the new version of the Rossby Centre regional atmospheric climate model (RCA3).* Norrköping: Swedish Meteorological and Hydrological Institute.

Kronvall, J. (1980). *Air flows in building components.* Lund: Lund University of Technology.

MathWorks. (2022a). *What Is Matlab?* Hämtat från MathWorks: https://se.mathworks.com/discovery/what-is-matlab.html?requestedDomain=

MathWorks. (2022b). *Help Center: MAT-File Versions*. Hämtat från MathWorks.: https://se.mathworks.com/help/matlab/import_export/mat-file-versions.html

MathWorks. (2022c). *Help Center: struct*. Hämtat från MathWorks: https://se.mathworks.com/help/matlab/ref/struct.html

Moran, M., & Shapiro, H. (2003). *Fundementals of engineering thermaldynamics.* New York: John Wiley & Sons.

Moss, R. H., Edmonds, J. A., Hibbard, K. A., Manning, M. R., Rose, S. K., van Vuuren, D. P., . . . Wilbanks, T. J. (2010). The next generation of scenarios for climate change research and assessment. *Nature*, 747-756.

Mundt-Petersen, S. (2015). *Moisture Safety in Wood Frame Buildings - Blind evaluation of the hygrothermal calculation tool WUFI using field measurements and determination of factors affecting the moisture safety.* Lund: Department of Building Physics. University of Lund. Hämtat från https://portal.research.lu.se/portal/files/3853018/4937649.pdf

Mundt-Petersen, S. (2016). *Fuktsäkra träkonstruktioner II: Vägledning för utformning av träbaserade takkonstruktioner.* Lund: Department of Building Physics. University of Lund.

Mundt-Petersen, S., & Harderup, L.-E. (2010). Importance of a Proper applied Airflow in the Façade Air Gap when Moisture and Temperature are Calculated in Wood Framed Walls. In B. Rosenthal (Ed.). *Reader manual: 5th International BUILDAIR-Symposium on Building and Ductwork Air thightness (former*

"European BlowerDoor-Symposium") October 21-22, 2010, Kgs. Lyngby near Copenhagen, Denmark., 37. Germany: Energie und Umweltzentrum am Deister GmbH (e.u.[z.]).

Mundt-Petersen, S., & Harderup, L.-E. (2011). Comparison of measured and calculated temperature and relative humidity with varied and constant air flow in the facade air gap. In J. Vinha, J. Piironen, & K. Salminen (Eds.). *Proceedings of the 9th Nordic Symposium on Building Physics - NSB 2011.* (ss. (Vol. 1, pp. 147-154)). Tammerfors: Tampere University of Technology.

Månhardt, G., & Odén, G. (2020). *Fuktsäkerhet i ventilerade parallelltak: Fallstudie med blinda beräkningar och utveckling av luftflödesmodell.* Lund: Lunds Universitet.

Nakicenovic, N., Davidson, O., Davis, G., Grübler, A., Kram, T., Lebre La Rovere, E., . . . Dadi, Z. (2000). *IPCC Special Report on Emissions Scenarios.* Cambridge: Intergovernmental Panel on Climate Change.

Nik, V. (2010). *Climate Simulations of an Attic Using Future Weather Data Sets: Statistical Methods for Data Processing and Analysis.* Gothenburg: Chalmers University of Technology.

Nik, V., Sasic Kalagasidis, A., & Kjellström, E. (2012). Assessment of hygrothermal performance and mould growth risk in ventilated. *Building and Environment 55*, 96-109.

Pachauri, R. K., & Meyer, L. A. (2014). *Climate change 2014: Synthesis Report. Contribution of Working Groups I, II and III to Fifth Assessment Report of the Intergovernmental Panel on Climate Change.* Geneva: Intergovernmental Panel on Climate Change.

Persson, G., Bärring, L., Kjellström, E., Strandberg, G., & Rummukainen, M. (2007). *Climate indices for vulnerability assessments.* Norrköping: Swidish Meteorology and Hydrological Institute.

Petersson, B.-Å. (2009). *Byggnaders klimatskärm: fuktsäkerhet, energieffektivitet, beständighet.* Lund: Studentlitteratur.

Svantesson, M., & Säwén, T. (2019). *Ventilation by Thermal Buoyancy in the Air Cavity of Pitched Roofs: An Experimental and Numerical Study of Air Cavity Design and Natural Convection in Parallel Roof Constructions.* Gothenburg: Chalmers University of Technology.

Taesler, R., & Andersson, C. (1984). A Method for Solar Radiation Computations Using Routine Meteorological Observation. *Energy and Buildings, 7*, 341-352.

The WUFI-Team. (2014). *Sources and Sinks in WUFI 2D*. Hämtat från Wufi-Wiki.de: https://wufi.de/de/wp-content/uploads/sites/9/2014/09/SourceStrengths_WUFI2D.pdf

Träguiden. (2020). *Tak*. Hämtat från Träguiden: https://www.traguiden.se/konstruktion/konstruktionsexempel/tak/

Wallentén, P. (2010). The treatment of long-wave radiation and precipitation in climate files for building physics simulations. *Proceedings of the 11th International Conference on Thermal Performance of the Exterior Envelopes of Whole Buildings (Clearwater) .*

Wallentén, P. (2018). *RäknadF 2018 -Stöd för kombinerade värme- och fuktberäkningar i byggnadsdelar.* Lund: Lund Universitet.

DEPARTMENT OF ARCHITECTURE AND CIVIL ENGINEERING
DIVISION OF BUILDING TECHNOLOGY
BUILDING PHYSICAL MODELLING
CHALMERS UNIVERSITY OF TECHNOLOGY
Gothenburg, Sweden 2022

CHALMERS
UNIVERSITY OF TECHNOLOGY